Nitrergic modulation of voltage-gated calcium channels and neuronal excitability

A thesis submitted for the degree of

Doctor of Philosophy

At the University of Leicester

By

Adam J.B. Tozer BSc (Leicester)

Department of Cell Physiology and Pharmacology

And MRC Toxicology Unit,

University of Leicester

August 2012

“Jeder Tag ist ein Schultag.”

Wise German words.

Abstract.

Nitric oxide is a regulator of voltage-gated calcium channels and neuronal excitability in the auditory pathway.

Adam J.B. Tozer

Nitric oxide (NO) is a diffusible messenger utilised body-wide for cellular signalling. In principal neurons of the medial nucleus of the trapezoid body (MNTB) NO is produced by the neuronal isoform of the nitric oxide synthase enzymes, nNOS. NO is known to inhibit $K_V3.1$ channels in these cells and to also reduce mini EPSC amplitudes (Steinert *et al.* 2008). In light of these known effects, NO-dependent modulation of the native voltage-gated calcium channels (Ca_Vs) in the principal neurons of the MNTB and the downstream superparaolivary nucleus (SPN) was investigated, and the functional relevance of the NO-dependent increase in Ca^{2+}influx in the MNTB explored.

Whole cell voltage clamp and pharmacological isolation of the high-voltage-activated (HVA) Ca_V subtypes in the MNTB revealed an NO-dependent potentiation of whole cell I_{Ca}, underlied by differential modulation of the channels, such that L-type channels were potentiated via a direct pathway, whereas P/Q were potentiated via the canonical NO-cGMP pathway. N-type channel activation was left-shifted by the NO-cGMP dependent pathway, and R-type channels were unaffected by NO.

Whole cell voltage clamp of SPN neurons revealed a low-voltage-activated (LVA) T-type current, which was sensitive to mibefradilMibefradil (2µM), and inhibited by NO (~50%). The T-type current contributed to the rebound firing phenotype of these cells following relief of glycinergic inhibition by the MNTB, and T-type blockers and NO exposure reduced the number of rebound action potentials (APs) generated.

Whole cell voltage clamp of MNTB principal neurons revealed an apaminApamin sensitive current which was potentiated by NO, suggesting the presence of SK channels in the MNTB. Further investigations using current clamp and synaptic stimulation revealed presynaptic expression of SK channels, which restrict synaptic release, as SK block increased evoked EPSC amplitude.

This research demonstrates that nitric oxide differentially modulates Ca_V channels expressed in two communicating nuclei of the auditory brainstem. This work also reveals the presence of SK channels both pre and postsynaptically at the calyx of Held synapse, and suggests a role for these channels in facilitating high-fidelity transmission at this auditory synapse.

Acknowledgements

I would like to thank and acknowledge the support, encouragement and supervision I have received from many people as I have made the journey through this PhD:

The great members past and present of the Forsythe group, especially Sue Robinson for her help with these investigations; my colleagues and friends in the MRC Toxicology Unit and the University of Leicester.

My Supervisors Professor Ian Forsythe and Joern R. Steinert, for hiring me, challenging me and ultimately never giving up on me.

Dr. Duncan Stanley, for his help in putting together this manuscript.

My family, for their support and unshaken belief in me and whatever it is I did during this PhD. This thesis is built on their support and would never have been achieved without it.

My Wife Rebecca, for making me the happiest man alive when she married me, and for all her love and support during the highs and lows of these studies. I especially want to thank her and acknowledge the sacrifices she has made in enabling me to undertake this PhD, and to follow my dream.

My little Son Joel, for reminding me that there is much more to life than the lab, and for making me feel like the proudest man alive every minute of every day from the moment I met him.

And my friends, those who have passed on and those still here, for shaping me as a person, for keeping my feet firmly on the ground, and for accompanying me to the pub.

Declaration

The work in this thesis is my own, and includes several collaborative projects outlined below.

PCR and immunohistochemistry was carried out by Sue Robinson.

Some of the synaptic stimulation experiments were done in conjunction with, and under the supervision of, Dr. Joern Steinert.

Parts of this thesis have been published in Kopp-Scheinpflug *et al.* 2011 and Tozer *et al.* 2012.

Major findings of this thesis.

- Four high voltage-activated Ca_V channels are expressed in the MNTB principal neurons, consistent with previous reports.
- Whole cell I_{Ca} is potentiated by NO and this is mainly due to the potentiation of L-type (Ca_V1) and P/Q-type ($Ca_V2.1$) channels, which switches the relative contribution of Ca_V channels to whole cell I_{Ca}.
    - This differential modulation occurs via distinct NO-dependent pathways.
- Low-voltage-activated (LVA) Ca_V channels are expressed in neurons of the superior paraolivary nucleus (SPN) and, together with HCN1 and 2 channels, these contribute to a rebound burst firing phenotype in these neurons, thought to underlie gap detection in sound.
    - The LVA T-type current is inhibited by NO.
- SK channels are present in the MNTB, both pre and post synaptically.
    - I_{SK} is potentiated by NO via its augmentation of I_{Ca}.
    - I_{SK} contributes to an After Hyperpolarising Potential following a presynaptically induced but not postsynaptically injected AP train.
    - Presynaptic SK current restricts glutamate release at the calyx of Held.

Table of Contents

Table of Figures

Introduction

Materials and Methods

Results.

Nitric Oxide (NO) differentially modulates voltage-gated calcium channels (Ca_V) in principal neurons of the Medial Nucleus of the Trapezoid Body (MNTB)

Nitric oxide (NO)-dependent inhibition of T-type (Ca_V3) channels in the Superior Paraolivary Nucleus (SPN).

Nitric oxide (NO) potentiates an SK-mediated after hyperpolarising potential (AHP) in mouse MNTB neurons.

Discussion and future work

Table of Tables

Table of Abbreviations

7-NI: 7-nitroindazole

AP: Action Potential

aVCN: Anteroventricular Cochlea Nucleus

BK: Large conductance Ca^{2+}-dependent Potassium Channel

cAMP: Cyclic Adenosine Monophosphate

CaRF: Calcium Response Factor

Ca_V: Voltage-Gated Calcium Channel

cGMP: Cyclic Guanosine Monophosphate

CREB: Calcium Response Element Binding Protein

DEA: Diethylammonium nonoate

EPSC: Excitatory Post Synaptic Current

EPSP: Excitatory Post Synaptic Potential

GBC: Globular Bushy Cell

HVA: High Voltage-Activated

I_{Ca}: Calcium Current

I_h: Hyperpolarisation-activated Potassium Channel

IHC: Inner Hair Cell

IK: Intermediate conductance Ca^{2+}-dependent Potassium Channel

IPSC: Inhibitory Post Synaptic Current

IPSP: Inhibitory Post Synaptic Potential

I_{TCa}: T-type Calcium Channel

K_V: Voltage-Gated Potassium Channel

LVA: Low Voltage-Activated

MAPK: Mitogen Activated Protein Kinase

MNTB: Medial Nucleus of the Trapezoid Body

Na_V: Voltage-Gated Sodium Channel

NFAT: Nuclear Factor of Activated T-Cells

nNOS: Neuronal Nitric Oxide Synthase

NO: Nitric Oxide

ODQ: 1H-[1,2,4]oxadiazolo[4,3-a]quinoxalin-1-one

OHC: Outer Hair Cell

PKG: Protein Kinase G

SBC: Spiny Bushy Cell

sGC: Soluble Guanylyl Cyclase

SK: Small conductance Ca^{2+}-dependent Potassium Channel

SNP: Sodium Nitroprusside

SPN: Superparaolivary Nucleus

TEA: Tetraethylammonium

TTx: Tetrodotoxin

V_m: Membrane Potential

1. Introduction.

The focus of this work was to characterise the voltage-gated calcium (Ca_V) channels present in the postsynaptic neurons of the medial nucleus of the trapezoid body (MNTB) and the downstream superparaolivary nucleus (SPN), and to investigate any nitric oxide (NO) dependent modulation of their currents. The consequence of any NO-Ca_V modulation on cellular excitability in these nuclei was then investigated.

1.1 Nitric oxide (NO) is a diffusible messenger utilised body-wide for cellular signalling.

Nitrogen monoxide or nitric oxide (NO) is a diatomic gas molecule with the chemical formula NO. It is a small amphiphyllic diffusible messenger utilised as a ubiquitous signalling molecule by vertebrates, invertebrates, bacteria and plants (Wendehenne *et al.*, 2001). Composed of a single nitrogen atom bonded to an oxygen atom, this simple molecule can diffuse within a cell and through the membrane to exert its signalling effect in its cell of origin or in adjacent cells and tissues. With a diffusion coefficient of 848µm/s in arterioles (Liu *et al.*, 2008), and a modelled volume-dependency of diffusion in the brain (Steinert *et al.*, 2008), NO is able to exert its signalling effects at distant sites. Its versatility and employment in intra and intercellular signalling in different systems within multiple organisms underlies its importance and conservation with evolution.

In mammals, NO's significance in intercellular signalling was discovered when it was characterised as the endothelium-derived relaxing factor, being generated in the endothelium and signalling in the adjacent smooth muscle cells to generate

vasodilation of blood vessels (Furchgott & Zawadzki, 1980; Ignarro *et al.*, 1987; Palmer *et al.*, 1987). The scientists behind this work, Furchgott, Ignarro and Murad received the 1998 Nobel Prize in Physiology or Medicine for investigating the role of nitric oxide in the cardiovascular system.

As 1992's molecule of the year (Koshland, 1992), NO has historically received a lot of scientific interest. In this section I will: explain how NO is synthesised; highlight the importance and breadth of NO signalling in the brain; and describe the pathways by which it can exert its signalling, and their regulation.

1.1.1 NO is synthesised by three NOS enzymes.

NO is synthesised in cells by the nitric oxide synthase (or synthetase) family of enzymes. They are a small family of enzymes of which there are three NOS isoforms, named after the tissues from which they were first cloned: neuronal NOS (nNOS, NOS1)(Bredt *et al.*, 1991); endothelial NOS (eNOS, NOS3)(Marsden *et al.*, 1992; Michel & Lamas, 1992); or induced during an immune response (iNOS, NOS2)(Chartrain *et al.*, 1994)(Figure 1.1.). The enzymes form homodimers where each NOS monomer is a bi-domain enzyme consisting of an N-terminal oxidase and C-terminal reductase with a central calmodulin binding region. To form the dimers each monomer must associate with heme, tetrahydrobiopterin (BH_4) and L-Arginine. The dimerisation brings the N-terminal oxidase of one monomer into close proximity of the C-terminal reductase of the other. To finally permit the catalytical breakdown of L-Arginine to L-citrulline and the production of NO, calmodulin must first bind to its binding region on the enzyme.

As NO cannot be stored, like other cellular messengers, its signalling specificity must be controlled at the level of its synthesis, which means that the enzymes are tightly

regulated. For nNOS and eNOS, calmodulin binding is dependent on intracellular Ca^{2+} activation of the protein, but for iNOS, calmodulin binding is independent of Ca^{2+}. This means that nNOS and eNOS are switched on by increases in intracellular calcium and are said to be constitutively expressed. iNOS is switched on as soon as it is transcribed and assembled, and this is why it is said to be inducible, prototypically this enzyme is induced in macrophages and cells of the immune response, like microglia. There are many good reviews that describe the large body of work done to elucidate the mechanism of action of the NOS enzymes (Nathan & Xie, 1994; Alderton *et al.*, 2001; Vallance & Leiper, 2002; Stuehr, 2004; Stuehr *et al.*, 2004).

Four nNOS (Nos1) isoforms are known to exist, nNOSα,β,γ and μ. The nNOSα isoform has an N-terminus PDZ domain and colocalises with NMDA receptors at the postsynaptic density (Figure 1.1. B), and is the isoform expressed in the MNTB.

As the focus of this thesis is on NO signalling in neuronal cells at a described synapse, and its effect on their excitability via modulation of their natively expressed ion channels, the rest of this section will focus on NO's action in the brain and brain tissue.

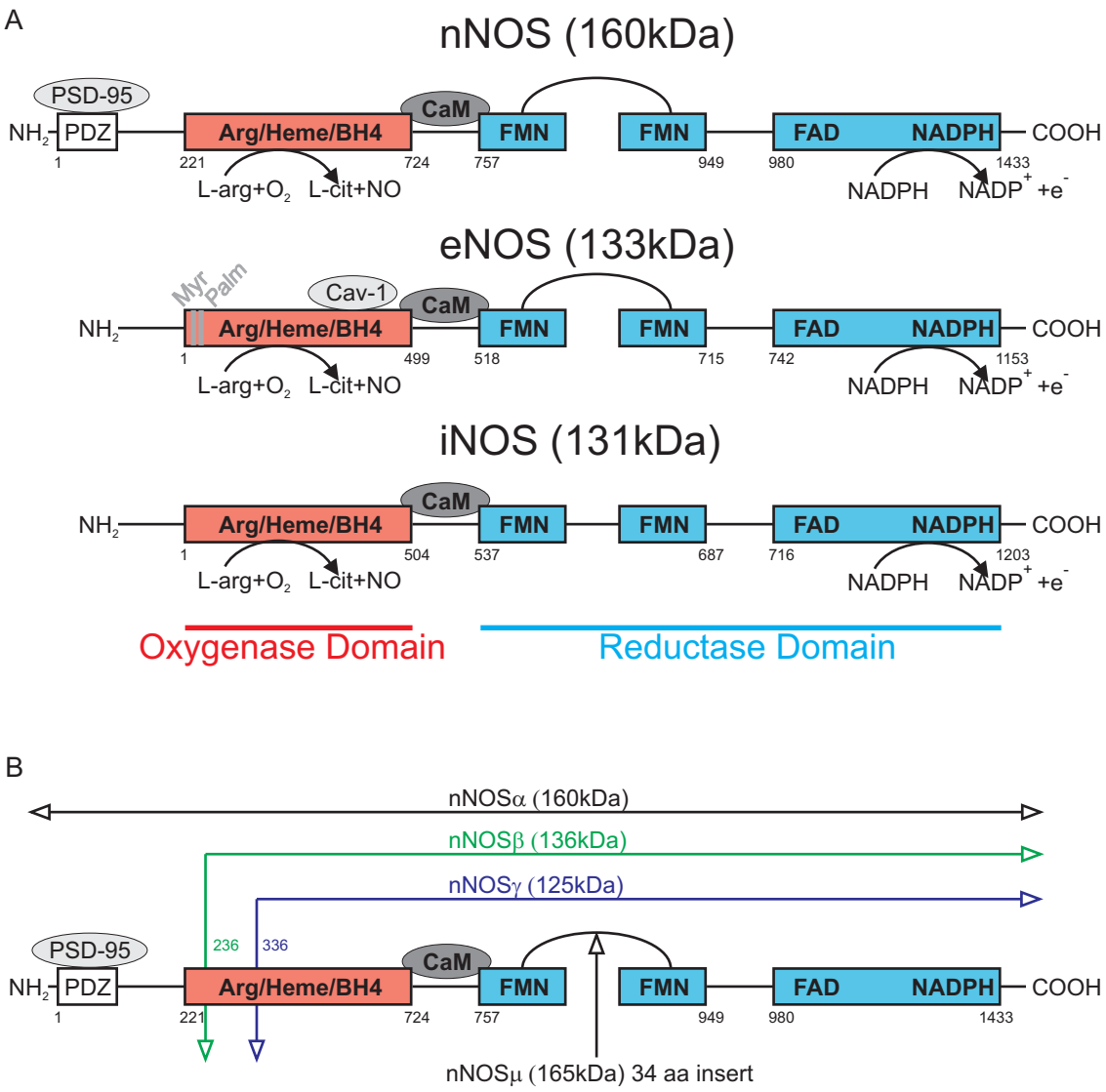

Figure 1.1. NOS structure.
Structure of human nNOS, eNOS and iNOS. **A.** NOS contains N-terminal oxygenase and C-terminal reductase domains that can be separated by a calmodulin binding motif. The reductase domain binds NADPH and has a site for FMN and FAD. The oxygenase domain is the site of L-Arginine binding. It also binds the tetrahydrobiopterin (BH4) and contains the heme-active site. Electrons (e^-) that transfer from the reductase domain to the oxygenase domain via FMN and FAD are donated by NADPH. The caveolin-1 (cav-1) binding site is located at the oxygenase domain. Only nNOS has a PDZ domain, and so can bind to PSD-95 proteins. The different domains are denoted by solid boxes, and the amino acid residue number at the start/end of each domain is shown. Palmitoylation and myristoylation sites of eNOS are shown. **B.** The protein products of the nNOS gene, nNOSα is the only isoform to have a PDZ domain and so colocalise with PSD-95 proteins at postsynaptic densities. (Adapted from Steinert *et al.* 2010).

1.1.2 NO has multiple roles in the brain.

The functional signalling cells of the brain are the neuronal cells, glial cells and cerebrovascular cells. The interplay of these cells in supporting and maintaining brain function is of obvious importance, and the coordination of this interplay would probably need a diffusible intercellular messenger. What better than a gasotransmitter like NO (Mustafa *et al.*, 2009)?

This concept has excited and driven the field for many years (Garthwaite, 2008), and has spawned countless investigations as researchers look to understand NO signalling in the: development, mature function and degeneration of the various different cell types present in the brain, using many different experimental models and animals. For example, research has investigated NO's role and effect: as a regulator of glial cell development in the hippocampus of transgenic nNOS knockout mice (Bechade *et al.*, 2011); as a regulator of cerebrovascular tone in mice (Atochin & Huang, 2011); in inducing synaptic plasticity in rat cerebellum (Jacoby *et al.*, 2001); sustaining long term memory formation in pond snails (Kemenes *et al.*, 2002); and pathology of cell death and neurodegeneration in mouse models (Liberatore *et al.*, 1999).

Most of these examples highlight NO's role as a regulatory molecule in these physiological functions. As I will describe, NO production and diffusion is tightly regulated, so there is regulation of the regulatory gas molecule. Pathological situations are known to arise in the brain in which NO is implicated (Lipton *et al.*, 1994) such as in Alzheimer's Disease (Cho *et al.*, 2009), whether NO is the primary cause or whether loss of regulation of NO leads to the pathology is unknown, especially as NO is also known to be neuroprotective in an Alzheimer's model (Puzzo *et al.*, 2009).

Whilst discussing this breadth of work in detail is beyond the scope of this thesis, it is important to emphasise NO's varied roles and employment in the brain, which are underlined by: a non-uniform expression of NOS enzymes and differential response of cells to NO; combined with the fact that NO is not continuously generated and, when liberated, it is tightly buffered due to its high reactivity with cellular proteins.

What follows is an explanation of the classically acknowledged pathway by which NO is generated and exerts its signalling within neuronal cell types.

1.1.3 NO signalling pathway in neurons and its regulators.

NO's presence in the brain was first speculated by the observation that it activated soluble guanylyl cyclase in brain tissue (Arnold *et al.*, 1977) (Miki *et al.*, 1977), and later proved to be present in brain slices and dependent on NMDAR activation (Garthwaite *et al.*, 1988). Shown to be bound to the same postsynaptic density proteins as NMDARs, the close proximity allows coupling of NMDAR opening to nNOS activation (Wu *et al.*, 1996). Breakdown of L-Arginine (as described above) generates NO which can exert its signalling properties via: a) direct interaction (S-nitrosylation) with cellular proteins via exposed thiol groups (Ahern *et al.*, 2002); or via formation of the peroxynitrite ion ($ONOO^-$) and redox interaction, or b) by activation of the metalloprotein soluble guanylyl cyclase (sGC) and induction of the NO-cGMP pathway. The NOS enzymes can be inhibited by the compound 7-nitroindazole (7-NI), which is the blocker used in this investigation (Figure 1.3).

Termed soluble because it is not membrane bound, sGC exists as a heterodimer in the cytosol of the cell. Consisting of an α and β subunit, the latter containing a heme group, NO is attracted to and binds the ferrous pore (Martin *et al.*, 2012) which causes

a conformational change in the enzyme activating its catalytic domain and initiating the conversion of GTP to cGMP with the production of pyrophosphate (PPi) (Bellamy *et al.*, 2002). The guanylyl cyclases and therefore the NO-cGMP pathway can be disrupted experimentally by addition of the antagonist oxodiazoquinylone (ODQ) (Figure 1.3).

Although levels of cellular cGMP are restricted by phosphodiesterases (PDEs), four molecules of the cyclic nucleotide can activate their dependent protein kinase (PKG) by binding to its regulatory subunits, causing a conformational change. The kinase is then free to exert its phosphorylatory effects within the cell (Figure 1.3.).

At the cellular level, NO signalling which terminates on ion channels and modulates their function, can be observed as changes in neuronal electrical excitability. Using electrophysiological techniques it is possible to measure NO-dependent modulation of the ionic currents that underlie neuronal excitability and neurotransmission.

The Medial Nucleus of the Trapezoid Body (MNTB), a well characterised nucleus in the auditory brainstem, is a good model for electrophysiological investigation of NO modulation of neuronal excitability and synaptic physiology for the reasons I will describe below.

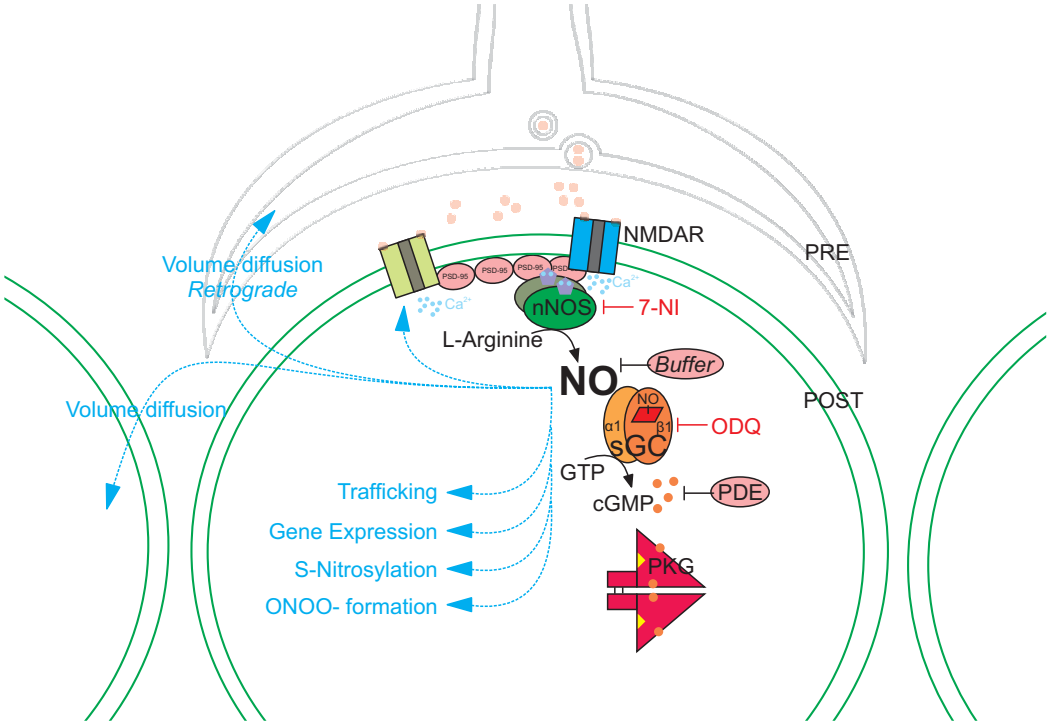

Figure 1.2. Nitric oxide signalling in neurons.
Glutamate activation of NMDA receptors allows Ca^{2+} influx which activates nNOS, producing a molecule of nitric oxide (NO) from the breakdown of L-Arginine to L-Citrulline. NO is a diffusible messenger which can pass through the lipid bilayer to exert its signalling actions at distant sites, in a volume dependent manner. NO can directly interact with exposed thiol groups on cellular proteins by S-Nitrosylation, and can affect gene expression and protein trafficking. It can also form the peroxynitrite ion. The alternative pathway of action is the NO-cGMP pathway, which involves binding to the heme group of soluble Guanylyl Cyclase (sGC) to catalyse the conversion of GTP to cGMP and the activation of its dependent protein kinase (PKG).

1.2 The Medial Nucleus of the Trapezoid Body is a high-fidelity inhibitory relay in the brainstem auditory pathway.

There is immunohistochemical (Steinert *et al.*, 2008) and in situ hybridisation (Fessenden *et al.*, 1999) (Allen atlas) evidence for nNOS expression in the medial nucleus of the trapezoid body (MNTB), where NO is known to modulate cellular excitability via inhibition of the $K_V3.1$ channels (Steinert *et al.*, 2008).

The MNTB is a nucleus of the superior olivary complex (SOC) and forms an inhibitory relay in the brainstem auditory pathway (Figure 1.4.). Sound innervation of the cochlea is transduced into electrical activity by the inner hair cells (IHCs) of the cochlea. The pitch of the sound is encoded by the position of the IHC along the basilar membrane of the cochlea, as high pitch sounds cause membrane resonance and activation of IHCs at the base of the cochlea whereas low frequency waves resonate to the apex. This frequency gradient or tonotopy of IHCs along the basilar membrane is maintained through the auditory brainstem (Kandler *et al.*, 2009). The IHCs depolarise on activation, generating action potentials (APs) in the spiral ganglion cells. The APs are then propagated along the auditory (VIII) nerve to the cochlear nucleus, and the frequency of the AP firing encodes the volume of the sound (Forsythe, 2001).

From the Cochlea, the auditory nerve bifurcates to innervate the dorsal and ventral part of the cochlear nucleus to form the first relay centre in the auditory brainstem. Most importantly for this thesis, innervation of the globular (GBCs) and spherical bushy cells (SBCs) in the antero-ventricular cochlear nucleus (aVCN) is conveyed along glutamatergic fibres which project across the midline of the brainstem to the contralateral SOC. Firing of the GBCs and SBCs is said to be primary-like as it follows

the auditory nerve firing with high fidelity (Forsythe, 2001), due to the large excitatory synaptic inputs converging on the cells to form the end bulbs of Held (Held, 1893; Lin *et al.*, 2011), 1-3 forming on SBCs and up to 4 or 5 forming on GBCs (Cao & Oertel, 2010).

As well as projecting to the contralateral LSO, Figure 1.4. shows axonal projections from the GBCs of the aVCN terminate in the MNTB forming large giant synapses onto the postsynaptic principal neuron soma (Held, 1893). These calyx of Held synapses envelope the postsynaptic neuron like a hand enclosing a fist, with many finger-like fenestrations innervating the postsynaptic soma developing with the onset of hearing (Ford *et al.*, 2009). The MNTB maintains the tonotopic gradient (Sonntag *et al.*, 2009), and is an inhibitory relay centre in the auditory brainstem and the axonal projections from the principal neurons form inhibitory glycinergic terminals in the downstream nuclei of the SOC: medial superior olive (MSO), superior paraolivary nucleus (SPN) and lateral superior olive (LSO) (Banks & Smith, 1992); as well as project to the lateral lemniscus, ventral and lateral trapezoid bodies and ipsilateral cochlea nucleus (Thompson & Schofield, 2000). From here the nuclei project to higher auditory brain centres.

Principal neurons of the MNTB are characterized by their globular or oval cell body which is ~20µm in size containing an eccentric nucleus, and relatively short dendrites, which branch extensively near the cell (Smith *et al.*, 1998). As well as the calyx, the principal neurons also receive a small amount of inhibitory input (Hamann *et al.*, 2003).

Whilst the majority of the experiments in this study were carried out in the MNTB, the SPN or (SPON in rats) was the focus of the experiments described in the second results chapter of this thesis. It is downstream of the MNTB and receives strong inhibitory input from the nucleus during MNTB firing. A high level of activity in the MNTB means a lot of suppression of the SPN. However, as soon as the inhibition is relieved the SPN responds with short latency rebound spiking (Felix *et al.*, 2011; Kopp-Scheinpflug *et al.*, 2011), thought to be important for detecting gaps in sounds (Kadner & Berrebi, 2008). This rebound firing spiking activity is facilitated by expression of a different suite of ion channels compared to the MNTB neurons, as will be explained.

Physiologically the SOC is thought to be important for sound source localisation as it facilitates comparison of intra-aural level differences (sound volume) and intra-aural timing differences (sound latency) between ears, this enables directional sensitivity to sound. This is made possible by the high fidelity firing of the neurons in this binaural auditory pathway, who maintain the pitch encoded at the cochlea as a tonotopic gradient throughout the cochlea nucleus and SOC, and encode volume as firing rate.

Given nNOS's expression in the MNTB, NO's diffusibility, and the known firing properties and function of the MNTB and SPN in audiology, it was interesting to investigate the functional relevance of NO, and how this could affect the ion channels that underlie cellular excitability in these nuclei.

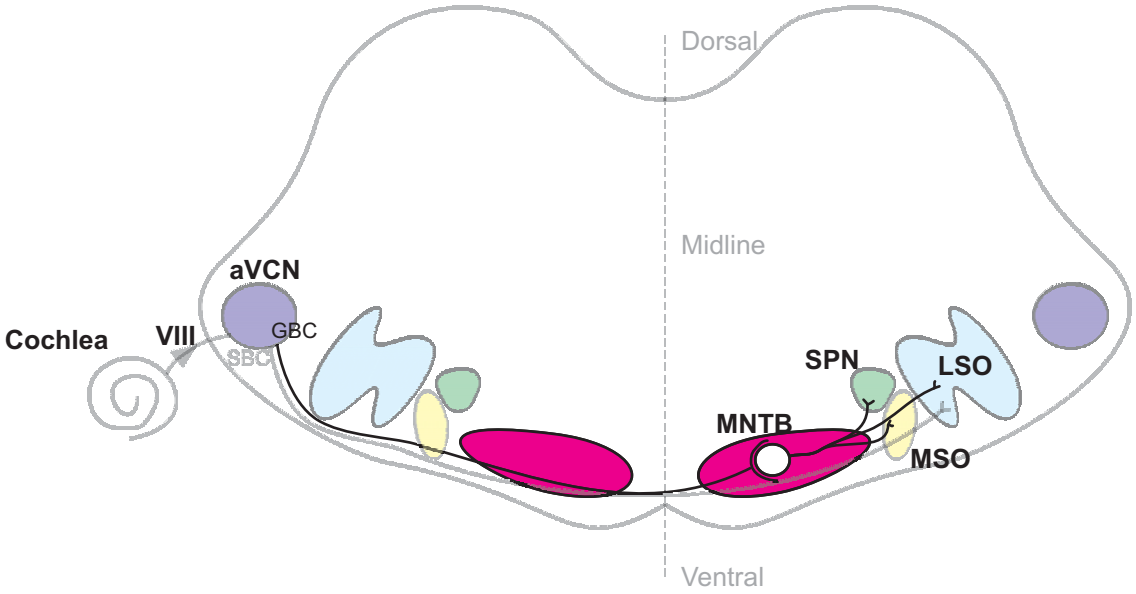

Figure 1.3. The brainstem auditory pathway.
Sound innervation at the cochlea is transduced along the 8th (VIII) nerve to the anteroventricular cochlea nucleus (aVCN). From here spiny bushy cells (SBCs) and globular bushy cells (GBCs) send out large glutamatergic projections across the midline of the brainstem. SBCs project to the contralateral LSO, whereas GBCs project to the medial nucleus of the trapezoid body (MNTB). The terminals in the MNTB form the giant synapses known as the Calyces of Held. These form directly on to the MNTB principal neuron soma. From here the MNTB sends out a glycinergic inhibitory projection to the medial superior olive (MSO),superior paraolivary nucleus (SPN) and lateral superior olive (LSO).

1.3 Ion channel expression governs neuronal excitability and neurotransmission.

Ion channels are pore-forming proteins that allow movement of ions across the lipid membrane bilayer.

Without the discrete expression of ion channels in the membranes of neurons of the auditory brainstem pathway, the nuclei would not be able to fulfil their roles in sound source localisation. The different firing properties and behavioural responses of the neurons to depolarisation and hyperpolarisation are completely dependent on the ion channels and ionic pumps/transporters that exist in the membrane of the excitable cells (Hille, 2001).

Ion channels generally show selectivity for an ion species and facilitate the movement of the ion through the pore by lining it with hydrophilic residues, known as the waters of hydration, passively allowing the charged species to move through and down their electrochemical gradient (Hille, 2001). The opening of the channels and hence ionic conductance is normally regulated by: membrane voltage, ligand binding, mechanical stress, pH or intracellular messengers like G-proteins, although there are some channels that do not exhibit such regulation.

Transporters and pumps are different to ion channels in that they do not have pores, and so have to undergo conformational changes to move ions across the membranes, meaning ionic movement is not as rapid as through channels. This can be against the electrochemical gradient of the ion, requiring either metabolic energy, ATP (Na^+/K^+ ATPase) or the electrochemical gradient of another ion species (Na^+/Ca^{2+} exchanger).

There are different families and subfamilies of ion channels which I will discuss, with particular focus on the voltage-dependent calcium channel family (Ca_V) and the small conductance calcium activated channel (SK) family, as my research particularly focussed on these.

1.3.1 Ligand-gated ion channels.

Ligand-gated channels open in response to ligand binding. These channels mediate fast synaptic transmission in response to specific neurotransmitters such as, glutamate, glycine, γ-amino butyric acid (GABA), ATP, cyclic nucleotides, acetylcholine, and serotonin (5-HT). In addition to the number of different ligands there is also a structural heterogeneity between the channel families. A functional channel is an assembly of poreforming subunit proteins, and: ATP-sensitive P2X receptors are known to have 3 subunits (Jiang *et al.*, 2003); glutamate receptors, such as N-methyl D-aspartate (NMDA) (Cull-Candy *et al.*, 2001), 2-amino-3-(5-methyl-3-oxo-1,2- oxazol-4-yl)propanoic acid (AMPA) (Lu *et al.*, 2009) and kainate receptors (Mulle *et al.*, 2000) have 4 subunits; and GABA (Sigel *et al.*, 1990) and nicotinic acetyl choline receptors have 5-subunits (McGehee & Role, 1995).

AMPA receptors are hetero-tetrameric assemblies of four GluA1-4 subunits which can conduct Na^+, Ca^{2+} and K^+ on activation, although only GluA2 lacking channels conduct Ca^{2+}. In the MNTB the calyx of Held is a glutamatergic synapse, and NMDA and AMPA receptor currents underlie the large excitatory postsynaptic currents (~10nA) generated on pre-synaptic release (Forsythe & Barnes-Davies, 1993). The receptors rapidly open and desensitise, eliciting fast, large conductance depolarising currents

(Postlethwaite *et al.*, 2007). Experimentally kainate and AMPA receptors can be blocked by the quinoxalinedione drug family, such as CNQX (Honore *et al.*, 1988).

NMDARs are dimer-dimers of GluN1-3 subunits. Glycine and glutamate binding activates the channel, but the channel pore is susceptible to Mg^{2+} block, and an ion can sit in the pore of the channels. Depolarisation removes Mg^{2+} block, and depolarisation in the presence of glycine and glutamate will activate the channel allowing Na^{+}, Ca^{2+} and K^{+} current flow. Because of this, NMDARs are considered to be coincidence detectors of pre and post synaptic activity (Malenka & Nicoll, 1999). The influx of Ca^{2+} can activate downstream signalling molecules, in the MNTB this can induce activation of nNOS, in the hippocampus this can induce mechanisms of synaptic plasticity via activation of CamKII (Bliss & Collingridge, 1993; Malenka & Nicoll, 1999; Thalhammer *et al.*, 2006). In the MNTB, NMDA current amplitude reduces with development in the mouse, correlating with a reduction in channel expression (Steinert *et al.*, 2011a) (Selvaskandan *in preparation*).

Experimentally NMDARs can be blocked by the uncompetitive inhibitor MK-801 (Wong *et al.*, 1986) and the competitive inhibitor D-AP5 (Olverman *et al.*, 1984).

1.3.2 Voltage-gated Sodium channels (Na_V)

Sixty years ago Na_V channels were shown to underlie the initiation and upstroke of the action potential in the squid giant axon (Hodgkin *et al.*, 1952). Since then Na_V channels have also been shown to be necessary for action potential generation in mammalian neurons (Llinas, 1988; Hille, 2001). Na_V channels are fast activating fast inactivating sodium conducting channels that open at ~-40mV (Bendahhou *et al.*, 1999). They consist of a pore-forming α subunit made up of ~2000 amino acids arranged into 4

homologous domains of six transmembrane (TM) spanning segments which conveys the ion selectivity and voltage sensitivity of the channel (Catterall, 2012), and when expressed by themselves the α subunits can form functional sodium channels (Goldin *et al.*, 1986; Noda *et al.*, 1986a ; Noda *et al.*, 1986b). There are 10 genes that encode the alpha subunits named $Na_V1.1$- Na_x. $Na_V1.1$-1.9 are known voltage-gated sodium channel subunits, whereas the Na_x subunits form atypical sodium channel-like proteins with greater than 50% homology to the Na_V1 family (Catterall, 2012).

$Na_V1.1$, $Na_V1.2$, $Na_V1.3$ and $Na_V1.6$ are the primary sodium channels in the central nervous system (Catterall *et al.*, 2003). Two β subunits also associate with the alpha subunit and there are four known members of this family (Na_Vβ1-4) (Isom *et al.*, 1992; Isom *et al.*, 1994). The auxiliary subunits are necessary for correct cellular localisation (Brackenbury *et al.*, 2010), but have also been shown to regulate A-type potassium channels (Marionneau *et al.*, 2012). The latter evidence for interaction between protein and signalling domains of different ion channel families has been seen in other instances, such as between K_V and Ca_V channels (Anderson *et al.*, 2011).

Na_V channels are blocked by low concentrations of tetrodotoxin (TTx), which is a pore blocker of the sodium channels (Hille, 1968). They can also be blocked by the synthetic compound Qx314, but this has been shown not to be a specific blocker (Mulle *et al.*, 1985).

In the MNTB principal neurons $Na_V1.1$ channels are present in neonatal mice and increase in channel density up to the onset of hearing at P11 (Ming & Wang, 2003 ; Leao *et al.*, 2006b) . In the calyx, Na_V channels are restricted to the large heminode, meaning APs do not actively invade the terminal, but do so passively (Leao *et al.*,

2005a). As well as fast-gated channels there is also a persistent current that contributes to presynaptic activity, and may underlie part of the afterdepolarisation seen following presynaptic APs (Huang & Trussell, 2008).

1.3.3 Voltage-gated potassium channels (K_V)

Voltage-gated potassium channels conduct potassium ions out of the cell in response to membrane depolarisation and underlie the delayed rectification of the AP (Hodgkin *et al.*, 1952). They are the largest and most diverse family of voltage-gated ion channels with over 40 known subunit genes in the mammalian genome, divided into twelve subfamilies, K_V1-12 (Coetzee *et al.*, 1999 ; Gutman *et al.*, 2005). Their expression is necessary in all excitable cells.

A functional channel usually consists of four six transmembrane (TM) spanning α subunits from the same subfamily which associate to form the channel pore. This is in contrast to the single pore-forming α subunit of Na_V channels (described above, Figure 1.5. A.). The assembly of the proteins in the channel determines its functional properties, such as voltage dependence, channels are low-voltage-activated (LVA) or high-voltage-activated (HVA), or gating kinetics, e.g. fast or slow time course of activation/inactivation. Given the large number of subunit genes it is easy to see how heteromeric assembly of the channels can generate currents with very different properties. These heterotetrameric channels can associate with β subunits which are known to modulate channel gating (Rettig *et al.*, 1994).

In the MNTB, LVA K_V1 and HVA K_V3 channels are expressed and are known to control cellular excitability contributing to the rapid single AP firing phenotype of the principal neurons (Brew & Forsythe, 1995). K_V2 channels are known to be expressed in these

neurons and restricted to the axon initial segment (Johnston *et al.*, 2008b). Their activity is upregulated following prolonged exposure to NO (Steinert *et al.*, 2011b). K_V4 channels which mediate A-type current (Johnston *et al.*, 2008a) are also expressed in MNTB neurons, as is another fast activating LVA channel, the *ether-à-go-go* related gene (ERG) channel (Hardman & Forsythe, 2009).

Presynaptically at the calyx of Held, $K_V1.1$, 1.2 and K_V3 are expressed and control excitability and AP waveform, which gets faster with the onset of hearing (Wang *et al.*, 1998; Elezgarai *et al.*, 2003; Ishikawa *et al.*, 2003 ; Dodson & Forsythe, 2004). The LVA channels act to restrict excitability and prevent firing on the depolarising afterpotential (Ishikawa *et al.*, 2003). K_V1 knockout mice show a loss in temporal fidelity at this synapse *in vivo* (Kopp-Scheinpflug *et al.*, 2003). K_V7 channels which underlie the M-current have also been shown to be expressed in the calyx (Garcia-Pino *et al.*, 2010), and are open at resting membrane potential, restricting depolarisation and release at the terminal (Huang & Trussell, 2011).

The rich variety of K_V expression underlies the distinct firing phenotype of the MNTB, where the principal neurons fire a single input-specific rapid AP (0.25ms) on depolarisation (Dodson & Forsythe, 2004). This enables fast input-specific responses to depolarisation, facilitating high frequency following at this relay (Wang *et al.*, 1998).

A multitude of pharmacological agents can be used to block the different K_V channels expressed in the MNTB, but most are sensitive to high concentrations (5mM+) of the quaternary amine cation pore blocker tetraethylammonium (TEA)(Armstrong, 1969; Stanfield, 1970), and K_V3 channels are sensitive to this compound at lower concentrations (1-3mM) (Wang *et al.*, 1998).

1.3.4 Cyclic nucleotide-gated potassium channels.

Similar in structure to potassium channels, the hyperpolarisation activated cyclic nucleotide-gatedcyclic nucleotide-gated (HCN) channels conduct both K^+ and Na^+ ions on opening, although 5x more K^+ is conducted than sodium. The channels activate at potentials more negative than -70mV, but cAMP or cGMP (or even cCMP, (Zong *et al.*, 2012)) binding to intracellular C-terminal domains can shift their activation to the right (Wahl-Schott & Biel, 2009). Four genes encode the HCN family, HCN1-4, and these can assemble as heterotetramers (Biel *et al.*, 2009).

HCN channels are differentially expressed in the auditory brainstem (Leao *et al.*, 2006a). HCN2 and HCN4 channels are present in MNTB principal neurons (Koch *et al.*, 2004 ; Leao *et al.*, 2006a), and I_h is known to be modulated by cAMP here (Banks *et al.*, 1993). In the calyx, I_h contributes to maintaining membrane potential (Cuttle *et al.*, 2001) and may prevent temporal summation during high frequency firing (Leao *et al.*, 2005b). In the SPN, a nucleus downstream of the MNTB, HCN1 and 2 channels are expressed and mediate a large I_h (Kopp-Scheinpflug *et al.*, 2011).

Experimentally, I_h can be blocked by the compound ZD 7288 at low micromolar concentrations (BoSmith *et al.*, 1993).

1.3.5 Calcium dependent potassium channels (K_{Ca})

The K_{Ca} family consists of the large conductance (BK, $K_{Ca}1.1$), intermediate conductance (IK, $K_{Ca}3.1$), small conductance (SK1-3, $K_{Ca}2.1$, 2.2, 2.3) calcium dependent potassium channels, and also confusingly the sodium dependent potassium channels (slack, slick and slo 3) (Coetzee *et al.*, 1999).

Like K_V channels, K_{Ca} channels are tetrameric assemblies of four 6-TM subunits with intracellular N and C-termini which assemble to form a functional channel. The difference being that they are gated by intracellular Ca^{2+} levels.

BK channels are voltage-dependent potassium channels whose open probability increases in response to intracellular Ca^{2+}, when it binds to the C-terminal calcium binding domains (CBDs) of the α subunits (Cui *et al.*, 1997). They have large single channel conductances and are sensitive to low concentrations of TEA (Coetzee *et al.*, 1999), and also to the specific blocker Iberiotoxin (Galvez *et al.*, 1990). The channels are recruited during high levels of AP firing activity and their activation leads to a broadening of the AP waveform, and generates the fast initial phase of the after hyperpolarisation (fAHP) following this activity (Shao *et al.*, 1999; Faber & Sah, 2003).

IK and SK (Figure 1.4. A.) channels are not voltage-dependent and do not have CBD domains, instead each subunit monomer has a constitutively bound molecule of calmodulin (Xia *et al.*, 1998). Ca^{2+} binding causes a conformational change in the molecule and facilitates opening of the channel. IK and SK have intermediate and small single channel K^+ conductances respectively, but are more sensitive to changes in intracellular Ca^{2+} than BK channels.

IK was originally cloned from pancreatic cells (Ishii *et al.*, 1997) and evidence for IK in the CNS is only just emerging, but it has recently been implicated in restricting synaptic input summation in the cerebellum in association with LVA T-type Ca_V channels (Engbers *et al.*, 2012), and also seems to have a role in AP propagation at the Nodes of Ranvier in pukinje cell axons (Clark, *oral communication at Physoc 2012*). IK channels can be blocked by the synthetic compound TRAM-34 (Jensen *et al.*, 2002).

SK current is known to have a wide expression in the CNS and to have many roles within these neurons (Faber & Sah, 2007). As well as having a molecule of calmodulin associate with the intracellular domain immediate to the 6th transmembrane segment, they also have a constitutively bound casein kinase (CK2) and protein phosphatase (PP2A) (Figure 1.4. B). CK2 is associated with the pore-forming subunits, but phosphorylates the calmodulin molecule at a known residue (threonine 80), but only when the channel is in its closed state, and this reduces Ca^{2+} sensitivity. PP2A is associated with the channels subunits at a site C-terminal to the calmodulin, and acts to dephosphorylate calmodulin, increasing Ca^{2+} sensitivity but only when the channel is in its open state (Allen *et al.*, 2007).

In addition to this multi component assembly of the channel, there are known phosphorylation sites on the channel subunits (Kohler *et al.*, 1996). These are important for cellular expression, as phosphorylation reduces SK trafficking and membrane expression in the amygdala (Faber *et al.*, 2005) and also in the hippocampus (Lin *et al.*, 2010), which facilitates induction of long term potentiation (LTP).

In the hippocampus, SK channels sit in the postsynaptic membrane and restrict depolarisation induced relief of Mg^{2+} block of the NMDARs (Ngo-Anh *et al.*, 2005). If depolarisation overcomes Mg^{2+} block, Ca^{2+} activation of CamKII (a kinase) leads to increased expression of AMPARs and decreased expression of SK channels, facilitating a potentiated response to a synaptic input, and this is LTP. Blocking SK channels in hippocampal neurons can mimic this effect, inducing LTP (Behnisch & Reymann, 1998; Norris *et al.*, 1998). More physiologically, it has been shown that activation of the M_1

muscarinic receptor can lead to inhibition of SK channels and induction of LTP in these neurons by theta burst protocols (Buchanan *et al.*, 2011).

By being closely associated with NMDARs, SK channels are important for synaptic plasticity in the CNS. However, SK channels are also important in regulating intrinsic neuronal excitability, and have been implicated in the intermediate phase of the AHP following burst of cellular firing and activity (Adelman *et al.*, 2011). The source of Ca^{2+} does not seem to be that relevant as SK channels have been shown to be activated following Ca^{2+} release from internal stores (Seutin *et al.*, 2000), or by close association with different Ca_V subtypes (Kohler *et al.*, 1996; Marrion & Tavalin, 1998). Tight or lose coupling of SK channels to sources of Ca^{2+} may enable the cell to tone its response to Ca^{2+} influx and membrane excitability (Fakler & Adelman, 2008). And restriction of SK channels to different cellular compartments can facilitate further toning of these responses (Bowden *et al.*, 2001; Ohtsuki *et al.*, 2012).

Pharmacologically low concentrations of the selective antagonist apamin (100nM) (Kohler *et al.*, 1996) can block SK channels, modulating cellular excitability, most notably by reducing the amplitude of the intermediate portion of the AHP. Alternatively, SK channel activation can be enhanced by the agonist 1-EBIO or CyPPA.

It has been shown in snail neurons that nitric oxide can modulate neuronal firing activity, causing a burst of activity before silencing the neuron via SK and BK channels (Artinian *et al.*, 2010). In mammals NO has been shown to activate BK channels by S-nitrosylation (Ahern *et al.*, 1999), but no relationship or direct link between NO and SK channels has been shown.

The role of K_{Ca} in synaptic physiology has mainly been shown postsynaptically in the hippocampus and amygdala, but there is evidence for K_{Ca} expression pre-synaptically in the CNS. SK channels are expressed in the vestibular calyx of the gerbil, and shown to contribute to AHPs in these terminals, but whether or not they modulated vesicular release was not investigated (Meredith *et al.*, 2011). Pre-synaptic terminals in the CA3 hippocampal region are known to express BK channels, but their role in spike broadening did not influence synaptic release at these synapses (Hu *et al.*, 2001). BK channels are also expressed and well characterised in the calyx of the chick ciliary ganglion, but their effect on synaptic release is not known (Sun *et al.*, 1999). In the Neurohypophyseal terminals of the pituitary, BK channels are expressed and contribute to cellular activity, but their involvement in release has only been theorised (Ahern *et al.*, 1999).

In the MNTB, BK channels are known to exist in the calyx of Held (Nakamura & Takahashi, 2007), but again their role in synaptic release has not been characterised. No evidence for IK or SK channels in the calyx or principal neurons of the MNTB has been reported.

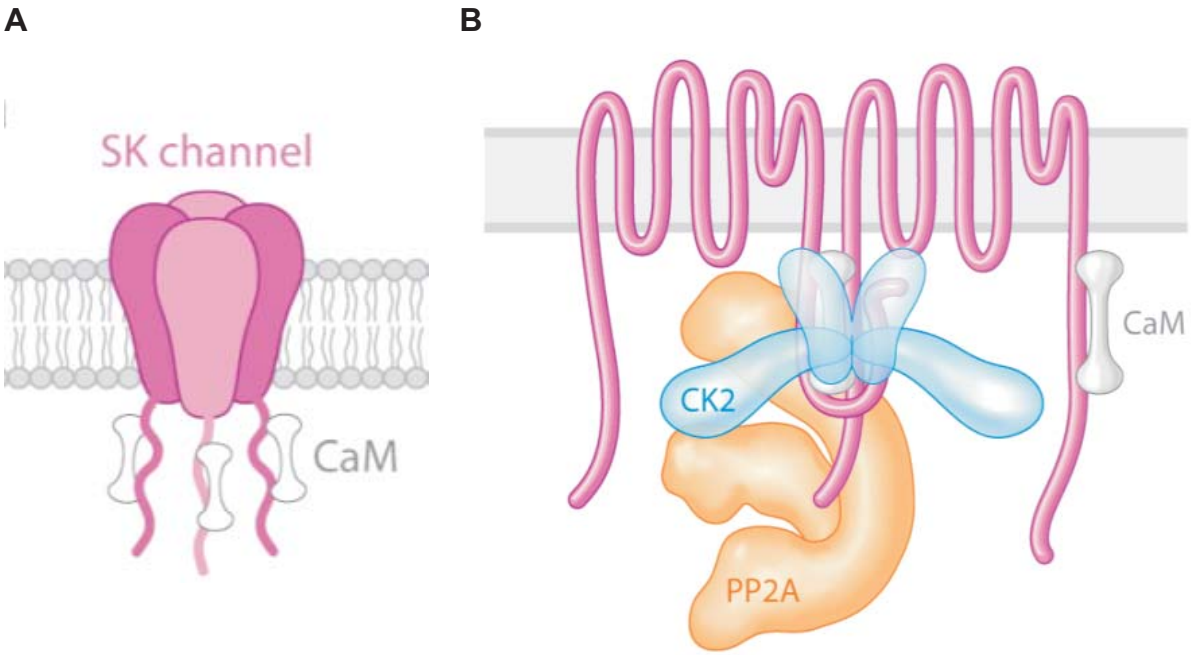

Figure 1.4. SK channels are gated by constitutively bound calmodulin.
A. A representative diagram of an SK channel. The four pore-forming subunits are shown in pink with each of their intracellular C-terminal tails associated with a molecule of calmodulin (CaM). **B.** An enlargement of two of the subunits, showing the assemblage of the modifying casein kinase 2 (CK2) protein and protein phosphorylase 2A (PP2A), which also associate with the channel. Adapted from Adelman *et al.* 2012.

1.3.6 Voltage-gated calcium channels (Ca_V)

Voltage-gated calcium channels (Ca_V) are the third member of the voltage-gated ion channel superfamily. They allow calcium influx into the cell in response to membrane depolarisation, which effectively links the cell's internal environment to its membrane excitability (Hille, 2001). The ensuing influx of Ca^{2+} gives rise to a multitude of cellular functions such as: gene transcription (Dolmetsch *et al.*, 2001; Gomez-Ospina *et al.*, 2006; Ma *et al.*, 2011), calcium release from internal stores (Tully & Treistman, 2004), excitation contraction coupling in the heart (Fozzard, 1991), and secretion and neurotransmitter release in neurons (Wheeler *et al.*, 1995).

1.3.6.1 Ca_V channels are composed of multiple subunits.

The channels are a multimeric assembly of subunits (Figure 1.5. B), the α_1 subunit is the pore-forming subunit, containing the voltage-sensitive domains and gating apparatus. It is also the subunit to which most blockers and second messenger substances interact, facilitating regulatory control over the channel. Four homologous six transmembrane (TM) spanning domains (I-V) make up the α_1 subunit (Figure 1.5. C), the 4^{th} TM segment of each domain confers the voltage-sensing apparatus, and the pore forming loop between TM domains 5 and 6 confers the ionic selectivity and Ca^{2+} conductance. Each of the four homologous domains is similar in structure to one α subunit of K_v channels, and the α_1 subunit as a whole is homologous to the α-subunit of Na_v channels, and three amino-acid changes in the pore-loop regions of domains I, III and IV will alter channel selectivity from Ca^{2+} to Na^+ (Catterall *et al.* 2005) (Figure 1.5. A).

Ca_V channels can be grouped according to their voltage activation characteristics, either high-voltage-activated (HVA), activating at potentials more positive than -40mV or low-voltage-activated (LVA), activating at potentials more positive than -80mV (Fox *et al.*, 1987; Bean, 1989). HVA channels are known to associate with the auxiliary $\alpha_2\delta$ and β subunits, where as LVA subunits do not need to associate with auxiliary subunits to form a function channel, but expression systems have shown that coexpression with the subunits improves current density (Isom *et al.*, 1994) (Figure 1.5 .C).

Four genes encode the $\alpha_2\delta$1-4 subunit proteins, Cacna2d1-4 (Davies *et al.*, 2007). These proteins sit extracellularly, held in the membrane by the partially membrane spanning δ-subunit, and are essential for membrane expression. Together with β-subunits they aid trafficking of the α_1 protein from the ER to the membrane, but most importantly are involved in locating Ca_V channels to the correct cellular compartments. $\alpha_2\delta$ mRNA has been shown to have a differential distribution in the CNS, with $\alpha_2\delta$3 showing strongest expression in the auditory brainstem (Cole *et al.*, 2005). In neurons $\alpha_2\delta$2 is needed for membrane targeting of Ca_V2.1 channels in the cerebellum (Davies *et al.*, 2006), $\alpha_2\delta$1 targets Ca_V2.1 to presynaptic active zones in the hippocampus (Hoppa *et al.*, 2012). Interestingly, overexpression of $\alpha_2\delta$ increases vesicular release at hippocampal synapses independently of increased Ca_V2.1 expression (Hoppa *et al.*, 2012), suggesting a role for the subunit in mechanisms of synaptic release.

There are four genes, Cacnb1-4, that encode the β1-4subunits and their splice variants (Buraei & Yang, 2010) which associate intracellularly with the α_1 subunit via the alpha subunit interaction domain (AID) between TM1 and 2. β subunits are known to facilitate cellular trafficking of the channel, promoting release from the ER (Bichet *et*

al., 2000) and preventing proteasomal degradation of the channel (Waithe *et al.*, 2011), and also to directly interact (Van Petegem *et al.*, 2004) and modulate channel gating and activation (Walker *et al.*, 1999).

In skeletal muscle, but not in neurons (Ahlijanian *et al.*, 1990), a γ subunit associates with the complex, and this is similar in structure to the stargazing proteins found to modulate AMPA receptors (Letts *et al.*, 1998).

1.3.6.2 Ca_V subunits confer multiple sites for channel modulation.

Ca_V channels and their associated subunits confer multiple sites for channel modulation and interaction with regulatory proteins. L-type currents in the cerebellum are potentiated by mGluR activation leading to increase Ca^{2+} release from internal stores, which then inhibits L-type channels (Chavis *et al.*, 1996). G-protein βγ subunits modulate Ca_V channels by precluding their inhibition by noradrenergic pathways in sympathetic neurons (Herlitze *et al.*, 1996), and this modulation is mediated via the Ca_Vβ subunit (Buraei & Yang, 2010).

Ca_V channels are also modulated by direct phosphorylation by protein kinase A (PKA) and protein kinase C (PKC), and this can interfere with G-protein regulation of the channels (Zamponi *et al.*, 1997). Ca_Vs are also modulated by calmodulin, which facilitates the calcium induced changes in channel kinetics (Peterson *et al.*, 1999).

Nitric oxide is known to modulate Ca_V channels in the CNS and the vasculature, but with contrasting effects in different signalling systems, as will be discussed in the following chapters of this thesis.

1.3.6.3 Experimentally, Ca_V channels can be separated by their pharmacological sensitivities and voltage dependence.

The channels can be further separated by their pharmacology, in addition to their α_1 subunit relatedness (Ertel *et al.*, 2000), such that L-type channels are sensitive to dihydropyridine block (e.g. nifedipine, 10μM) and make up the Ca_V1 family, which has four members: Ca_V1-4. The Ca_V2 family of channels, made up of P/Q-type ($Ca_V2.1$), N-type ($Ca_V2.2$) and R-type ($Ca_V2.3$) are insensitive to dihydropyridine block, but are selectively blocked by peptide toxins. P and Q-type channels are splice variants of the same gene (Bourinet *et al.*, 1999) and can be separated pharmacologically by their sensitivity to low concentrations of ω-agatoxinIVA (Mintz *et al.*, 1992), as shown in cerebellar granule neurons, P-type channels were blocked with an EC_{50} concentration of 1-3nM and Q-type with an $EC_{50}$of ~90nM (Randall & Tsien, 1995). N-type channels are inhibited by the cone snail toxin derivative ω-conotoxin GVIA (2μM) (Boland *et al.*, 1994), and R-type channels are somewhat inhibited by the synthetic peptide SNX-482 (Newcomb *et al.*, 1998). The low-voltage-activated T-type channels, which make up the Ca_V3 family ($Ca_V3.1$-3) show the least relatedness in α_1 subunit sequence homology. T-type channels are sensitive to dihydropyridine block, but can be separated by their sensitivity to low concentrations of mibefradil (2μM) (Martin *et al.*, 2000) or to NNC 55-0396 (Huang *et al.*, 2004).

It was by exploiting their pharmacological and voltage sensitivities using voltage clamp techniques that physiologists confirmed the presence of different Ca_V channels in neurons (Nowycky *et al.*, 1985; Fox *et al.*, 1987), determined the role of these channels in different cells, and the importance of their targeted expression to neuronal function

(Catterall, 2012). In the hippocampus, N-type and Q-type (a splice variant of P-type channels) channels were shown to underlie presynaptic release between CA3 and CA1 regions based on the sensitivity of postsynaptic potential to ω-conotoxin GVIA and low concentrations of ω-agatoxin IVA (30nM) (Wheeler *et al.*, 1994). L-type channels are known to contribute to synaptic integration and to couple excitation to gene transcription (Ma *et al.*, 2011), as blocking them with dihidropyridines prevents these processes. T and R-type channels are important for synaptic integration and oscillatory activity, and are known to be expressed at postsynaptic regions in dendrites (Catterall *et al.*, 2005).

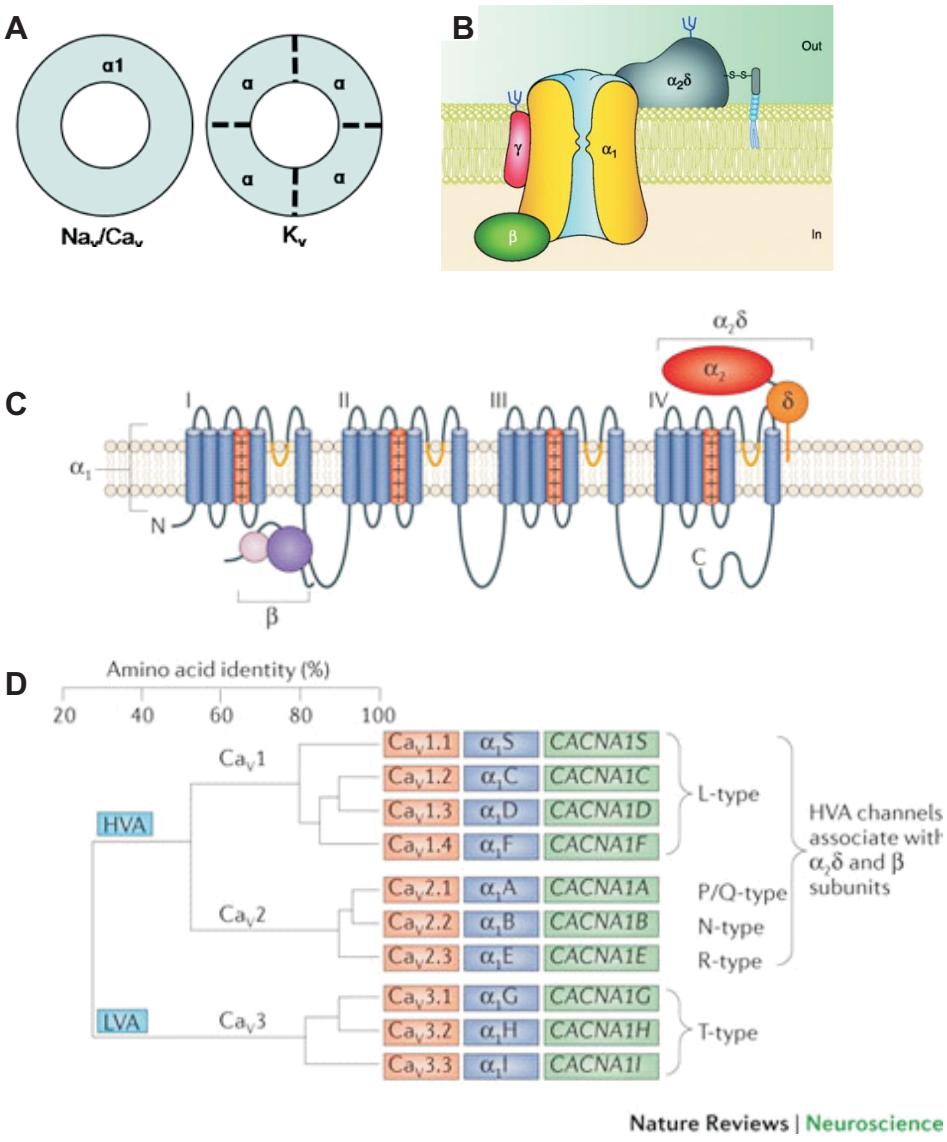

Figure 1.5. Ca$_v$ channels are multimeric assemblies.
A. Na$_v$ and Ca$_v$ channels have single poreforming α/α$_1$subunits respectively. K$_v$ channels are made up of four α homo/heteromeric subunits. **B.** A cartoon of the functional channel assembly (taken from Buraei and Yang 2010). **C.** The different subunits that assemble to form a functional Ca$_v$ channel. The α$_1$ subunit is composed of four segments of 6TM spanning region with the pore-forming loops between TM5 and TM6, and the voltage sensitive residues in TM4. The α$_2$δ subunit is composed of the extracellular α$_2$ protein (red) disulphide bonded to the membrane anchored δ subunit (orange). The β subunit is composed of a Src homology domain (pink) and guanylate kinase (GK) domain (purple), and assembles with the α$_1$ subunit via GK at the alpha subunit interaction domain (AID) between segment 1 and 2, no γ subunit associates with neuronal Ca$_v$s. **D.** Clustal analysis of the α1 subunit shows the genetic relatedness of the different channel families: Ca$_v$1 family makes up the L-type channels; Ca$_v$2.1 the P/Q-type, Ca$_v$2.2 the N-type, Ca$_v$2.3 the R-type; and Ca$_v$3 the T-type channels (taken from Dolphin 2012).

1.3.6.4 A suite of HVA Ca_V channels are expressed in the MNTB

The somas of the globular bushy cells (GBCs) of the aVCN express LVA T-type channels as well as HVA Ca_Vs (Doughty *et al.*, 1998), whereas the mature calyx of Held terminal only expresses P/Q-type channels (Forsythe, 1994; Iwasaki & Takahashi, 1998).

Presynaptic Ca_V expression in the rat calyx of Held changes with development from N and P/Q-type to solely P/Q type following the onset of hearing at P10 (Iwasaki & Takahashi, 1998). The P-type channels are closely associated with docked vesicles in the active zones (Wadel *et al.*, 2007) and facilitate efficient and fast release at this synapse (Inchauspe *et al.*, 2007), but interestingly are functionally compensated for by N-type channels in a P-type knock out model (Inchauspe *et al.*, 2004).

In Rat MNTB principal neurons, four HVA Ca_V subtypes, L, P/Q, N and R, are known to be expressed (Barnes-Davies *et al.*, 2001). Each has a different contribution to the whole cell I_{Ca}, such that L-type contribution is negligible, and most of the voltage-gated Ca^{2+} entry is through P/Q (60%), N (30%) and R-type (30%). In mice this relationship is different, with a bigger contribution of L-type (15%), and P/Q, N and R-type (30±5%) (Leao *et al.*, 2004), suggesting a species difference in Ca_V expression.

1.3.6.5 $Ca_V2.1$ and Ca^{2+} influx underlies plasticity at the calyx of Held.

The calyx is specialised for its role as an auditory relay pathway by its ion channel expression but also by its morphological properties. In the mature calyx there is a greater degree of fenestration (Ford *et al.*, 2009), allowing better access for glial cells to the synapse to mop up excess glutamate, and contribute to signalling at the synapse

(Reyes-Haro *et al.*, 2010; Uwechue *et al.*, 2012). There are also bouton-like varicosities along the filopodia, and clustering of mitochondria and surrounding vesicles into doughnut like domains (Wimmer *et al.*, 2006), and these domains are full of active zones, regions where vesicles cluster and are docked for release, which get smaller but greater in numbers in the adult calyx.

The calyx does not exhibit long term plasticity changes, unlike other model synapses in the CNS, such as LTP in the hippocampus (Bliss & Collingridge, 1993). However, the calyx does exhibit short term plasticity changes, such as short term depression, short term potentiation and post tetanic potentiation, similar to other synapses.

Short term depression can be caused by depletion of the vesicles in the readily releasable pool, usually due to high frequency firing (Wu & Borst, 1999), Ca^{2+} dependent inactivation of P/Q-type calcium channels (Forsythe *et al.*, 1998), again during high frequency activity, and postsynaptic receptor desensitisation (Wong *et al.*, 2003).

Short term potentiation is a form of potentiation of the response to presynaptic input that lasts for up to a few hundred milliseconds (Zucker & Regehr, 2002), and is generated by an increase in residual Ca^{2+} following an AP. If the residual Ca^{2+} is not buffered, then the Ca^{2+} influx caused by the following AP will be additive and the release response potentiated (Zucker & Regehr, 2002; Awatramani *et al.*, 2005). Experimentally this type of facilitation can be observed as paired-pulse facilitation where the second response of the pair is greater than the first owing to the priming effect of the residual Ca^{2+} (Cuttle *et al.*, 1998). At frequencies greater than 500Hz, calmodulin has a potentiating effect before its inhibitory effect (Nakamura *et al.*, 2008)

suggesting that a modulation of the channel as well the Ca^{2+}influx may be necessary for paired-pulse facilitation. During a tetanus a large increase in $[Ca^{2+}]_i$ occurs, and this is buffered either by parvalbumin or sequestered by mitochondria (Billups & Forsythe, 2002). If the parvalbumin is saturated and the mitochondria slowly release the Ca^{2+} back into the terminal then the facilitated response lasts longer and is said to be post tetanic potentiation (Habets & Borst, 2005).

Synaptic release at a synapse is a product of the number of readily releasable vesicles (RRV) and the average probability that they will be released from the terminal (R_{Prob}), determined by Ca^{2+} influx and activation of the synaptic machinery. Synaptic strength is a measure of how much vesicular release is observed from the terminal per AP. If you have a large RRV and a high R_{Prob} then you would have a large amount of release per the first AP. However, you would quickly deplete your pool of readily releasable vesicles and depress your synapse with further incoming APs. The MNTB overcomes this by having a large RRV with a low average release probability. This is achieved by having an RRV of between 700 and 5000 vesicles (Schneggenburger *et al.*, 1999; Borst & Soria van Hoeve, 2011), but by having a heterogenous R_{Prob} between active zones. This was thought to be determined by the proximity of the vesicles to the Ca_V channels, Ca^{2+} influx through which determines release (Wadel *et al.*, 2007), but has been shown to critically depend on the actual number of Ca_V channels present within the active zone (Sheng *et al.*, 2012), which can differ between 5-218 channels.

When combining this with plastic changes it is interesting to investigate how a feedback messenger molecule like NO might affect cellular excitability both pre and

postsynaptically via modulation of Ca_V channels, as this could add another level of complexity to this already complicated puzzle.

1.4 Aims and objectives of this study

Given the role of voltage-gated calcium channels (Ca_Vs) in synaptic release and their influence on cellular excitability in the medial nucleus of the trapezoid body (MNTB), and in light of the evidence for nitric oxide (NO) as an activity dependent modulator of excitability in the MNTB via modulation of HVA of K_V channels (Steinert *et al.*, 2008; Steinert *et al.*, 2011b), the aim of this study was to investigate any NO-dependent modulation of native Ca_V channels in the MNTB and SPN using an electrophysiological approach (Figure 1.6.).

This would be achieved by completing three objectives: firstly, characterisation of any NO-dependent modulation of the high-voltage-activated Ca_V channels in the principal neurons of the MNTB; secondly, characterisation of the LVA current present in the downstream nucleus the SPN, and investigation of any NO-dependent modulation of this current; thirdly, by investigating NO-dependent effects or modulation of cellular excitability via Ca_V channels (Figure 1.6.).

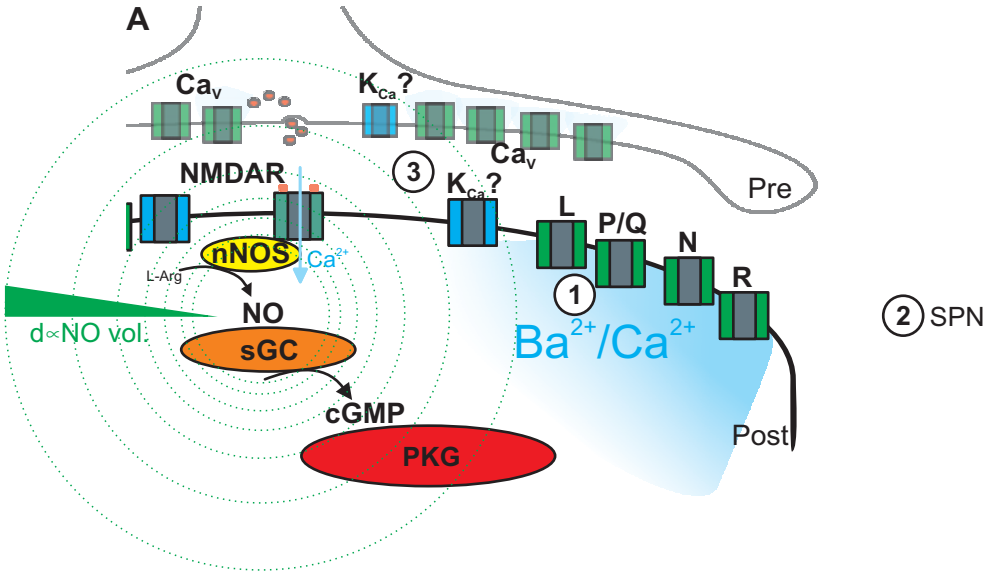

Figure 1.6. Nitrergic signalling in the MNTB.
A. Schematic illustration of the pathways by which NO could modulate cellular/synaptic excitability via modulation of Ca_V channels and K_{Ca} activation in the MNTB. The concentric cirlces and green bar illustrate the volume diffusion model, by which NO will diffuse further at higher volume of production as it over comes local buffering. Objectives (numbered circles): 1) to investigate NO-dependent modulation of expressed HVA channels in the principal neurons of the MNTB. 2) Characterisation of LVA Ca_V in downstream SPN nucleus and effect of NO there in. 3) To understand NO-dependent modulation of cellular excitability via Ca_V channels in the MNTB.

2. Materials and Methods

In this chapter I will describe the materials, methods and tools that I used to investigate the nitrergic modulation of the conductances described. Where experiments differ from those outlined here, they will be described in the relevant results section.

2.1 Tissue preparation and maintenance.

The protocol for tissue preparation follows that which is well characterised and used in the Forsythe lab (Kopp-Scheinpflug *et al.* 2011; Tozer *et al.* 2012), and is done with strict accordance to the Home Office use of animals for Scientific Procedures Act 1986.

2.1.1 Solutions.

Artificial cerebrospinal fluid (aCSF) was made to mimic physiological CSF, to maintain the brainslice *in vitro*, and to provide the ionic gradients necessary for experimentation. For slicing, slice maintenance and experimental recording, slightly different external aCSFs were used, and their compositions are listed in table 2.1. All aCSFs were continually bubbled with carbogen gas (95% O_2, 5% CO_2) to buffer the pH to 7.4. All divalent ions (Mg^{2+}/Ca^{2+}/Ba^{2+}) were added after 20-30 minutes bubbling, to allow pH stabilisation and prevent precipitation (Barnes-Davies & Forsythe, 1995). To observe I_{Ca} in MNTB neurons a Ba^{2+} (5mM) containing aCSF recording solution instead of physiological Ca^{2+} (2mM) was used, and a CsCl based pipette solution was also used (table 2.1) in order to better observe Ca_V currents. For the I_{Ca} measurements in the SPN and the SK measurements in the MNTB, normal aCSF was used.

However, for the SPN voltage clamp experiments a CsCl internal pipette solution was used, but a KCl/KGlu pipette solution was used for the current clamp experiments (Kopp-Scheinpflug *et al.*, 2011). In the SK experiments the normal aCSF external and KCl/KGlu pipette solutions were used for both voltage and current clamp experiments.

In all experiments the external pH was titrated to pH 7.4 and the internal pipette solution to pH 7.2 with a relevant hydroxide solution. External solutions had an osmolarity of between 310-320 mOsM, and internal pipette solutions had an osmolarity of 10-20mOsM lower to prevent cells swelling during whole cell patch clamp recording.

For dissection and slicing of the brain, low sodium slicing aCSF solution was used (table 2.1). Again divalents were added to this after bubbling with carbogen for 20-30 minutes. In this solution, sodium chloride was replaced with increased sucrose, and a higher Mg^{2+} concentration and lower Ca^{2+} concentration were used to reduce excitability and excitotoxicity by blocking NMDA receptors, with the aim of being neuroprotective. Slicing solution was used at temperatures ~0˚C, and slush was made from this using an ice cream maker (Magimix, UK). This was also neuroprotective, cryoprotecting the brain during extraction, dissection and slicing.

Compound / Solution (in mM)	Slicing aCSF	Normal aCSF	I_{Ca} measuring aCSF	Pipette sol. for I_{Ca}	Normal Pipette sol.
NaCl		125	95	10	
KCl	2.5	2.5			32.5
$MgCl_2$	4	1	1.3		1
$CaCl_2$	0.1	2			
NaH_2PO_4	1.25	1.25	1.25		
$NaHCO_3$	26	26	26.2		
Na^+ pyruvate	2	2	2		
Myo-inositol	3	3	3		
Ascorbic acid	0.5	0.5	0.5		
Glucose	10	10	10		
Sucrose	250				
HEPES				40	40
EGTA				1	5
CsCl				120	
KGlu					97.5
Phosphocreatine				5	5
Mg-ATP				2	2
Na-GTP				0.3	0.3
TEA-Cl			30	10	
$BaCl_2$			5		
pH	7.4	7.4	7.4	7.2	7.2
Omolarity (mOsM)	310-320	310-320	310-320	290-300	290-300

Table 2.1 Basic solutions for tissue maintenance and experimentation

Protein	Abb.	Blocker	[Conc.]
Potassium Channel	K_v2, K_v3	TEA	30mM
L-type Calcium Channel	$Ca_v1.2$	nifedipine	10 µM
P/Q-type Calcium Channel	$Ca_v2.1$	ω-agatoxin IVA	200nM
N-type Calcium Channel	$Ca_v2.2$	ω-conotoxin GVIA	2µM
Small conductance Ca^{2+} activated potassium channel	SK	apamin	100nM
GABA Receptor	GABAR	bicuculline	10µM
Glycine Receptor	GlyR	strychnine	1µM
Sodium Channel	Na_v	Qx314	2mM
Sodium Channel	Na_v	TTx	0.5µM
Hyperpolarisation activated Potassium Channel	HCN	ZD7288	10µM
Guanylyl Cyclase	sGC	ODQ	1µM
Neuronal Nitric Oxide Synthase	nNOS	7-NI	10µM

Table 2.2 Pharmacological blockers used in experiments

2.2 Dissection and slicing procedures.

2.2.1.1 Extraction from skull

P13-P16 CBA/Ca mice (P=postnatal day) were decapitated by scalpel (size 26 blade, swann-morton, UK) in accordance with the UK animals in scientific procedures Act (1986) in the designated procedure room within the MRC Toxicology Unit. The severed head was immediately placed in ice cold slicing solution (~0˚C). The scalp was removed by scalpel cutting rostral-caudally from forehead to spinal cord, the exposed skull then pierced by scalpel point and opened by scissors cutting in a 'cross' formation rostrally, caudally, and laterally from the centre of the skull. The quadrants of the skull are folded out and back on themselves revealing the cortex. The brain was then removed from the rest of the encasing skull with care, using scissors. By dissociating the brain from the olfactory bulb at the front of the skull the scissors can then cut through connective tissue and the optic nerves to tease the brain out of the skull. Care must be taken when severing connective tissue near to the brainstem. The brain is finally separated from the skull and stored again in cold slicing solution (~0˚C) for transport to the laboratory prep room.

2.2.1.2 Mounting brain on tissue block.

The brain is laid ventral surface up; the meninges are removed by fine forceps. The cortex is then separated from the brainstem by a 30˚-angled cut towards the cerebellum, at the level of the inferior and superior colliculus (Figure 2.1. A.), this is achieved by placing a pair of forceps at the required angle and slicing along these. The brainstem is then fixed cut-surface first (upside-down) to the vibratome tissue block by a blob of superglue, after the briefest touch of the cut-surface with filter paper to

remove excess moisture and improve glue mounting. A drop of slicing solution is pipetted down on to the mounted brainstem to wash the excess glue down, away from the brain and onto the stage. This prevents the glue rising up on to the tissue when the prep is resubmerged in slicing solution as the block and brainstem are then moved into the vibratome (either: Microslicer DTK-1000, DSK, Japan; or CI 7550, Campden Instruments, UK), ventral side towards the blade, for slicing. The tissue block should then be filled with slicing solution, ensuring coverage of brain stem, and the The vibratome blade was set to oscillate in the horizontal plane at 80Hz, and advanced 0.02mm s^{-1}. The slower the blade advance, the less debris was observed on the slices, improving imaging quality (personal observation).

Using the Cochlear nuclei and 7^{th} nerve as landmarks, 200µm slices were made at the level of the MNTB, Bregma level -4.84 to -5.68mm (Figure 2.1. B). Slices were placed directly into a lifesaving chamber containing normal aCSF and 10µM 7-nitroindazole (7-NI) at 37˚C for incubation for 1 hour, after which the chamber was allowed to cool to room temperature.

After slicing and incubation the slices are then ready for experimentation and are moved via transfer pipette to the CI 7800 visual patching and imaging chamber (Campden Instruments, UK) on the microscope stage of the electrophysiological rig for maintenance at 37˚C during recording.

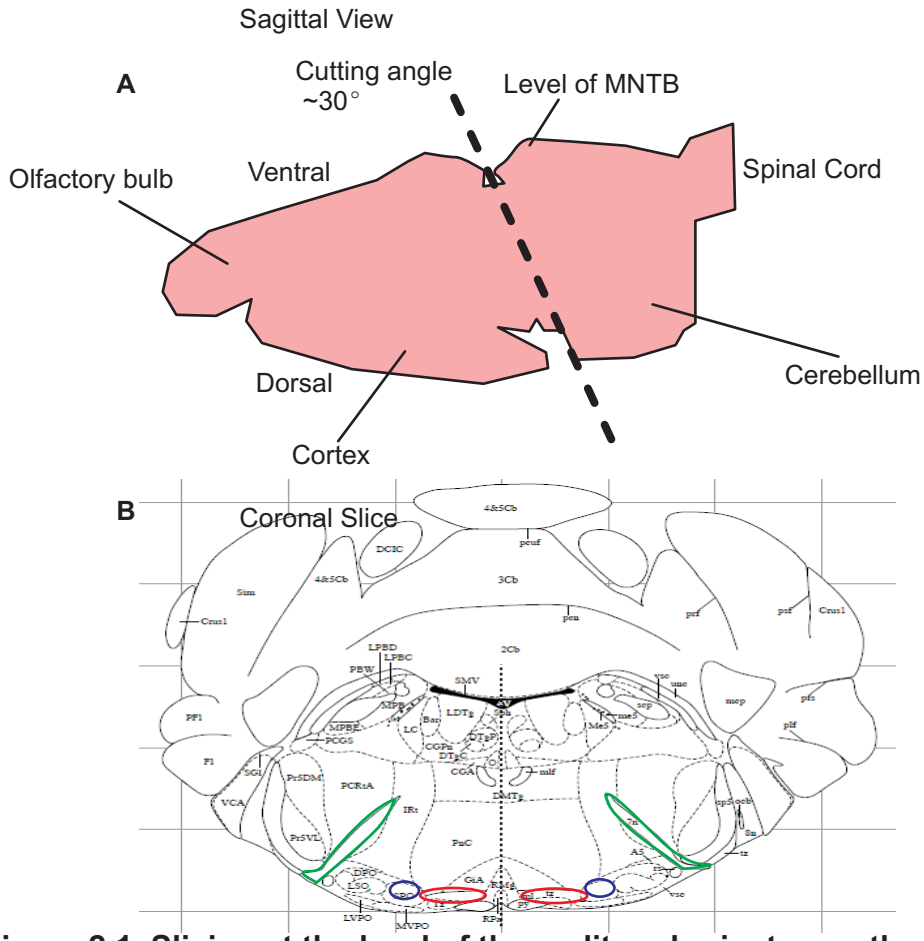

Figure 2.1. Slicing at the level of the auditory brainstem pathway. **A.** Cutting at a 30 degree angle to separate the cortex from the brainstem (dashed line) helps to preserve fibres when slicing the brain. **B**. 200μm slices are taken at the level of the 7th nerve (green), the MNTB nuclei (red) and SPN nuclei (blue) sit bilaterally to the midline (dashed line).

2.3 Experimental microscope and cell visualisation.

The upright Nikon (Japan) eclipse E600FN microscope was fitted with a 4x (N.A 0.1) dry objective, 60x (N.A 1.00) water immersion objective and configured with Nomarski optics enabling differential interference contrast (DIC) microscopy of the brain slices (Allen *et al.*, 1969). DIC optics allows the visualisation of cells with a pseudo-contrast, giving a 3D-feel to the image, making it easier to view cells and target them with patch pipettes.

Figure 2.2. shows how the light path, generated from a tungsten light source was directed up through a linear polarizer (1) and into the first condenser-Nomarski prism (2). The 45˚ shear angle of the prism splits the light beam into two parallel waves, the ordinary (red lines) and extraordinary (blue dots), which are spatially separated (but not to a greater distance than 2nm). The two waves are then focused by the condenser (3) to converge on the specimen (4), and the emerging light is collected by the objective (5) and converges at the rear focal plane where the second Nomarski prism is positioned inverted with respect to first prism (6). The recombined waves then pass through a second polarizer (analyzer, at 90˚ to the first), forming the image (7).

As the light waves pass through the tissue they have different optical paths and get refracted, as the phase-shifted wavefronts recombine in the Nomarski prism they generate elliptically polarized light. As a portion of this waveform is parallel to the transmission axis of the analyzing polarizer, it passes through the second polarizer (analyzer), generating an image with constructed contrast.

MNTB neurons in these aged animals are easily visible under the experimental scope, as to are SPN neurons, although there are fewer numbers of these as it is a comparatively smaller nucleus.

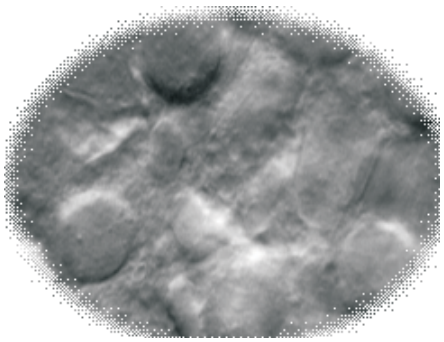

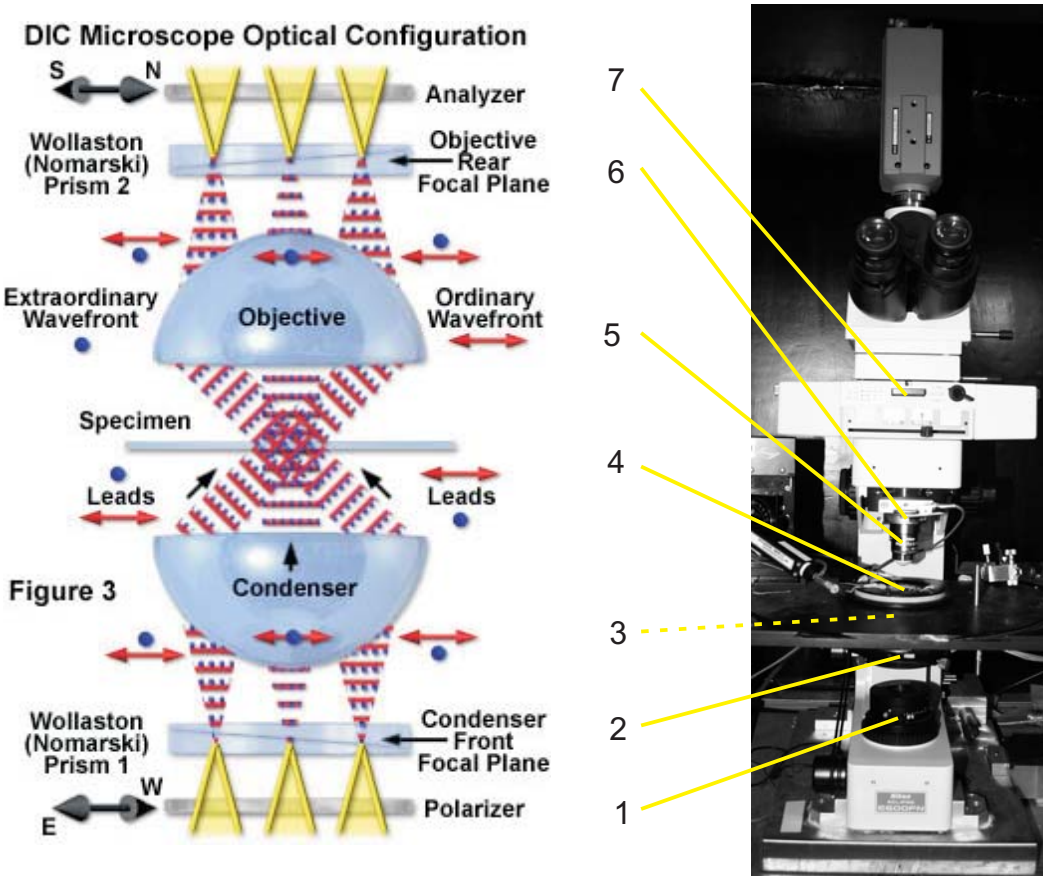

Figure 2.2. Light path through the experimental scope with Nomarski optics. The diagram shows the light path through the different components of the microscope (#1-7) before forming an image with pseudo contrast, like the one shown at the top of the figure. Image adapted from the Olympus website.

2.3.1 Tissue maintenance and pharmacological perfusion.

The brain slice was held under a U-shaped harp made of a flattened platinum frame and nylon strings, in a temperature controlled visual patching and imaging chamber (CI 7800, Campden Instruments, UK) situated on the microscope stage. Four lines were able to bring test solutions into the chamber after passing around and through the chamber heating element, bringing the solution to test temperature (37˚C). The solution volume was kept constant in the chamber by the matched extraction of solution at the opposite side of the bath by the extraction/outflow needle. The special needle was blunted, bent to allow better access to the bath, and its tip blocked with sylgard, allowing bath solution to be sucked out of a small slit cut into its front face (Figure 2.3.).

The four lines bringing solution to the bath were each connected to a bubble trap, made from an upright 5ml syringe with plunger removed. At the top, in the place of the plunger, the opening of the syringe was sealed by silicon, through which two needles were pushed, one to connect to the perfusion tubing arriving from the peristaltic pump and one to a 1ml syringe to maintain pressure in the bubble trap. The tip of the upright bubble trap (at the bottom) was attached to a three-way tap, before joining with the perfusion tubing (Tygon, Carlton Parmer, UK) which then went on to enter the heating chamber and arrive at the bath. The bubble traps served several purposes, firstly to prevent bubbles from entering the lines into the chamber by retaining a small amount of solution in the trap. Secondly, they prevent the solution from the reservoir to the chamber bath being electrically connected, as this would act as an aerial, adding noise to the recordings. A bubble trap also collects solution from

the bath via the extraction needle before channelling the solution to waste (Figure 2.3.)

When different lines were used for pharmacological addition during recording, they were primed prior to washing into the bath. This meant that the solution was pumped in-to the bubble trap, and as a drop emerged into the trap the perfusion tubes were clamped with a crocodile clip to maintain peristaltic pressure, but the peristaltic pump clamp removed to stop further advancement of the solution until needed. This made pharmacological addition quicker in the experiments, as movement through the perfusion tubing from reservoir to bath took 57 seconds.

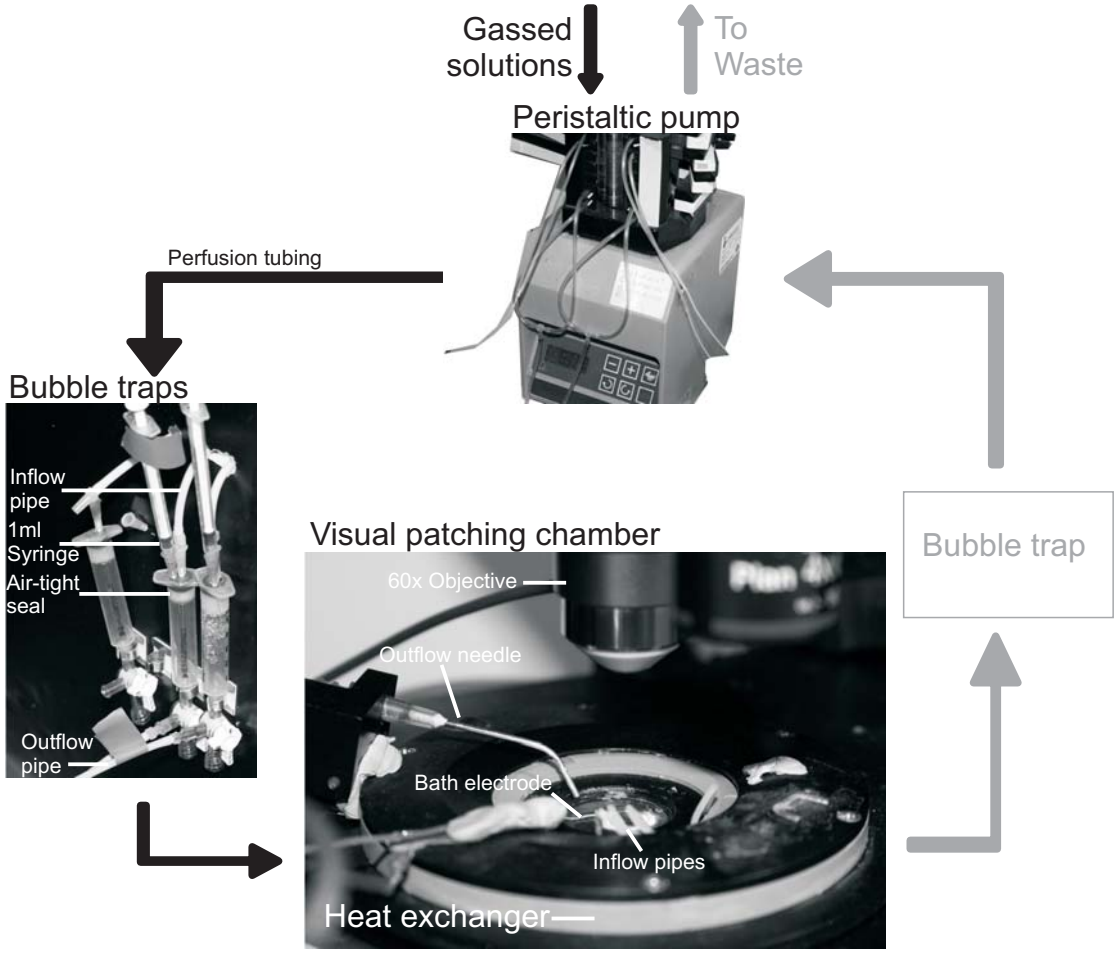

Figure 2.3. Peristaltic perfusion set up.
Gassed solutions are pumped between reservoir, patching chamber and waste pot by a peristaltic pump. Solutions are sucked into the small diameter tubing and pass around the peristaltic pump (minipuls, Gilson, France) before entering the bubble traps. In the airtight bubble traps the pressure flow of the solution is reduced by applying negative pressure with the 1ml syringe. This enables a head of solution to be maintained in the bubble trap, preventing bubbles moving on in to the patching chamber. Before entering the patching chamber from the bubble traps, the solution is passed around its 360º circumference, which is an aluminum heating element electrically powered by a resistive circuit board with feedback control. The solution enters the chamber at 37ºC, flows over the slice and is extracted by the outflow suction needle. The suction pressure is maintained by the Gilson pump, and the extracted solution encounters another bubble trap to ensure discontinuation of the solution between chamber and perfusion tubes, and from here the waste solution re-enters the pump before washing in to the waste pot. The perfusion speed is calibrated to a 1ml/min flow. Arrows indicate perfusion tubing and direction of flow.

2.4 Patch clamp recording from auditory brainstem neurons.

Electrophysiology involves the use of electrodes to measure the potential difference across a cell membrane, and to interpret changes in that potential difference as cellular excitability due to the movement of ions. Historically this has involved sharp electrode puncture of cells to compare the voltage difference between an internal electrode and an external reference electrode, and lead to the understanding of the ionic basis of the action potential (Hodgkin *et al.*, 1952).

An improvement on this method is the patch clamp technique, pioneered by Sakmann and Neher in the 1980s (Hamill *et al.*, 1981) and for which they shared the Nobel Prize for Physiology in 1991. It involves connecting a glass micropipette filled with ionic solution and containing a silver silver-chloride wire attached to a patch clamp amplifier, and putting this microelectrode in series with the cell membrane by forming a high resistance gigaohm seal between the patch and the glass in the mouth of the pipette. The different patch clamp configurations: cell attached, whole cell, inside-out and outside out; are shown in Figure 2.4. which is adapted from the original paper (Hamill *et al.*, 1981). The figure highlights the critical path used to carry out whole cell *in vitro* patch clamp recordings from visually identified neurons in brain slices (Edwards *et al.*, 1989) from the auditory brainstem.

2.4.1 Whole cell patch clamp enables observation of ionic flux across channels in the whole cell membrane.

The whole cell configuration is achieved by approaching the cell membrane with a capillary glass microelectrode (boroscillicate, OD 1.5mm, ID 0.86mm, Harvard Apparatus, UK) which has been micro-forge heated and pulled (Digitimer, UK) so that the mouth diameter is ~1µm, with a resistance of between 2 and 6MΩ, and pipette

offset zeroed. By filling the micropipette with internal solution and applying positive pressure (<2ml), a dimple is observed as the pipette comes into contact with the cell membrane. By commanding 5mV step pulse to the electrode we can use this as a seal test to understand when we have a patch seal with the cell. Release of positive pressure allows the membrane and pipette mouth to become contiguous, forming a loose patch, increasing resistance and reducing current observed in 5mV seal test. Light sucking advances a 'patch' membrane into the mouth of the pipette, this is known as the cell-attached configuration, and generates a high resistance (GΩ) seal between the capillary glass and the membrane patch. Thus normally reducing the observed seal test current to a flat line with two fast pipette capacitance transients at the start and end of the voltage step. These are removed by circuitry in the patch clamp amplifier.

Before going whole cell, the electrode is gently pulled out and up to the surface edge of the cell, removing the risk of the nucleus blocking the patch and increasing access resistance. The cell is held at a negative potential approximately equal to resting membrane potential (-60mV) and negative pressure is applied to rupture the membrane. The rupture means that the pipette solution is now continuous with the cytoplasm, and the electrical properties of the whole cell are in series with the pipette electrode.

The pipette solution and cytosol can now mix through the patch, known as dialysis. Dialysis is useful for washing pharmacological blockers from the pipette into the cell, but conversely can wash signalling molecules from the cell out into the pipette. In these experiments, dialysis is a problem as nitrergic signalling utilises soluble second messenger molecules, and dialysis will wash these out. To minimise the problem of

dialysis, experiments were conducted in an unpaired fashion such that the slices were treated with pharmacological agents prior to patching, and cells were patched and recorded from, before moving on to the next cell.

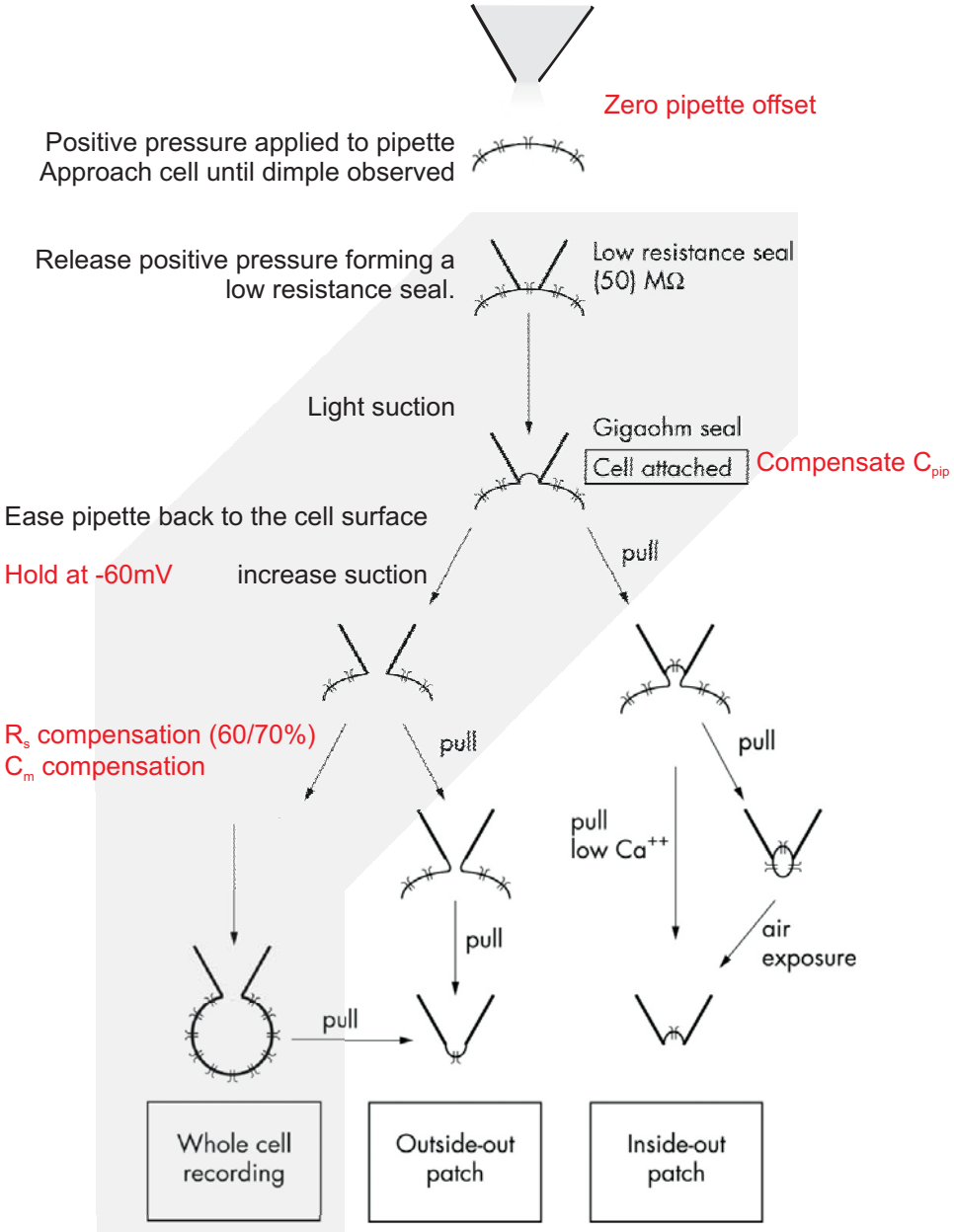

Figure 2.4. Achieving the whole cell patch clamp configuration.
Top - Bottom the steps taken to achieve the whole cell patch clamp configuration are highlighted in grey. The steps in red are the critical checkpoints needed to ensure good voltage control. Adapted from Hamill (1981).

2.4.2 Overcoming electrophysiological caveats to measure whole cell ionic currents.

It is important to understand the limitations of electrophysiology both in the technique and equipment used, but also those inherent to the preparation or system being studied. What follows is a description of the limiting factors in my experiments.

2.4.2.1 Electrodes in solution.

The ions in the pipette solution have a different mobility to the ions in the bath solution, and this sets up a liquid junction potential (LJP) (Neher, 1992). Practically the pipette offset zeros the current trace for the seal test before sealing with a cell. However, this does not remove the junction potential, so the pipette command that is given to the cell during an experiment is actually:

$$V_{command} - LJP$$

Equation 2.1. Where $V_{command}$ is voltage command in Volts, and LJP is liquid junction potential in Volts.

The LJP can be calculated by software in pClamp and can be subtracted offline. Unless otherwise stated the results shown are not corrected for the junction potential. In the calcium channel experiments in the MNTB the junction potential was -9mV. In the Ca_V measurements in the SPN the junction potential was -4mV. In the SK investigation the junction potential was -6mV.

2.4.2.2 Excitable cell membrane properties.

The phospholipid bilayer membrane is an electrical insulator. It prevents charged species (ions) from moving across it unless ion channel proteins are open allowing flux. Because of its thinness (order of nm), the charges inside and outside the cell can

influence each other, and as such the membrane acts as a capacitor C (capacitance measured in Farads), storing charge Q (coulombs).

When a voltage is applied across the membrane the capacitance must be re-equilibrated which involves movement of charge with time, termed capacitive current, I_C (amperes).

$$C = \frac{Q}{V} \qquad\qquad I_C = \frac{\Delta Q}{\Delta \mathrm{t}}$$

Equation 2.2. C is capacitance (farads), Q is charge (coulombs), V is membrane potential (volts), I_C is capacitive current (amperes), t is time (seconds).

The protein pores in the membrane act as conductors allowing current to flow across a resistor when they open. Therefore the membrane resistance R (ohms) is inversely proportional to the total conductance G (Siemens) of these channels:

$$\mathrm{R} = \frac{1}{G}$$

Equation 2.3. R is resistance (ohms), G is conductance (Siemens).

A high resistance means only a small number of channels are open in the membrane, and so there will be little current at that voltage. A bigger potential difference across the membrane could activate more channels, reducing resistance, meaning there will be greater membrane conductance and therefore greater current flow across the membrane, I_m.

As the membrane capacitance and resistance are in parallel, a change in membrane potential must first fulfill the membranes capacitive requirements, generating a fast I_C, before current I_m is generated through the membrane resistors. This means that the I_m generated on a given voltage step is equal to I_C + the ionic current through the membrane conductances (ion channels). Membrane potential V_m (volts) is the product of membrane current I_m and membrane resistance R_m, according to Ohm's law:

$$V = IR$$

Equation 2.4. Ohm's law. V is membrane potential (volts), I is current (amperes), R is resistance (ohms).

Injecting current into the cell will not cause the membrane potential to change instantly. Instead it will change exponentially, and the time constant (τ) of that change is the product of the resistance and the capacitance, such that:

$$\tau = \mathrm{RC}$$

Equation 2.5. membrane time constant τ (seconds), R is resistance (ohms) C is capacitance (farads).

2.4.2.3 Ion channels and ionic movement through membrane channels.

For a given V_m the amplitude of the current is dependent on membrane conductance. This is dependent on the number of ion channels (N) in the membrane and the

probability that they will be open (P_{open}), such that the ionic current through the membrane channels is a product of N, P_{open} and the single channel current (i):

$$I_m = NiP_{open}$$

Equation 2.6. I_m is membrane current (amperes), N is total number of ion channels, *i* is the current through a single channel, P_{open} is the probability of ion channel opening.

The reason the membrane has the electrical properties described above is because it separates ionic charges, setting up electrochemical gradients for ionic flow. A large negative charge is contained inside the cell due to the overall negative charge of cellular proteins, this is balanced by a high concentration of positive K^+ ions. Outside the cell, a high concentration of positive Na^+ and Ca^{2+} ions exist, balanced by a high Cl^- ion concentration. The electrochemical gradient is maintained by the Na^+/K^+-ATPase membrane pump.

An electrochemical gradient is one that takes into account the concentration differences of the ions across the membrane, meaning there is a diffusion gradient promoting movement of ions, but also the fact that ions are charged species and, as a voltage is applied across the membrane, these ions will be more (or less) driven to move through the membrane down these gradients.

The membrane potential at which there will be no ionic flux across the membrane, or at which the direction of ionic movement reverses (E_{rev}) can be calculated for each ionic species, by the Nernst equation:

$$E_{rev} = \frac{RT}{zF} \ln \frac{[ion]out}{[ion]in}$$

Equation 2.7. Nernst equation. E_{rev} is reversal potential (volts), R is gas constant (8.314 J K^{-1} mol^{-1}), T is temperature (K), z is ion valency, F is faraday's constant (96,485 C mol^{-1}).

My Ca_V recording experimental solutions contained 95mM external and 10mM internal Na^+ ions, giving a Nernst potential of +49.9mV. My Ca_V recordings also used Ba^{2+} as the charge carrying ion, and it was assumed that, if Ba^{2+} ions interact with the Ca_V channels in a similar fashion to Ca^{2+} ions, they would have a similar reversal potential. 5mM BaCl was used in the external aCSF for recordings, the equivalent concentration of Ca^{2+} ions with a nominal internal concentration of 125nM would have a reversal potential of +129mV.

The restriction of the Nernst equation is that it only calculates the reversal potential for a single ion species without accounting for the permeability of the ion. A better equation to use is the Goldman-Hodgkin-Katz (GHK) equation which accounts for the Nernst potential and permeabilities of the major permeating ions:

$$E_{rev} = \frac{RT}{F} \ln \frac{P_{Na}}{P_{Na}} \frac{[Na]o + \frac{P_K}{P_K}}{[Na]i + \frac{P_K}{P_K}} \frac{[K]o + \frac{P_{Cl}}{P_{Cl}}}{[K]i + \frac{P_{Cl}}{P_{Cl}}} \frac{[Cl]i}{[Cl]o}$$

Equation 2.8. Goldman Hodgkin Katz equation, extension of Nernst equation above, accounting for the permeability (P_{ion}) of each ion species.

2.4.2.4 Compensation of whole cell membrane properties enables accurate measurement of ionic currents.

In the whole cell configuration the pipette solution is continuous with the cytosol. Which means the pipette electrode resistance and solution is now in series with the membrane resistance and cytosol of the cell. However, the two compartments are either side of the patch, which is of a small diameter and has a resistance known as access resistance. The access resistance divides the compartments, inducing a voltage drop, meaning that the cell membrane never sees the potential commanded at the pipette. These resistances in series, termed the series resistance (R_s), are compensated by 60-70% by a potentiometer circuit within the amplifier to overcome this problem.

Practically, lower resistance electrodes and high seal resistance can reduce the problem of R_s. If R_s changes by more than 20% during a recording, the cell is abandoned as this is beyond an acceptable loss of voltage control.

Two large capacitive current deflections are observed at the start and end of the seal test pulse and these are generated by the cell membrane's intrinsic capacitance. These are compensated for by amplifier circuitry, minimizing capacitive current contribution to recordings of I_m as described earlier. Combined with the R_s compensation described above, this aims to improve resolution of ionic currents. In whole cell current clamp, only R_s needs compensating.

2.4.3 Voltage clamp enables the observation of ionic flux at a clamped V_m.

This method involves using a feedback amplifier (Axopatch 200B, Molecular Devices, US) and head stage to inject current to hold the membrane potential (V_m) of the cell at different command voltages, $V_{command}$. Ion channels open at these different $V_{commands}$,

and membrane resistance R_m changes allowing ionic current flow across the membrane, I_m. The feedback amplifier instantaneously compensates for this by injecting the reciprocal current to maintain the cell at $V_{command,}$ giving a read out of this injected current as the membrane current I_m.

Although it is not a physiological measurement of cellular ionic properties, it has proved very insightful in investigations of the conductances present in the membrane, and those that underlie cellular excitability (Cole, 1949 ; Hodgkin *et al.*, 1952).

Voltage clamp is the most heavily used technique in these investigations. It allowed for pharmacological isolation of my ion channel of interest meaning I could investigate current amplitudes at different V_m and generate current voltage relationships (IVs), and understand channel kinetics and availability.

2.4.4 Current clamp enables observation of membrane potential (V_m).

Current clamp involves applying a known current and measuring the change in V_m in response to that current injection. It is a useful technique because it can mimic physiological scenarios, like a synaptic input, enabling measurement of cellular excitability. The level of cellular excitability is defined as the current injection amplitude needed to elicit an action potential (AP).

In this way, pharmacological blockers of currents can be used to determine the blocked-channel's influence on cellular excitability.

Current clamp is used in the experiments investigating the role of SK channels in the afterhyperpolarisations (AHPs) generated in MNTB cells following trains of APs in results chapter 3.

2.4.5 Synaptic Stimulation

Whilst recording from a post synaptic cell in voltage clamp or current clamp mode it was possible to stimulate the presynaptic fibres. This was achieved using a DS2A isolated stimulator (Digitimer, UK; 1-10V, 0.01-0.2ms) connected to a bipolar platinum electrode placed at the midline of the slice across the trapezoid body nerve fibres (Haustein *et al.*, 2011). Stimulus trains were generated in Clampex 10.2 (pClamp 10.2, Molecular Devices, US) and transmitted to the stimulator via the digidata 1322A (Molecular Devices, US).

2.4.6 Protocol implementation and data analysis.

Voltage clamp, current clamp and synaptic stimulation protocols were designed in Clampex 10.2 using the protocol editor software. They were delivered via a digidata 1322A to the Axopatch 200B amplifier headstage, mounted on a MP-285 manipulator (Sutter, US).

Incoming signals were sampled at 100kHz and filtered at 5kHz, and analysed in clampfit 10.2 (Molecular Devices, US). IVs were drawn in clampfit and transferred to Excel (Microsoft, US). Leak subtraction was done offline in Excel, by subtracting the gradient derived from the portion of the IV where there was no voltage-dependent current flowing.

Conductance was measured from the IVs as G=I/(V-Erev) where V-Erev is equal to the driving force acting on the ion. G/G_{max} was then plotted against V_m and a Boltzmann function was then fitted of the form:

$$\frac{G}{Gmax} = \frac{1}{1 + e^{(\frac{V - V_{0.5}}{k})}}$$

Equation 2.9. Boltzmann function, K is the slope factor.

Average data curves are plotted as mean±SEM and drawn in Sigmaplot 12.0 (Systat). All statistical analysis was carried out using GraphPad Prism (GraphPad Software Inc., San Diego, CA) and InStat 3 (GraphPad Software Inc., San Diego, CA). One-way ANOVA tests with Tukey-Kramer post-hoc tests for pair-wise comparison were used to compare the groups described in the text. P values are described as fully as possible. However, due to the limitations of GraphPad and InStat 3, the post-hoc test p value could only be described as: $p>0.05$ considered not significant; $*p<0.05$, considered significant; $**p<0.01$ considered very significant; and $***p<0.001$ considered extremely significant. Other tests used, such as unpaired student's t-tests, are described in the text along with their p values, accordingly.

3. Nitric Oxide (NO) differentially modulates voltage-gated calcium channels (Ca_V) in principal neurons of the Medial Nucleus of the Trapezoid Body (MNTB)

Previous investigations of Ca_V channels in the MNTB have revealed a species difference in channel contribution to whole cell I_{Ca} between rat and mouse models. In the rat, neurons have a negligible L-type (Ca_V1) current, based on the minimal (<10%) whole cell current sensitivity to nicardipine (Barnes-Davies *et al.*, 2001), whereas mouse MNTB has an L-type current that contributes ~15% of the whole cell current (Leao *et al.*, 2004). Both papers agree on the presence of P/Q, N and R-type channels in these neurons, which are all high-voltage-activated (HVA) subtypes, and a lack of the low-voltage-activated (LVA) T-type subfamily of channels.

As there is a high expression of neuronal nitric oxide synthase enzyme (nNOS) in the MNTB of rat (Fessenden *et al.*, 1999) and mouse (Steinert *et al.*, 2008) (Allen Atlas) and, at the time of starting this project, NO-dependent inhibition of the HVA delayed rectifier $K_V3.1$ potassium channel had recently been characterised in this model (Steinert *et al.*, 2008), it seemed prudent to investigate its effect on Ca^{2+} entry through the native HVA Ca_V channels in the principal neurons of this nucleus. Also, given the importance of Ca^{2+} as a cellular signalling molecule, and the role of Ca_V channels in synaptic transmission, coupled with the convenience of this model in investigating synaptic physiology, it was thought that any observed effects of NO would not only have intrinsic consequences on cellular excitability, but may also provide clues to explain some of the presynaptic effects of NO that have been observed, such as smaller mini and evoked EPSC amplitudes (Steinert *et al.*, 2008).

Here I describe investigations into HVA Ca_V channel subtypes present in the MNTB of CBA mice, and their modulation by NO. The results show a non-equal contribution of the subtypes to whole cell I_{Ca}, and also reveal a differential modulation of each subtype by NO, involving distinct pathways. L-type (Ca_V1) current is potentiated by NO, as is P/Q-type ($Ca_V2.1$) current, although via a different signalling pathway. N-type ($Ca_V2.2$) voltage dependence of activation is leftward shifted by NO, but the peak amplitude of the current is unaffected. NO does not modulate R-type ($Ca_V2.3$) current.

In order to arrive at this conclusion and to tease out the modulatory effects of NO on the channels, it was necessary to employ some optimisation strategies to the experimental design.

3.1 The experimental design aimed to improve the resolution of the I_{Ca} and the modulatory effect of NO on the current(s).

The ideal experimental scenario for investigating NO-dependent modulation of Ca_Vs would have been paired investigations of pharmacologically isolated currents in the presence, and absence, of NO administered by donor molecules. This was attempted, but was found to be technically challenging: cells needed to be held for an extensive period of time whilst NO was applied by a donor molecule, over this time period the series resistance would increase and the I_{Ca} current would run down. Another problem associated with holding cells for a prolonged length of time in the whole cell configuration is dialysis of the cytosol with the pipette solution, which risked washing out parts of the signalling system. This made it difficult to discriminate NO-mediated effects from dialysis artifacts. Therefore unpaired experiments, in which the slices were treated with the relevant pharmacological agents prior to recording, were

performed. This allowed the cellular signalling systems to remain intact and functional up to the point of 'breaking-in' to the whole cell configuration with the patch pipette.

To optimise the resolution of NO's effect on the currents, slices were first incubated with the nNOS blocker 7-Nitroindazole (7-NI) to exclude endogenous production of the gas (7-NI was also included in the bath solution), and to remove or restrict the amount basal modulation of the I_{Ca} by NO. Currents were then measured from neurons in this 7-NI-control condition, and during treatment with NO donors, either Diethyl-ammononium nonoate (DEA, 100µM) or sodium nitroprusside (SNP, 100µM), which were added to the bath solutions. Removing endogenous nNOS activity and adding NO via a donor would help to emphasise the physiological effect of NO in these neurons.

As well as conducting the experiments at 37˚C (as described in the methods), further improvement of the current resolution was achieved by using Barium (Ba^{2+}) as the charge carrier, instead of Ca^{2+}. Ba^{2+} (5mM) has a greater conductance through Ca_V channels than physiological Ca^{2+} (2mM) (Catterall *et al.*, 2005), and also helps to block outward K^+ or Cs^+ movement which would pollute the data if not removed, by counteracting the inward movement of the I_{Ca}, decreasing the amplitude and distorting the reversal potential of the observed I_{Ca}. Despite being an un-physiological ion, and known to be toxic to cells with time, Ba^{2+} was a better choice for investigating Ca_V modulation in this investigation, and the following section explores the suitability of the optimisation strategies I have just described.

3.2 Barium (Ba^{2+}) as a charge carrier improved current resolution.

To measure the I_{Ca}, neurons were voltage clamped in the whole cell configuration in the presence of K_V and Na_V blockers (see methods), to isolate the current. The voltage

protocol used to generate a current/voltage relationship (IV) consisted of a hyperpolarising pre-pulse (300ms) to -90mV from a holding potential (V_h) of -60mV, before 5 or 10mV step depolarisations up to +40, +50mV for 300ms, before returning to the holding potential (Figure 3.1. A.). The hyperpolarising pre-pulse served two purposes, firstly to remove any voltage-dependent inhibition of the channels and, secondly, to allow recruitment of LVA channels should any exist in these neurons. The protocol is depicted in Figure 3.1. A with the pre-pulse excluded.

Na_V and K_V channels have to be blocked when using this protocol to isolate the I_{Ca} because the fast and large amplitude inward I_{Na}, and large amplitude yet outward flowing I_K, dominate the generated current traces occluding the smaller amplitude inward I_{Ca} present in these neurons (Figure 3.1. B. Note, this IV is generated in the presence of 1mM TEA). By adding Na_V blocker tetrodotoxin (TTx, 0.5µM) and K_V blocker tetraethyl-ammonium chloride (TEA, 30mM) to the bath solution, the physiological I_{Ca} generated by the voltage step protocol can be observed (Figure 3.1. C).

This is still not an optimal scenario however, due to a remaining unblocked outward current persisting and flowing against the inward I_{Ca}, confusing our picture of the I_{Ca}. The I_{Ca} peak generated by the depolarising voltage command steps similar to that mentioned above (only this time lasting 600ms) is depicted by the arrow in the raw current trace in figure 3.1. C. After the small inward peak an outward movement of the current is observed. This outward current persists for the length of the trace and could be due to a remaining K^+ conductance or Cs^+ permeability and outward ion movement. Leak currents (see methods) could also contribute to the obscuring outward current,

the raw current trace shown in Figure 3.1. C has not been leak subtracted. The small amplitude of the I_{Ca}, obscuring outward flowing current and confounding issue of leak currents would make the data accrued in these conditions difficult to analyse and interpret. In this scenario we are observing an underestimate of the amplitude of the I_{Ca} and because of this proceeding using physiological Ca^{2+} as the charge carrier is not practical.

Re-running the experiment with Na_V and K_V blockers and, substituting physiological Ca^{2+} (2mM) for 5mM Ba^{2+}, using the protocol described in Figure 3.1. A, generates inward currents that are ~4.5 times greater in amplitude. Furthermore there are no polluting outward flowing currents working against the inward flowing whole cell I_{Ba}, suggesting they are blocked by Ba^{2+}, and most likely a conductance through K_V channels. Representative raw traces from one cell are shown in Figure 3.1. D.

The peak amplitudes of the currents can be plotted against the depolarising voltage command steps at which they are generated, producing a current voltage relationship (IV). The IV of the I_{Ca} and I_{Ba} generated from the representative traces, after offline leak subtraction (methods), reveals the extent to which using Barium as the charge carrier improves the resolution of the inward I_{Ca}. Although both currents activate at potentials more positive than -50mV and produce a bell-shaped relationship which peaks at ~-10mV, the I_{Ca} IV peak is ~30% of the amplitude of the I_{Ba} peak. The I_{Ca} also has a reversal potential of ~30mV, which is more negative than expected, the Hodgkin Huxley model would predict a calcium reversal potential (E_{Ca}) of between 40 and 50mV, this is indicative of the outward flowing polluting current's influence on the IV. At more positive potentials (10mV+) there is a large driving force acting on K^+ ions,

even a small outward I_K can oppose the weaker inward I_{Ca} flow and the apparent more negative reversal we observe is the compound effect of the currents influence on each other.

Due to the block of the polluting outward current, the I_{Ba} looks to achieve a more expected reversal potential. The current however does not fully reverse in this scenario, and this is because there are no intracellular Ba^{2+} ions to flow out of the cell.

The trend for I_{Ba} peak amplitude to be threefold greater than I_{Ca} amplitude, as shown in the IVs (Figure 3.1. E), is maintained across the data set and this is summarised in the bar graph of the peak amplitudes from the IVs (Figure 3.1. F). I_{Ca} peak amplitude was 0.22±0.03nA (n=8, mean±SEM) where as peak I_{Ba} was 0.94±0.06nA (n=6, mean±SEM) (***$p<0.001$, unpaired t-test).

Barium as the charge carrier improves the resolution of the whole cell I_{Ca} current by having a greater amplitude than the I_{Ca} recorded in physiological Ca^{2+} and by blocking unwanted and polluting outward conductances.

Barium as the charge carrier should also remove the technical issue of calcium dependent channel inactivation. This is where Ca^{2+} influx through Ca_V channels can lead to inactivation of channels (Yue *et al.*, 1990; Imredy & Yue, 1992). In different preparations different levels of this inactivation have been observed. In an oocyte expression system L-type, but not P/Q-type channels are susceptible to Ca^{2+} influx induced inhibition (Cens *et al.*, 2006), whereas in the presynaptic terminals of the rat calyx of Held calcium dependent inhibition of P/Q-type channels leads to synaptic depression (Forsythe *et al.*, 1998).

As calcium dependent inhibition of the currents would cause a current run-down phenomenon, where each subsequent depolarisation of the cell would generate a smaller amplitude current, it would be difficult to separate an NO-dependent decrease in I_{Ca} from current run-down in the ideal paired experiment. To investigate if Ba^{2+} prevents current run-down, a neuron was patched and subjected to a depolarisation to -10mV every 2 minutes for 16 minutes, and then again at 25 minutes and 30 minutes. The I_{Ba} generated is plotted against the time of recording (Figure 3.1. G). This is only data from one cell, but the trend is for a rundown in the I_{Ba} amplitude with time, similar to that expected in physiological calcium. Therefore rundown still happens in the presence of Ba^{2+}, further supporting the use of unpaired experiments in this investigation.

Ba^{2+} is not a physiological ion, and is known to be toxic to cells over time (Dierickx, 1989). To explore this caveat, and to understand if Ba^{2+} affected current amplitudes with exposure, slices were exposed to the Ba^{2+} containing bath solution and unpaired recordings were taken from cells (n=7) over time. The peak currents were then plotted against time of Ba^{2+} exposure (Figure 3.1. H). The r^2 value of 0.02 denotes a lack of correlation between the variables, and the flat regression line further supports the argument that the cells are unaffected over ~30 minutes exposure to Ba^{2+}.

This evidence supports the choice of using Ba^{2+} as the charge carrier in this study. But, as Ba^{2+} is not a physiological ion, and in an effort to avoid any Ba^{2+} induced errors due to toxicity in these experiments, slices were only exposed to Ba^{2+} five minutes prior to recording.

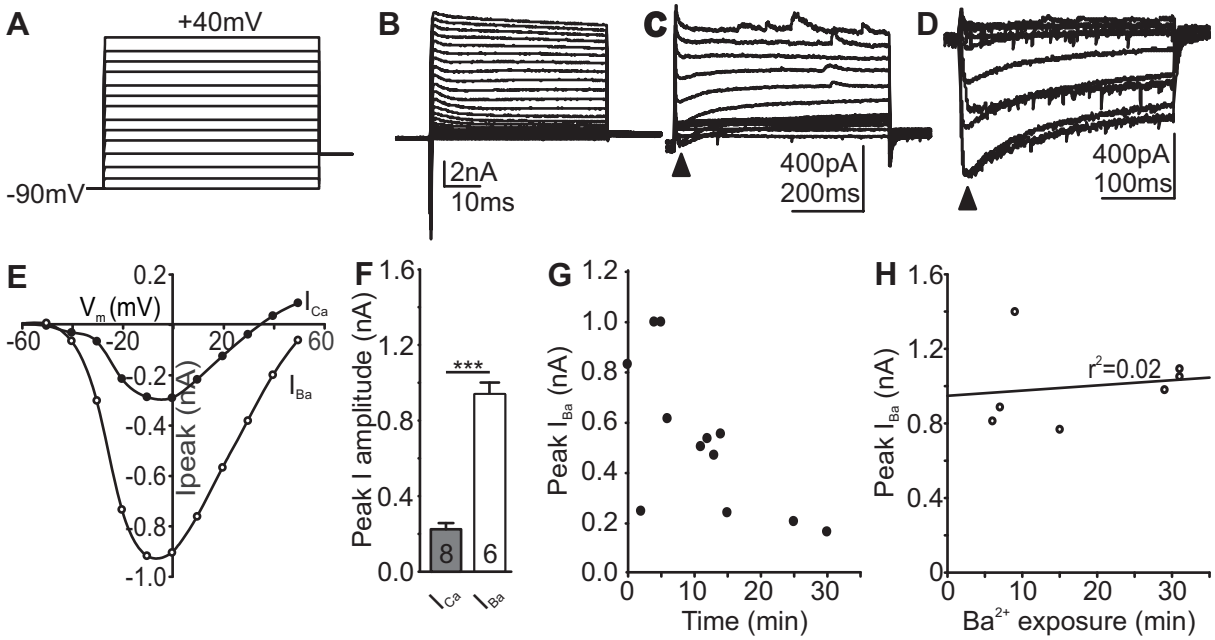

Figure 3.1. Barium (Ba^{2+}) as a charge carrier improved current resolution.

A. Voltage step protocol used to generate currents shown in **B-D**, and produce IVs shown in this figure and throughout the chapter. **B**. Whole cell currents evoked in normal aCSF (+1mM TEA). **C.** Whole cell currents evoked in presence of TTx (0.5μM) and TEA-Cl (30mM). **D**. Currents evoked with Ba^{2+} (5mM) in place of physiological Ca^{2+} (2mM). **E.** IV of I_{Ca} (black circles) vs I_{Ba} (open circles).**F.** Summary bar graph of mean±SEM peak currents generated in I_{Ca} (grey bar), I_{Ba} (white bar)(***p<0.001, unpaired t-test). **G.** Rundown of I_{Ba} with time, peak I_{Ba} generated from step depolarisation to -10mV (black circles) recorded from one cell over time. **H.** plot of peak I_{Ba}

3.3 Basal nNOS activity was removed to improve resolution of NO-dependent modulatory effects.

nNOS will still be active in the slices during and after brain slice preparation, and therefore NO will still be produced in the neurons, and any NO liberated by the other NOS enzymes during the preparation could also act on our neurons of interest. This would mean that different neurons could be exposed to different levels of NO, producing another source of variability in the recordings. To control for this, slices were incubated with the NOS inhibitor 7-nitroindazole (7-NI, 10µM) whilst in their incubation chambers, and 7-NI was also included in the bath solution. In later experiments NO was applied exogenously to the slices by means of a donor molecule, either diethyl ammonium nonoate (DEA, 100µM) or sodium nitroprusside (SNP, 100µM).

To investigate the level of basal nNOS activity and NO-dependent modulation of the slices, unpaired recordings of the whole cell I_{Ba} were made from neurons from untreated and 7-NI treated slices.

Data from the various treatment goups (7-NI, DEA and SNP treated) were compared to the control group using a one-way ANOVA followed by Tukey's post-hoc tests for pairwise comparison (Figure 3.3.). Post-hoc tests were only performed if significant difference between groups was observed.

The IVs generated by these experiments are shown in Figure 3.2. A, 7-NI (black circles) slightly reduces the amplitude of the I_{Ba} compared to untreated control conditions (open circles), and hints at a rightward shift in voltage dependence of activation. However this amplitude difference is not significant as confirmed in the summary bar

graph in Figure 3.2. B: I_{Ba} peak amplitude was 0.94±0.06nA (n=6); I_{Ba}+7-NI peak amplitude was 0.98±0.09nA (n=6, Tukey's: p>0.05). The activation curves in Figure 3.2. C confirm a lack of effect of 7-NI on the voltage dependence of the currents, plotted as G/G_{Max} fitted with a Boltzmann function of the form: $I=I_{max}/(1+\exp(V-V_{1/2}/k)$. I_{Ba} $V_{1/2}$ was -20.25±0.4mV (n=6) and I_{Ba} +7-NI $V_{1/2}$ was -25.5±1.5mV (n=6) (p>0.05)

These data suggest that blocking NOS activity with 7-NI has little effect on the I_{Ba}. This could mean that there is little residual basal modulation of the I_{Ba} or that, what modulation there is, is not removed by blocking NOS activity.

Despite the lack of a significant effect of 7-NI on I_{Ba}, it was decided that the most accurate way to observe NO dependent modulation of the calcium channels would be to always include 7-NI in the incubation chamber and recording solutions. Henceforth all data is in the presence of 7-NI unless otherwise stated.

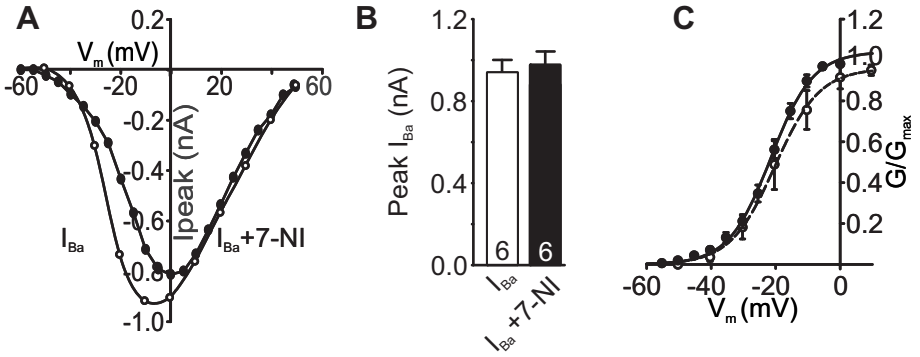

Figure 3.2. Basal nNOS activity was removed to improve resolution of NO-dependent modulatory effects.

A. IV of I_{Ba} (white circles) vs I_{Ba}+7-NI (black circles) from two cells. **B.** Summary bar graph of mean±SEM peak I_{Ba} current (white bar) and I_{Ba}+7-NI treated cells (black bar). **C.** Activation curve showing voltage dependence of activation of I_{Ba} (white circles) vs I_{Ba} +7-NI treated cells (mean±SEM).

3.4 NO potentiates whole cell I_{Ba}.

Using the optimisation strategies described it was then possible to move on to characterising NO's effect on the whole cell I_{Ba}. Following NOS inhibition by 7-NI, slices were exposed to NO by means of exogenous donor molecules, either diethyl ammonium nonoate (DEA, 100µM) or sodium nitroprusside (SNP, 100µM). This aimed to push the physiology in such a way as to maximise any NO-dependent effect.

Data from DEA and SNP treated cells were compared with data from 7-NI treated cells presented in Figure 3.2. using one-way ANOVA with Tukey's post-hoc test.

Neurons were patch clamped in the whole cell configuration and subjected to the voltage command protocol described in Figure 3.1. A. The raw currents generated by a step depolarisation to -10mV in 7-NI(black trace), DEA (green trace) and SNP (red trace) treated cells are shown in Figure 3.3. A. The representative traces show a potentiation of I_{Ba} in the NO-treated cells compared to the 7-NI cell. The IV in Figure 3.3. B shows that this potentiation is maintained across the data set. The potentiation of the peak amplitude by the NO donors is statistically significant when the groups are compared using one-way ANOVA, however pairwise comparison using a Tukey's post-hoc test reveals no significant differences. This is shown in the summary Bar graph in Figure 3.3. C, mean±SEM peak amplitudes: 7-NI amplitude was 0.98±0.09nA (n=6, black bar); 7-NI + DEA amplitude was 1.5±0.2nA (n=5, green bar); and 7-NI + SNP amplitude was 1.6±0.4nA (n=3, red bar) (Tukey's: 7-NI vs 7-NI+DEA, and 7-NI vs 7-NI+SNP: $p>0.05$). Despite this, there is a clear trend for an NO-dependent potentiation of the whole cell current.

No effect of NO on the inactivation time course (τ) of the currents was observed, as calculated by plotting the exponential decay from the peak of the current to the end of the voltage step: 7-NI τ was 134±8ms; DEA τ was 134±6ms; and SNP τ was 133±5ms (one-way ANOVA: p=0.9) (Figure 3.3. D). Also, the voltage dependence of the current was not affected by NO, as shown in Figure 3.3. E: 7-NI $V_{1/2}$ of activation was -25.5±1.5mV (black circles, n=6); 7-NI+DEA $V_{1/2}$ was -30.4±2.0mV (green circles, n=5) and 7-NI+SNP $V_{1/2}$ was -23.5±1.5mV (red circles, n=3) (one-way ANOVA:p=0.06). Boltzmann curves were fitted according to the equation described in section 1.2.

NO delivered by donor molecules DEA and SNP potentiates the whole cell I_{Ba} without affecting the time course of inactivation or its voltage dependence, but how does it affect each Ca_V subtype and their contribution to the whole cell I_{Ba}?

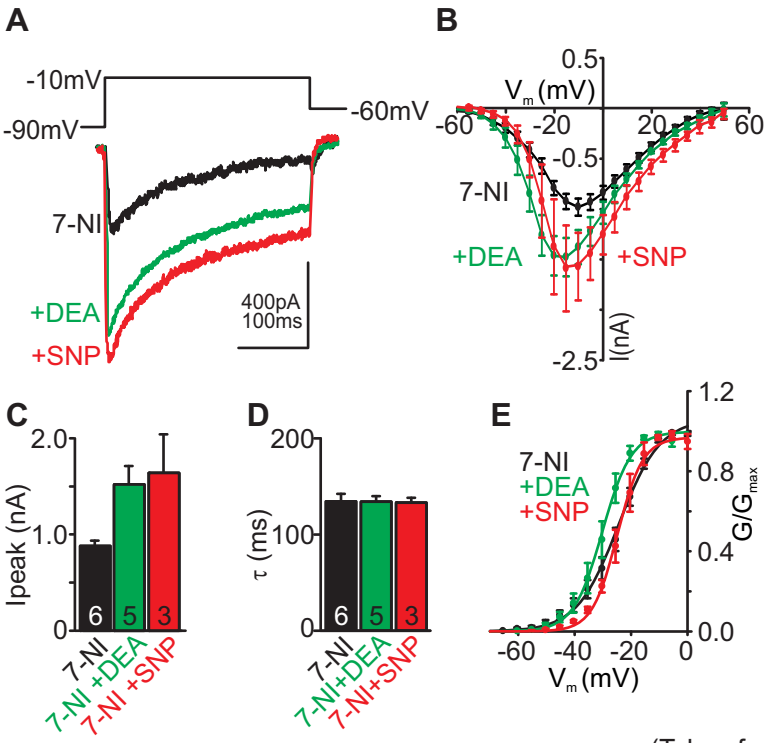

(Taken from Tozer *et al.* 2012)

Figure 3.3 Nitric oxide augments whole-cell barium currents.

A. (bottom) Raw traces of unpaired I_{Ba} recorded from a 7-NI neuron (black trace), one treated with NO donor DEA (100μM, green trace) and one with SNP (100μM, red trace) using the protocol shown (top). **B.** Average mean±SEM IV curves for I_{Ba} from neurons treated with 7-NI (black circles), 7-NI+DEA (green circles) or 7-NI+SNP (red circles). **C.** Summary bar graph of mean±SEM peak I_{Ba} currents of 7-NI (black bar) and 7-NI+NO-donor treated, DEA (green bar) and SNP (red bar). **D.** Summary bar graph of Mean±SEM inactivation kinetics (τ) of currents evoked by step depolarisation to -10mV. **E.** Activation curve of normalised mean±SEM I_{Ba} conductance in 7-NI (black circles), 7-NI+DEA (green circles) and 7-NI+SNP (red circles) treated neurons. Curves show a Boltzmann fit.

3.5 NO differentially modulates natively expressed Ca_Vs.

As both NO donors potentiated the I_{Ba} without affecting its kinetics or voltage dependence, and as DEA has a shorter half-life (2 minutes) in solution than SNP (Keefer *et al.*, 1996), it was decided to pursue this question using SNP as the NO donor. Each subtype was isolated pharmacologically along with R-type current, as the available blocker of R-type current (SNX-482) is known not to be 100% effective (Newcomb *et al.* 2006), and so was not used. The isolated currents were measured from neurons in the presence of 7-NI or 7-NI+SNP. Slices were allowed 15 minutes treatment with SNP before neurons were patched to allow for sufficient wash on and activation of downstream NO pathways.

3.6 NO potentiates L-type (Ca_V1) current.

L-type (and R-type) current was isolated by blocking P/Q-type currents and N-type currents with known antagonists, ω-agatoxin IVA (200nM) (Mintz *et al.* 1992) and ω-conotoxin GVIA (2μM) (Boland *et al.*1994; Barnes-Davies, 2001) respectively.

Data from these cells in 7-NI and 7-NI+SNP treated conditions were compared with data from cells in L+R-type +7-NI+SNP+ODQ treated conditions presented in Figure 3.10. using one-way ANOVA with Tukey's post-hoc test for pair-wise comparison.

Neurons were patch clamped in the whole cell configuration and subjected to the voltage command protocol described in Figure 3.1. A. The representative raw traces from a control and NO treated cell reveal a marked potentiation of the L-type (+R-type) current by NO (Figure 3.4. A), the potentiation is maintained across the data set as shown by the averaged IV (Figure 3.4. B): L+R-type 7-NI peak amplitude was 0.36±0.04nA (n=5, black trace), and was increased to 0.64±0.11nA (n=5, red trace,

p<0.05) by NO treatment. No effect on the inactivation time course (τ) of the current was observed in the presence of 7-NI+NO compared to 7-NI as summarised in the bar graph: L+R-type +7-NI τ was 179±10ms (n=5, black bar) and L+R-type +7-NI +SNP τ was 214±18ms (n=5, red bar, p=0.07) (Figure 3.4. C). Similarly, No effect of NO on the voltage dependence of activation was observed either: L+R-type +7-NI half-activation voltage ($V_{1/2}$) was -26.5±1.7mV (n=5, black circles) and L+R-type +7-NI +SNP $V_{1/2}$ was -26.1±1.3mV (n=5, red circles, p=0.13), curves fitted to a Boltzmann as described earlier.

NO significantly potentiated the peak amplitude of the L+R-type +7-NI current without affecting the inactivation tau or the voltage dependence of activation of the currents.

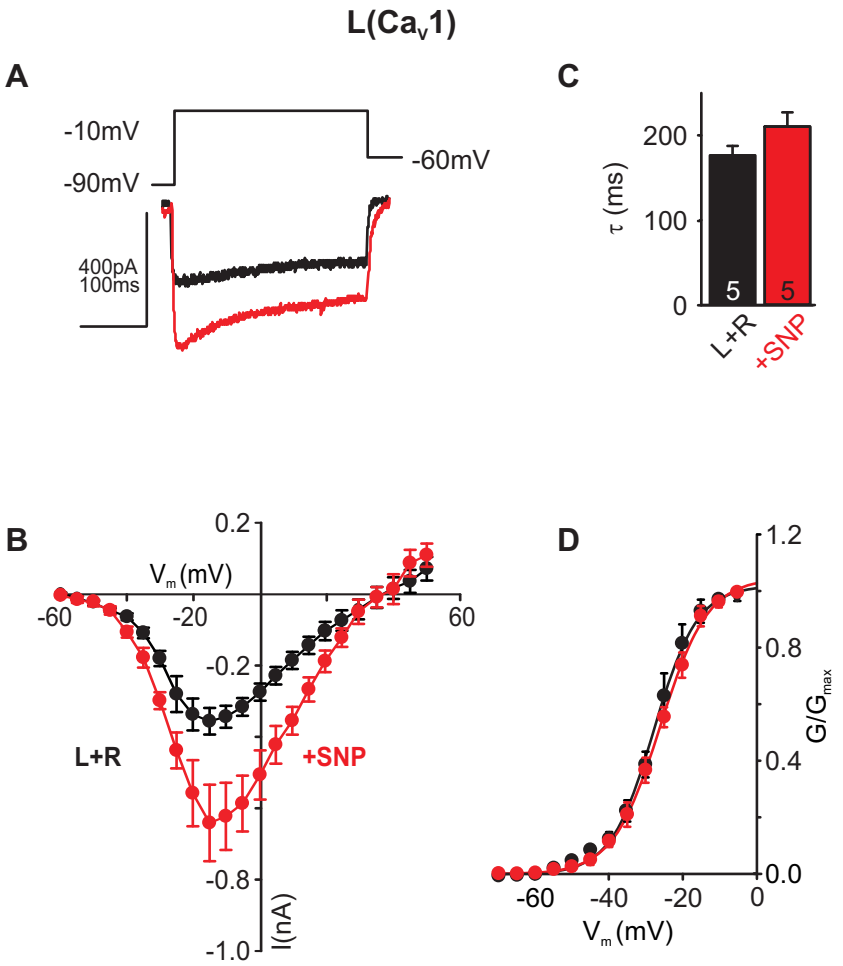

(Adapted from Tozer *et al.* 2012)

Figure 3.4. NO potentiates L-type (Ca_V1) current.

A. (bottom) Raw traces of unpaired L+R-type current recorded from a 7-NI neuron (black trace) and SNP treated (100μM, red trace) using the protocol shown (top). **B.** Average mean±SEM L+R-type IV curves from 7-NI neurons (black circles) and 7-NI+SNP treated (red circles). **C.** Summary bar graph of mean±SEM inactivation kinetics (τ) of L+R-type currents in 7-NI (black bar) and 7-NI+SNP treated (red bar) cells. **D.** Activation curves of normalised mean±SEM L+R-type conductance in 7-NI (black circles) and 7-NI+SNP treated (red circles) neurons. Curves show a Boltzmann fit.

3.7 NO potentiates P/Q-type ($Ca_V2.1$) current.

P/Q-type (and R-type) current was isolated by blocking L-type and N-type currents with known antagonists, nifedipine (10μM) and ω-conotoxin GVIA (2μM), respectively.

Data from these cells in 7-NI and 7-NI+SNP treated conditions were grouped with data from cells in 7-NI+SNP+ODQ treated conditions presented in Figure 3.11. and compared using one-way ANOVA with Tukey's post-hoc test for pair-wise comparison.

Neurons were patch clamped in the whole cell configuration and subjected to the voltage command protocol as described previously. The representative raw traces from a 7-NI and 7-NI+SNP treated cell reveal a marked potentiation of the P/Q-type (+R-type) current by NO (Figure 3.5. A), the potentiation is maintained across the data set as shown by the averaged IV (Figure 3.5. B): P/Q+R-type 7-NI peak amplitude was 0.55±0.10nA (n=4, black circles), and 7-NI+SNP treatment increased peak amplitude to 0.94±0.05nA (n=4, red circles, p=0.06). No effect on the inactivation time course (τ) of the current was observed in the presence of NO compared to 7-NI as summarised in the bar graph: P/Q+R-type +7-NI τ was 123±12ms (n=4, black bar) and 7-NI +SNP treated τ was 158±15ms (n=4, red bar, p=0.06) (Figure 3.5. C).Similarly, no effect of NO on the voltage dependence of activation was observed either: P/Q+R-type +7-NI $V_{1/2}$ was -19.7±4.1mV (n=4, black circles) and 7-NI+SNP-treated $V_{1/2}$ was -21.5±3mV (n=4. Red circles, p=0.8), curves fitted to a Boltzmann.

As with the L+R-type current, 7-NI+SNP potentiated the peak amplitude of the P/Q+R-type current, although this was not quite statistically significant, without affecting the inactivation tau or the voltage dependence of activation of the currents.

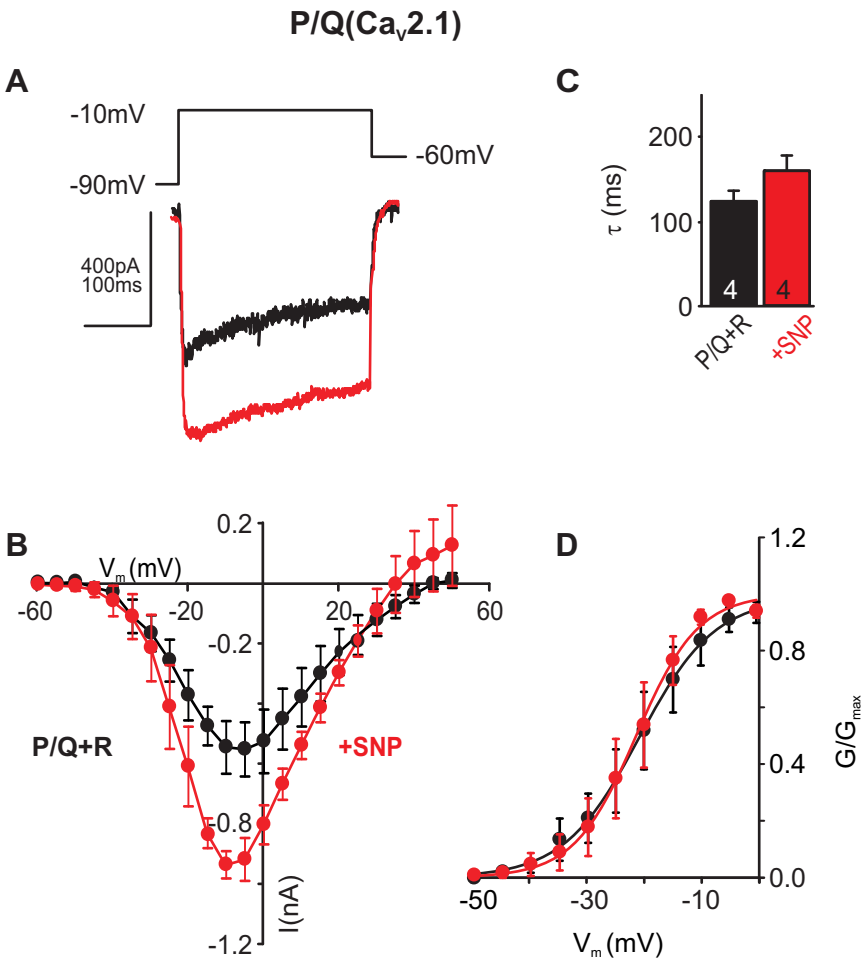

(Adapted from Tozer *et al.* 2012)

Figure 3.5. NO potentiates P/Q-type ($Ca_V2.1$) current.

A. (bottom) Raw traces of unpaired P/Q+R-type current recorded from a7-NI neuron (black trace) and 7-NI+SNP treated (100μM, red trace) using the protocol shown (top). **B.** Average mean±SEM P/Q+R-type IV curves from7-NI neurons (black circles) and 7-NI+SNP treated neurons (red circles). **C.** Summary bar graph of Mean±SEM inactivation kinetics (τ) of P/Q+R-type currents in 7-NI (black bar) and 7-NI+SNP treated (red bar) cells. **D.** Activation curves of normalised mean±SEM P/Q+R-type conductance in7-NI (black circles) and 7-NI+SNP treated (red circles) neurons. Curves show a Boltzmann fit.

3.8 NO induces a leftward shift in voltage dependence of the N-type ($Ca_V2.2$) current, but does not affect its amplitude.

N-type (and R-type) current was isolated by blocking L-type currents and P/Q-type currents with known antagonists, nifedipine (10μM) and ω-agatoxin IVA (200nM) respectively.

Data from these cells in 7-NI and 7-NI+SNP treated conditions were grouped with data from cells in 7-NI+SNP+ODQ treated conditions presented in Figure 3.12. and compared using one-way ANOVA with Tukey's post-hoc test for pair-wise comparison.

Neurons were patch clamped in the whole cell configuration and subjected to the voltage command protocol as described previously. The representative raw traces from a 7-NI and 7-NI+SNP treated cell reveal no effect of NO on the N-type (+R-type) current (Figure 3.6. A), this lack of amplitude modulation is maintained across the dataset as shown by the averaged IV (Figure 3.6. B): N+R-type +7-NI was 0.70±0.10nA (n=6), and N+R-type 7-NI+SNP was 0.69±0.08nA (n=8, p=0.98). Although there was no effect on the peak amplitude of the current, the IV hints at a more negative activation of the current in the presence of NO. No effect on the inactivation time course (τ) of the current was observed in the presence of NO compared to control as summarised in the bar graph: N+R-type +7-NI τ was 158±18ms (n=6, black bar) and 7-NI+SNP-treated τ was 146±9ms (n=8, red bar, p=0.29) (Figure 3.6. C).

NO induced a significant leftward shift in the voltage dependence of the current, as described in the activation curve where the normalised conductance of the channels is plotted as G/G_{max}: N+R-type +7-NI $V_{1/2}$ was -20.9±2.8mV (n=6, black circles), whereas

the 7-NI+SNP-treated $V_{1/2}$ was -29.7±2.6mV (n=8, red circles, $p<0.05$), curves fitted to a Boltzmann as described earlier (Figure 3.6. D).

In contrast to NO's effect on L and P/Q-type currents, NO did not potentiate the amplitude of the N-type current, but it did cause a leftward shift in the voltage dependence of the current.

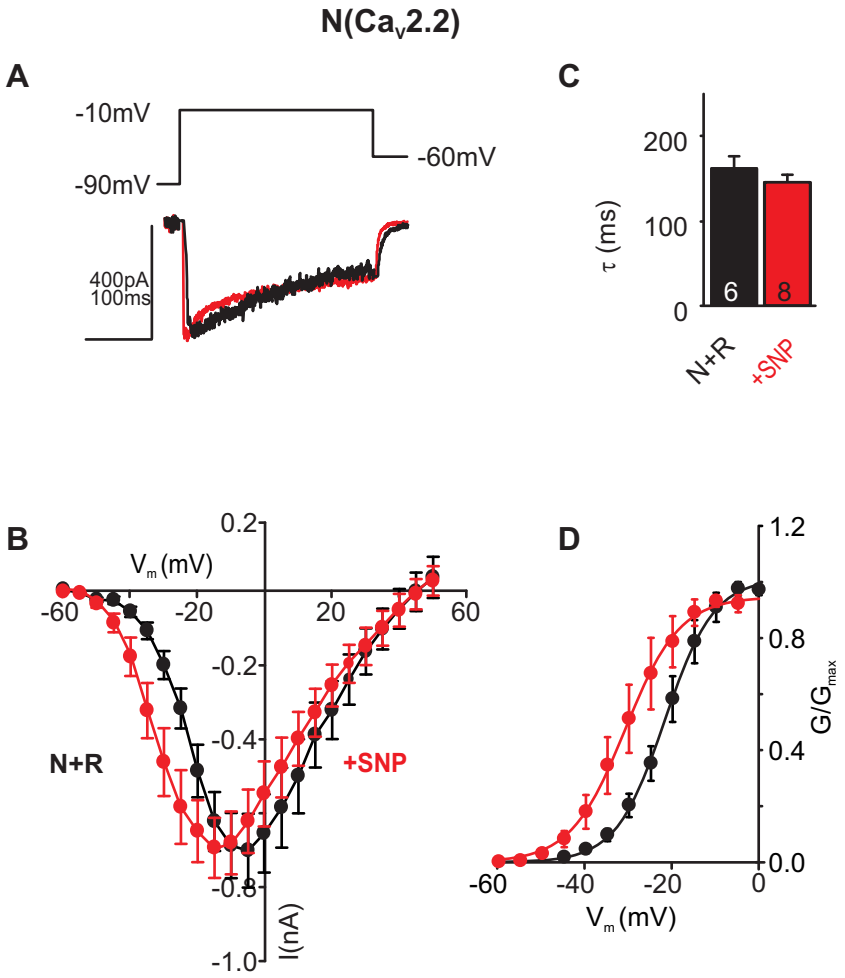

(Adapted from Tozer *et al.* 2012)

Figure 3.6. NO induces a leftward shift in voltage dependence of the N-type ($Ca_V2.2$) current, but does not affect its amplitude.

A. (bottom) Raw traces of unpaired N+R-type current recorded from a 7-NI neuron (7-NI, black trace) and 7-NI+SNP treated (100μM, red trace) neuron using the protocol shown (top). **B.** Average mean±SEM N+R-type IV curves from 7-NI neurons (black circles) and 7-NI+SNP treated neurons (red circles). **C.** Summary bar graph of mean±SEM inactivation kinetics (τ) of N+R-type currents in 7-NI (black bar) and 7-NI+SNP treated (red bar) cells. **D.** Activation curves of normalised mean±SEM N+R-type conductance in7-NI (black circles) and 7-NI+SNP treated (red circles) neurons. Curves show a Boltzmann fit.

3.9 NO does not modulate R-type ($Ca_V2.3$) current

R-type current was isolated by blocking L-type, P/Q-type and N-type currents with known antagonists, nifedipine (10μM), ω-agatoxin IVA (200nM) and ω-conotoxin GVIA (2μM) respectively. The pharmacological agents were allowed to wash on for 10 minutes before recording, and were continually perfused at 1ml/min.

Neurons were patch clamped in the whole cell configuration and subjected to the voltage command protocol as described previously. The representative raw traces generated by a step depolarisation to -10mV reveal no effect of NO on the R-type current (Figure 3.7. A), this lack of effect on current amplitude is maintained across the dataset as shown by the averaged IV (Figure 3.7. B): R-type +7-NI was 0.42±0.08nA (n=8) and R-type +7-NI+SNP was 0.30±0.13nA (n=4, p=0.48, unpaired t-test). The inactivation tau was calculated by plotting the exponential decay of the first 50ms following the peak of the R-type current because it was thought there may be more than one component contributing to the decay phase in this scenario. This could be explained by incomplete block of the other currents by the pharmacological agents. The results of this method of tau analysis are summarised in the bar graph in Figure 3.7. C and show that there is no significant difference between 7-NI and 7-NI+SNP treated neurons: R-type +7-NI τ was 55±6ms (n=8) and 7-NI+SNP-treated τ was 74±19ms (n=4, p=0.41, unpaired t-test). No effect of NO on the voltage dependence of activation was observed either: +7-NI $V_{1/2}$ was -21.7±3.1mV (n=8) and NO-treated $V_{1/2}$ was -28.2±6.0mV (n=4, p=0.39, unpaired t-test).

NO does not modulate R-type current in these neurons. Of the four HVA subtypes expressed in the MNTB: L-type and P/Q-type I_{Ba} amplitudes are potentiated by NO; N-type voltage dependence is leftward shifted; and R-type is unaffected.

The next question to address is by which pathways are these modulatory effects happening? Are they all happening via the same pathway? Are the observed modulatory effects sustained over time or are they transient? We are only viewing a snapshot of NO's effect on the currents and so investigating their modulation with time of NO exposure could help to answer some of these questions.

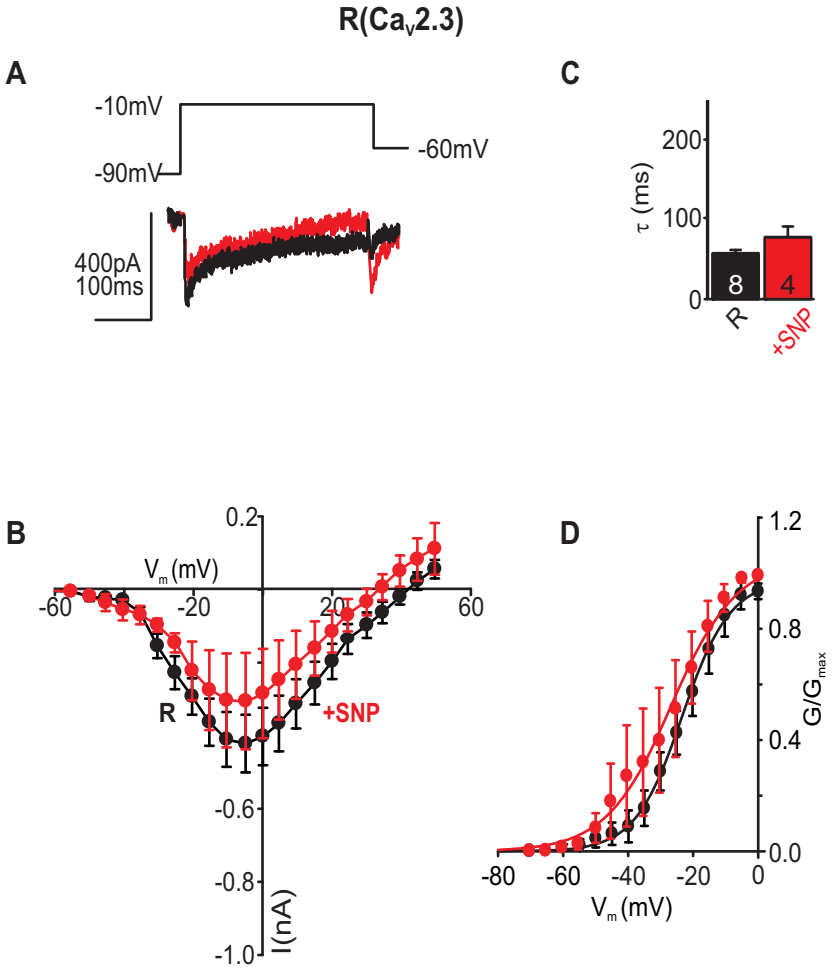

(Adapted from Tozer *et al.* 2012)

Figure 3.7. NO does not modulate R-type ($Ca_V2.3$) current.

A. (bottom) Raw traces of unpaired R-type current recorded from a 7-NI neuron (black trace) and 7-NI+SNP treated (100μM, red trace) neuron using the protocol shown (top). **B.** Average mean±SEM R-type IV curves from 7-NI neurons (black circles) and 7-NI+SNP treated neurons (red circles). **C.** Summary bar graph of Mean±SEM inactivation kinetics (τ) of R-type currents in 7-NI (black bar) and 7-NI+SNP treated (red bar) cells. **D.** Activation curves of normalised mean±SEM R-type conductance in 7-NI (black circles) and 7-NI+SNP treated (red circles) neurons. Curves show a Boltzmann fit.

3.10 Observed modulation does not change over time.

A temporal dependence of the observed effects could shed some light on the pathway by which the channels are modulated i.e. by the NO-cGMP pathway or by S-nitrosylation, one of the pathways could have a faster onset of modulation than the other, for example. It was also considered that NO-dependent modulation could lead to a change in channel expression with time, such as that shown with K_V2 channels (Steinert *et al.* 2011), although this happens after ~1hour NO exposure. Any such effects could be observed as a change in peak amplitude of currents in cells treated with NO over time.

7-NI treated slices were exposed to NO donors and cells were patched, their peak currents were plotted against their time of NO exposure. Slices were allowed 15 minutes prior to patching to allow for the donor to wash on and generate NO. This meant however that any transient or fast NO-dependent modulation that happened within 0-15 minutes of NO exposure was missed.

The averaged 7-NI (black circles, mean±SEM) and 7-NI+NO-exposed (SNP, red circles; DEA, green circles) whole-cell peak current amplitudes are shown in Figures 3.8. A-E. The potentiation of total whole-cell, L+R-type and P/Q+R-type currents observed in the previous figures was maintained over 5-60min of NO exposure (Figure 3.8. A-C). Similarly, the null-effect of NO on N+R- and R-type current amplitudes was also maintained over the 60min of NO exposure (Figure 3.8. D and E). Due to the lack of a temporal aspect to the NO-dependent modulation of the currents it was possible to summarise the observed current amplitude changes in the bar graph in Figure 3.8. F.

Data from these cells were compared using one-way ANOVA with Tukey's post-hoc test for pair-wise comparison.

The bar graph shows the potentiating effect of the pooled NO donors (100µM DEA and 100µM SNP) on the whole-cell I_{Ba}: 7-NI treated peak I_{Ba} was 0.98±0.09nA (n=6) and 7-NI+NO treated was 1.52±0.18nA (n=8, $p<0.05$). It also shows the potentiation of L+R- and P/Q+R-type currents by the NO donor SNP (100µM): L+R-type +7-NI was 0.36±0.04nA (n=5), and L+R-type+7-NI+SNP increased to 0.64±0.11nA (n=5)($p<0.05$); P/Q+R-type +7-NI was 0.55±0.10nA (n=4), and P/Q+R+7-NI+SNP increased to 0.94±0.05nA (n=4, $P<0.01$). N+R-type +7-NI and R-type +7-NI current amplitudes were unaffected in cells treated with SNP (100µM): N+R-type +7-NI was 0.70±0.10nA (n=6) and N+R-type +7-NI +SNP was 0.69±0.08nA (n=8, $p>0.05$); R-type +7-NI was 0.42±0.08nA (n=8) and R-type +SNP was 0.30±0.13nA (n=4, Figure 3.8. F).

Overall the NO-dependent modulation of the HVA currents was constant and unchanged, meaning that the modulation observed in the previous sections is maintained over an hour. Unfortunately these data do not tell us anything about the pathway by which these channels are modulated, the resolution of any temporal aspect that could provide a clue to this is clouded by the fact that SNP is given 15minutes to wash on to the slice before recordings. Also, if recordings were made during this 15 minute window, it would be difficult to separate an artefact of the NO concentration increasing in the bath from an actual temporal effect on the channels.

The maintenance of the channel modulation over time suggests that NO does not cause a change in Ca_V subtype expression. If channels were internalised due to NO I might expect a decrease in the current amplitude, if there was increased expression I

would expect the opposite. The only subtype which might hint at a temporal change in amplitude is the R-type, as it shows a trend for a decrease in amplitude with time. However, with such a small data set, and a recording at ~35minutes that bucks this trend, it is difficult to draw a conclusion from this experiment.

These data suggest the relative contribution of each subtype to the whole cell current is changed by NO, swinging from being mainly N and R-type dependent to L and P/Q.

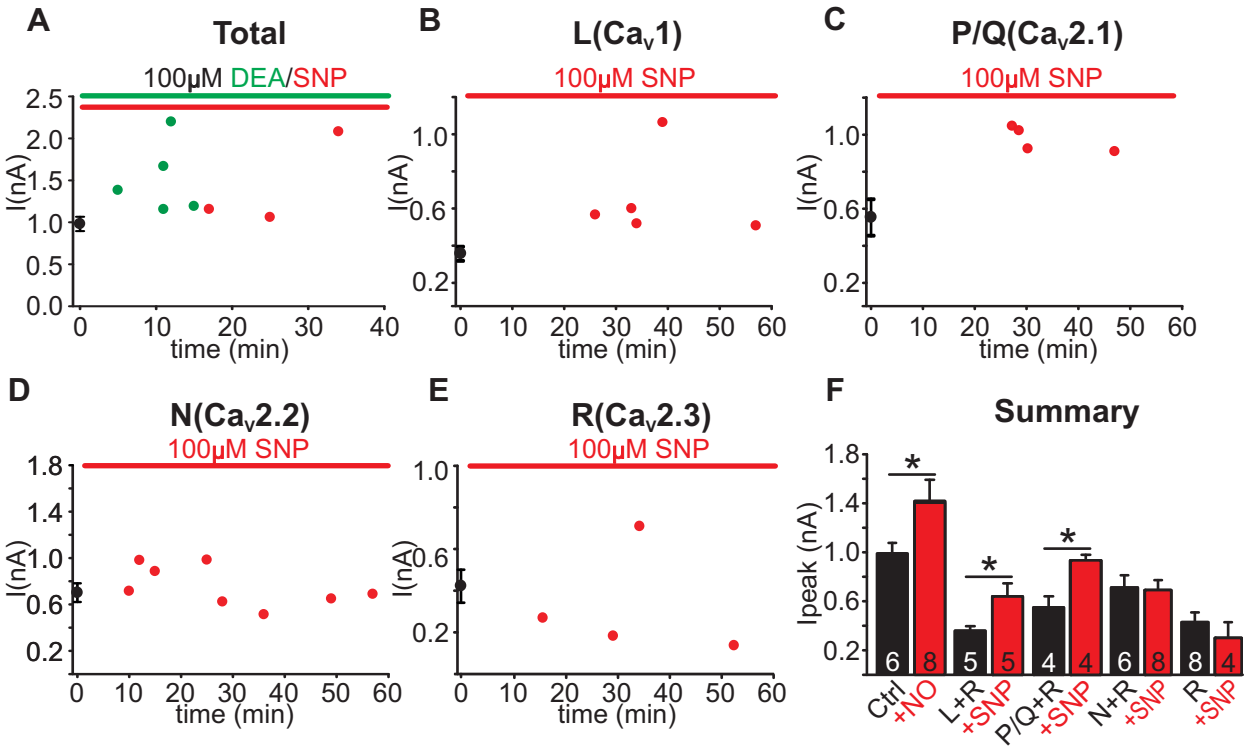

Figure 3.8. NO-dependent modulation of channel subtypes is maintained over time.

A, Peak whole-cell I_{Ba} amplitudes from unpaired recordings, 7-NI (black , mean±SEM), 7-NI+SNP (red)- and 7-NI+DEA (green)-treated neurons. **B**, Peak L-type (+R-type) current amplitudes from unpaired recordings made from 7-NI (black, mean±SEM) and 7-NI+SNP-treated (red) neurons. **C**, Peak P/Q-type (+R-type) current amplitudes from unpaired recordings made from 7-NI (black, mean±SEM) and 7-NI+SNP-treated (red) neurons. **D**, Peak N-type (+R-type) current amplitudes from unpaired recordings made from 7-NI (black, mean±SEM) and 7-NI+SNP-treated (red) neurons. **E**, Peak R-type current amplitudes from unpaired recordings made from 7-NI (black, mean±SEM) and 7-NI+SNP-treated (red) neurons. **F**, Contribution of the different Ca_V subtypes to whole-cell currents under 7-NI (black) and nitrergic conditions (red). R-type current was present throughout all recordings. Note the large proportional increase in L- and P/Q-type currents following NO exposure. Data denote mean±SEM, n=number of neurons, one-way ANOVA with Tukey's post-hoc tests, *P<0.05, **P<0.01.

3.11 NO changes the relative contribution of each of the Ca_V subtypes to the whole cell current.

NO differentially modulates the Ca_V subtypes and so changes their relative contribution to the whole cell current. This might be important for the cell as different routes of calcium entry could lead to or underlie specific cellular, functional or signalling changes (Steinert *et al.*, 2010). Calculating each subtype's contribution to the whole cell current is difficult, except for R-type, as each current is isolated pharmacologically with R-type. Therefore any variability in the size of the R-type current amplitude will sum with any variability in the amplitude of the current of interest. It is also important to acknowledge that no pharmacological blocker is one hundred percent effective or even selective. So again, the act of adding pharmacological blockers could have variable effects between cells and slices. Taken together with the inherent variability between cells (location in the nucleus, age of animal, for example), and the emerging evidence that the MNTB is not a nucleus of homogenous cells (Grande & Wang, 2011), there are a number of sources of variation that will contribute to error when averaging measured currents.

Table 3.3 shows the recorded mean peak current amplitude data for the isolated Ca_V subtypes in the absence and presence of NO, and their associated standard error (SEM). As R-type is the only subtype that is solely isolated, we could calculate the size of the other currents by subtracting its amplitude from them, and observing their contribution to the whole cell current. This is loosely achieved using the mean values, not accounting for the SEM, and we arrive at this conclusion for control conditions: R-type, 0.422nA; N-type, 0.28nA; L-type, 0.066nA; P/Q-type, 0.131nA; summing gives a

total estimated I_{Ba} of 0.767nA. In the presence of NO the current amplitudes change: R-type, 0.303; N-type, 0.391; L-type, 0.338; P/Q type, 0.634, which gives an estimated total I_{Ba} of 1.666nA. From this gross calculation we can see that NO greatly potentiates L and P/Q type currents whilst not affecting N and R-type currents, and this underlies the 2 fold increase in the whole cell I_{Ba} amplitude.

	-NO		+NO	
Channel	Current (nA)	SEM	Current (nA)	SEM
R	0.422	0.080	0.303	0.129
N+R	0.702	0.010	0.694	0.081
L+R	0.356	0.037	0.641	0.107
P/Q+R	0.553	0.090	0.937	0.045
Estimated IBa	0.767	0.211	1.666	0.294
Observed Iba	0.980	0.085	1.519	0.175

Table 3.3 Averaged amplitude of Cav subtypes +/- NO

However we cannot simply ignore the standard error and this can be propagated. If the whole cell mean is equal to: R+N+R+L+R+PQ+R-3R, then the errors (Δ) can be propagated as such: $\Delta I_{Ba}{}^2 = (\Delta N+R^2) + (\Delta L+R^2) + (\Delta PQ+R^2) + 2^2 (\Delta R^2)$. Therefore ΔI_{Ba}= 0.211. This large propagated error could account for the discrepancy between the observed (measured) I_{Ba} amplitude and the estimated. Interestingly the discrepancy between the means is smaller in the NO treated cells.

To visualise the shift in Ca_V contribution to the whole cell I_{Ba} I have included the pie charts shown in Figure 3.9. It is clear from the charts that in the presence of NO the whole cell I_{Ba} is larger (2 fold) and the relative contribution of P/Q and L-type channels has increased from 17.1% and 0% to 38% and 20.3% respectively. In control conditions

N and R-type Ca_Vs contribute 36.5% and 55% of voltage-gated Ca^{2+} entry on depolarisation, which is reduced to 18.2% and 23.5% respectively in the presence of NO.

I will discuss the possible reasons for, or point of, this underlying shift in Ca_V contribution and increase in intracellular Ca^{2+} later. The more pressing question to answer was by which pathway does NO cause these changes?

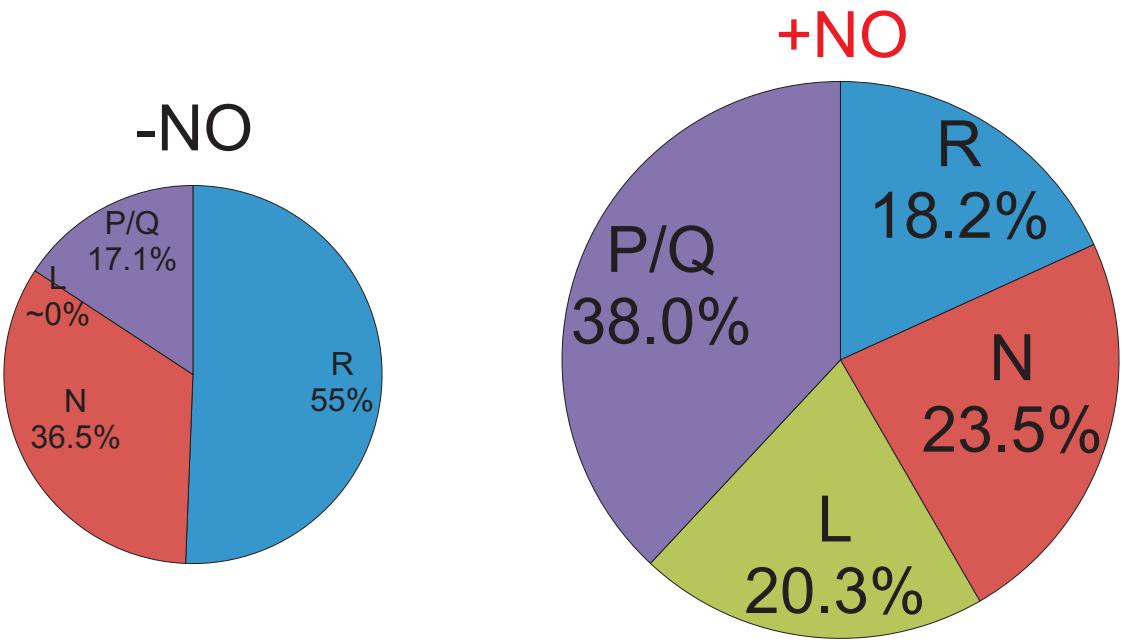

Figure 3.9. NO changes the relative contribution of each Ca_V subtype to the whole cell current.

A. Pie chart describes relative contribution of each Ca_V channel subtype to whole cell I_{Ba}. **B.** Pie chart shows how whole cell I_{Ba} is potentiated by NO, and how this changes the overall contribution of each Ca_V channels to whole cell I_{Ba}.

3.12 NO potentiates L and P/Q-type Ca_V subtypes by distinct pathways.

As NO has a differential effect on the expressed Ca_V subtypes, which is maintained over an hour, I asked whether this modulation happened when the NO-cGMP pathway was inhibited. To do this the currents were pharmacologically isolated as previously described, and SNP was added to nNOS inhibited cells as before, but this time the soluble guanylyl cyclase (sGC) blocker 1H-[1,2,4]oxadiazolo[4,3-a]quinoxalin-1-one (ODQ, 1μM) was included, inhibiting the NO-cGMP pathway.

3.13 NO-cGMP pathway does not underlie L-type potentiation.

L-type (and R-type) current was isolated by blocking P/Q-type currents and N-type currents with known antagonists ω-agatoxin IVA (200nM) and ω-conotoxin GVIA (2μM), respectively.

Neurons were patch clamped in the whole cell configuration and subjected to the voltage command protocol previously described. Data from these cells were grouped with data from cells in L+R-type +7-NI+SNP treated conditions presented in Figure 3.6 and compared using one-way ANOVA with Tukey's post-hoc test.

The representative raw traces from a 7-NI and 7-NI+SNP+ODQ treated cell reveal a potentiation of the L-type (+R-type) current by NO in the presence of the sGC blocker (Figure 3.10. A), the potentiation is maintained across the data set as shown by the averaged IV (Figure 3.10. B): L+R-type +7-NI peak amplitude was 0.36±0.04nA (n=5, black trace), and L+R-type +SNP+ODQ was 0.62±0.06nA (n=5, red trace, $p>0.05$). Although not statistically different from L+R-type+7-NI, the amplitude of the L+R-type +7-NI+SNP+ODQ treated current is also not statistically different from the 7-NI+SNP

treated current, suggesting the NO-dependent effect is not removed by blocking sGC activity.

No effect on the inactivation time course (τ) of the current was observed in the presence of SNP+ODQ compared to control as summarised in the bar graph: L+R-type τ was 179±10ms (n=5, black bar, p=0.73) and SNP+ODQ-treated L+R-type τ was 171±7ms (n=5, red bar) (Figure 3.10. C). Similarly, No effect of SNP+ODQ on the voltage dependence of activation was observed either: L+R-type half-activation voltage ($V_{1/2}$) was -26.5±1.7mV (n=5, black circles) and L+R-type +SNP+ODQ-treated $V_{1/2}$ was -22.9±0.4mV (n=5, red circles) (p=0.1), curves fitted to a Boltzmann as described earlier.

The NO-dependent augmentation of the L-type amplitude observed in Figure 3.4 is still maintained in the presence of ODQ. This implies that the NO-cGMP pathway does not have to be intact for the modulation to occur and suggests NO must be modulating this current by another route.

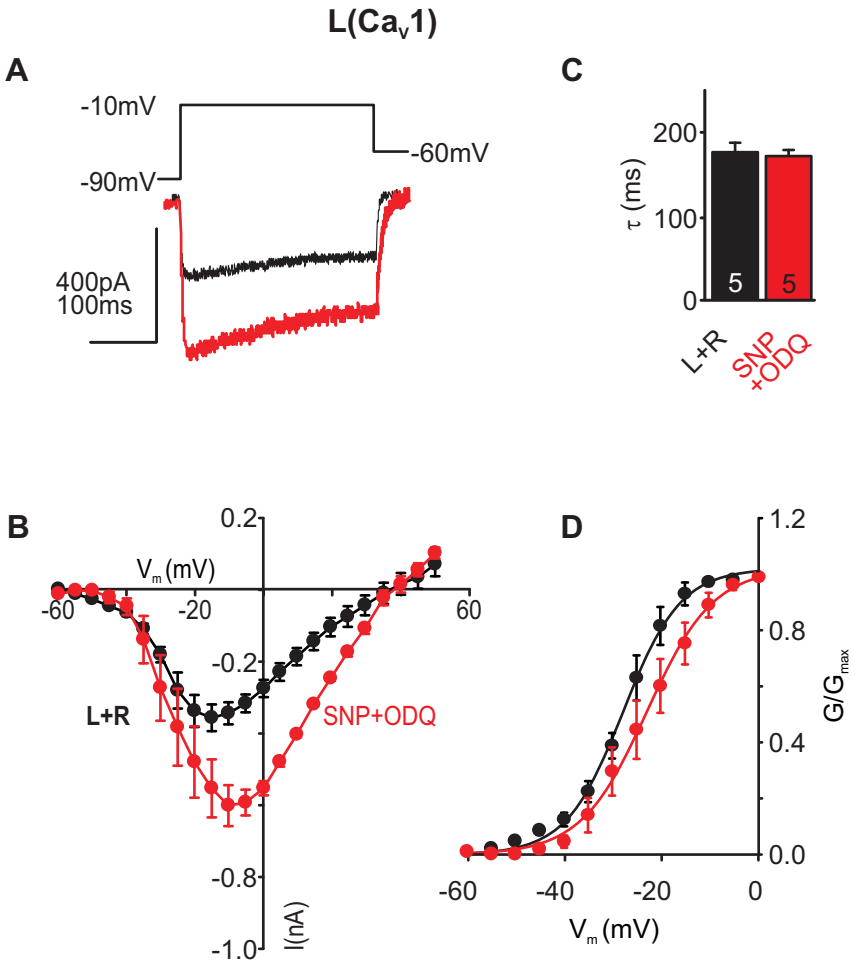

(Adapted from Tozer *et al.* 2012)

Figure 3.10. NO-cGMP pathway does not underlie L-type potentiation. **A.** (bottom) Raw traces of L+R-type current from 7-NI (black trace) and 7-NI+SNP+ODQ treated cells (red trace). Traces generated by a depolarising step from -90mV to -10mV (top). **B.** Average (mean±SEM) IVs of L+R-type current from 7-NI (black circles) and 7-NI+SNP+ODQ-treated (red circles) neurons. **C.** Bar graph shows mean±SEM inactivation kinetics (τ) of L+R-type current in 7-NI (black bar) and 7-NI+SNP+ODQ treated (red bar) neurons. **D.** Mean±SEM activation curves of L+R-type normalised conductance from 7-NI (black) and 7-NI+SNP+ODQ treated (red) neurons. Curves are fitted using a Boltzmann equation.

3.14 NO-dependent augmentation of P/Q-type current is removed by disrupting the NO-cGMP pathway.

P/Q-type (and R-type) current was isolated by blocking L-type currents and N-type currents with known antagonists: nifedipine (10μM) and ω-conotoxin GVIA (2μM), respectively.

Neurons were patch clamped in the whole cell configuration and subjected to the voltage command protocol as described previously. Data from these cells were grouped with data from cells in P/Q+R-type +7-NI+SNP treated conditions presented in Figure 3.5 and compared using one-way ANOVA with Tukey's post-hoc test.

The representative raw traces from a control and NO+ODQ treated cell reveal a removal of the previously observed potentiation (shown in Figure 3.5 A) of the P/Q-type (+R-type) current (Figure 3.11 A). The removal of the potentiation is maintained across the data set as shown by the averaged IV (Figure 3.11. B): P/Q+R-type +7-NI peak amplitude was 0.55±0.10nA (n=4, black circles), and in the presence of 7-NI+SNP+ODQ was 0.70±0.12nA (n=5, red circles) ($p>0.05$ in this pair-wise comparison). No effect on the inactivation time course (τ) of the P/Q+R-type current was observed in the presence of 7-NI+SNP+ODQ compared to 7-NI as summarised in the bar graph: P/Q+R-type+7-NI τ was 123±12ms (n=4, black bar) and P/Q+R-type+7-NI+SNP+ODQ-treated τ was 109±10ms (n=5, red bar) ($P=0.06$) (Figure 3.11. C), similarly, no effect of 7-NI+SNP+ODQ on the voltage dependence of activation was observed either: P/Q+R-type+7-NI $V_{1/2}$ was -19.7±4.1mV (n=4, black circles) and P/Q+R-type+7-NI+SNP+ODQ-treated $V_{1/2}$ was -18.8±0.4mV (n=5. Red circles) ($p=0.8$), curves fitted to a Boltzmann as described earlier (Figure 3.11. D).

The apparent NO-dependent augmentation of the P/Q-type current is removed by sGC block, meaning that an intact NO-cGMP pathway is needed for this modulation, which is in contrast to L-type current, and suggests that both currents are potentiated via different pathways.

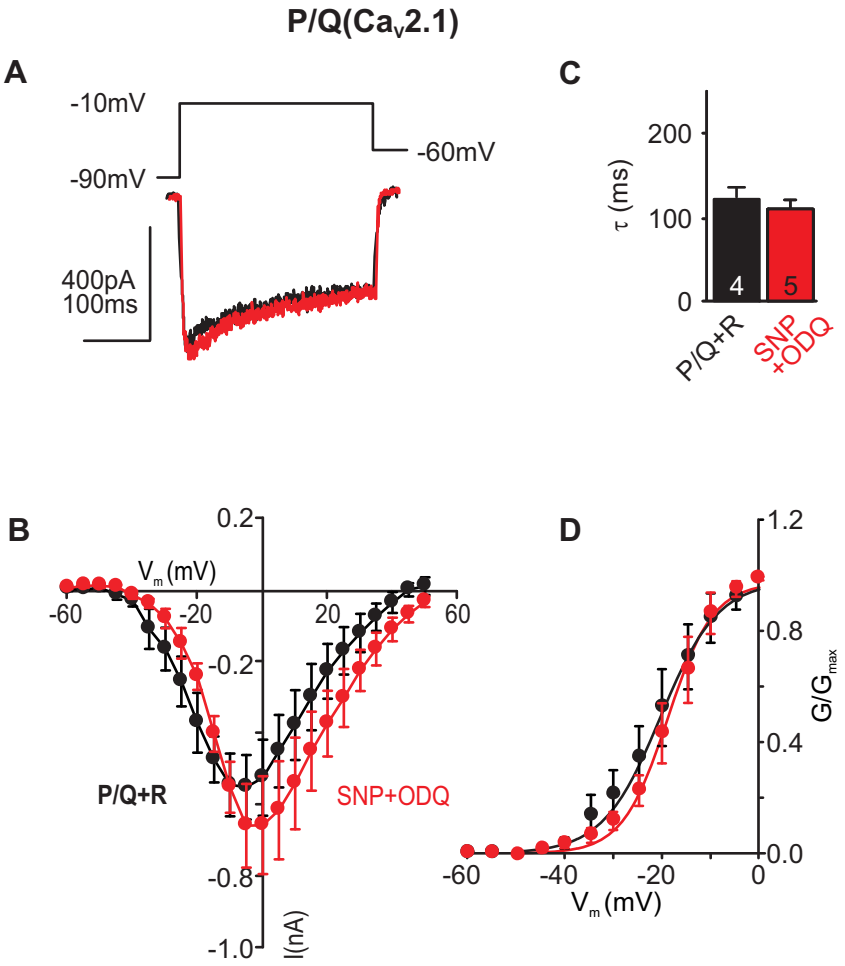

(Adapted from Tozer *et al.* 2012)

Figure 3.11. NO-dependent augmentation of P/Q-type current is removed by disrupting the NO-cGMP pathway.

A. (bottom) Raw traces of P/Q+R-type current from 7-NI (black trace) and 7-NI+SNP+ODQ treated cells (red trace). Traces generated by a depolarising step from -90mV to -10mV (top). **B.** Average (mean±SEM) IVs of P/Q+R-type current from 7-NI (black circles) and 7-NI+SNP+ODQ-treated (red circles) neurons. **C.** Bar graph shows mean±SEM inactivation kinetics (τ) of P/Q+R-type current in 7-NII (black bar) and 7-NI+SNP+ODQ treated (red bar) neurons. **D.** Mean±SEM activation curves of P/Q+R-type normalised conductance from 7-NI (black) and 7-NI+SNP+ODQ treated (red) neurons. Curves are fitted using a Boltzmann equation.

3.15 NO-cGMP pathway underlies leftward shift in N-type voltage dependence.

N-type (and R-type) current was isolated by blocking L-type currents and P/Q-type currents with known antagonists, nifedipine (10μM) and ω-agatoxin IVA (200nM) respectively.

Neurons were patch clamped in the whole cell configuration and subjected to the voltage command protocol as described previously. Data from these cells were grouped with data from cells in N+R-type +7-NI+SNP treated conditions (Figure 3.6) and compared using one-way ANOVA with Tukey's post-hoc test.

The representative raw traces from a 7-NI and 7-NI+SNP+ODQ treated cell reveal no effect of NO on the N-type (+R-type) current (Figure 3.12. A), this lack of amplitude modulation is maintained across the dataset as shown by the averaged IV (Figure 3.12. B): N+R-type+7-NI peak amplitude was 0.70±0.10nA (n=6), and 7-NI+SNP+ODQ treated was 0.67±0.92nA (n=5) (p=0.98). Although there was no effect on the peak amplitude of the current, the more negative activation of the current observed in NO treated cells is removed by the presence of ODQ. No effect on the inactivation time course (τ) of the current was observed in the presence of NO+ODQ treated neurons compared to control as summarised in the bar graph: N+R-type+7-NI τ was 158±18ms (n=6, black bar) and 7-NI+SNP+ODQ-treated τ was 128±6ms (n=5, red bar) (p=0.2) (Figure 3.12. C).

As hinted at in the IV, the NO-induced significant leftward shift in the voltage dependence of the current, shown earlier by the activation curves in Figure 3.6. D, was removed by the presence of ODQ: N+R-type+7-NI $V_{1/2}$ was -20.9±2.8mV (n=6, black

circles), whereas the 7-NI+SNP+ODQ-treated $V_{1/2}$ was -23.6±0.4mV (n=5, red circles, p>0.05 in this comparison), curves fitted using a Boltzmann fit.

The NO-induced leftward shift in voltage-dependence of the N-type current was removed by the presence of the cyclase blocker ODQ, suggesting that intact NO-cGMP signalling underlies this modulation.

These data show that the NO-cGMP pathway is necessary for the potentiation of P/Q-type current and the leftward shift in N-type current voltage dependence, but is not necessary for the potentiation of L-type current. Therefore NO is causing these modulatory effects by at least two distinct pathways.

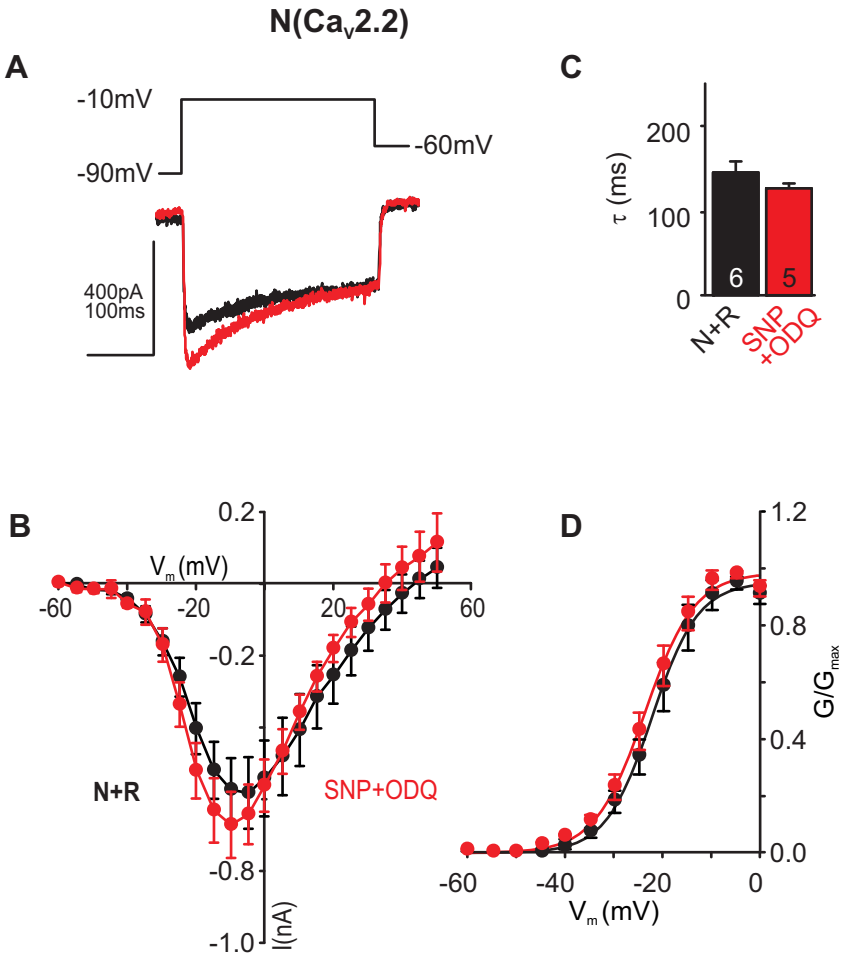

(Adapted from Tozer *et al.* 2012)

Figure 3.12. NO-cGMP pathway underlies leftward shift in N-type voltage dependence.

A. (bottom) Raw traces of N+R-type current from 7-NI (black trace) and 7-NI+SNP+ODQ treated cells (red trace). Traces generated by a depolarising step from -90mV to -10mV (top). **B.** Average (mean±SEM) IVs of N+R-type current from 7-NI (black circles) and 7-NI+SNP+ODQ-treated (red circles) neurons. **C.** Bar graph shows mean±SEM inactivation kinetics (τ) of N+R-type current in 7-NI (black bar) and 7-NI+SNP+ODQ treated (red bar) neurons. **D.** Mean±SEM activation curves of N+R-type normalised conductance from 7-NI (black) and 7-NI+SNP+ODQ treated (red) neurons. Curves are fitted using a Boltzmann equation.

3.16 Discussion

In this chapter I have described the steps I took to best investigate the effect of NO on the natively expressed Ca_V channels in the principal neurones of the MTNB. Using an experimental scenario where unpaired recordings were made using Ba^{2+} as the charge carrier, endogenous production of NO by nNOS was excluded, and NO was added to the cells by exogenous donor, at physiological temperature, allowed for an improved resolution of Ca_V channel modulation. Using this approach, I have shown that a suite of natively expressed Ca_V subfamilies are modulated differently by NO and by distinct pathways, such that L and P/Q-type currents are potentiated, N-type activation is leftward shifted and R-type is unaffected. This work has been published (Tozer *et al.*, 2012). These results reveal another piece in the jigsaw of NO-mediated modulation of cellular proteins and perhaps neuronal excitability.

Ba^{2+} was a suitable charge carrier in these experiments for the reasons already described in the above text, and has previously been used to investigate Ca_V channels in the aVCN neurons of the auditory brainstem of the rat (Doughty *et al.*, 1998) (10mM) and in the MNTB of the rat (5mM) (Barnes-Davies *et al.*, 2001). In the aVCN neurons a maximal HVA current of ~0.8nA was observed, which is comparable to the size of the I_{Ba} observed here in the MNTB, whereas in the rat MNTB a peak I_{Ba} of ~2.5nA was observed. As I used the same concentration of Ba^{2+} (5mM), I am surprised I only saw a control I_{Ba} of ~0.9nA, but this could be due to a species difference in the number of expressed channels for example. The peak I_{Ba} amplitude observed in CBA mice by the Walmsley group was 0.602±0.08nA (Leao *et al.*, 2004), which is ~1/3

smaller than in my observation. However, their I_{Ca} amplitude of 0.26±0.06nA was of similar amplitude to my observation of 0.22±0.03nA.

My observations confirm the presence of 4 HVA Ca_V conductances in the MNTB of CBA mice, which is in accordance with previous work from mice (Leao *et al.*, 2004) and rat (Barnes-Davies *et al.*, 2001). However, the L-type current I observed does not make a significant contribution to whole cell I_{Ba} until after NO exposure, whereas the Walmsley group, who present their data in relative terms, suggest 14±5% of the whole cell I_{Ba} is nifedipine sensitive, yet it is still the smallest contributor to whole cell I_{Ba}, which is in agreement with my findings. Perhaps this difference could be explained by the inclusion of 7-NI and removal of NOS activity in my control experiments? Meaning that NO-dependent modulation of L-type current could be necessary for normal channel function. The Walmsley group also show the proportional contribution of P-type to be 32±4%, N-type to be 30±4% and R-type to be 28±9%, which is in contrast with my findings (P/Q-type 38%, N-type 23.5% and R-type 18.2%). Several differences in the methodology could explain the disparity between the observed current contributions such as, the inclusion of 7-NI in my solutions, and the recording temperature used(37˚C in my investigations, as opposed to room temperature in the Walmsley group's observations).

The observed NO-dependent modulation of the currents: L-type and P/Q-type potentiation; leftward shift in voltage dependence of N-type; and a null effect on R-type, were maintained over time, which suggests that there is no change in expression levels of the Ca_V channels with exposure to NO over an hour. This is in contrast to published findings on NO's effect on K_V subunits, as K_V2 expression has been shown

increase with NO exposure (Steinert *et al.*, 2011b). Perhaps over longer periods of time some changes in Ca_V expression could take place? This is not something I will look into but nevertheless is an interesting point to consider. However, extended potentiation of Ca^{2+} influx cannot be good for a cell, especially at high levels of activity.

Which leads me to ponder the reason for NO's potentiation of the Ca_Vs as we have a scenario in a neuron where at least four different Ca_V subtypes are natively expressed, and each one is modulated differently by NO. The extent of this modulation is summarised in the bar graph in Figure 3.13. A, which shows the peak current amplitudes of all the grouped treatment conditions (statistics are one-way ANOVA with Tukey's post-hoc test, *$p<0.05$), and diagram in Figure 3.13. B. L-type channels are modulated by direct NO interaction, or by a pathway that is distinct from the NO-cGMP pathway, which could indicate S-Nitrosylation. P/Q and N-type channels need soluble guanylyl cyclase (sGC) activity for their modulation to take place, as confirmed by its removal in the presence of sGC blocker ODQ. And so their modulation is down stream of cGMP production. R-type channels are seemingly unaffected by NO's presence, at least in these cells.

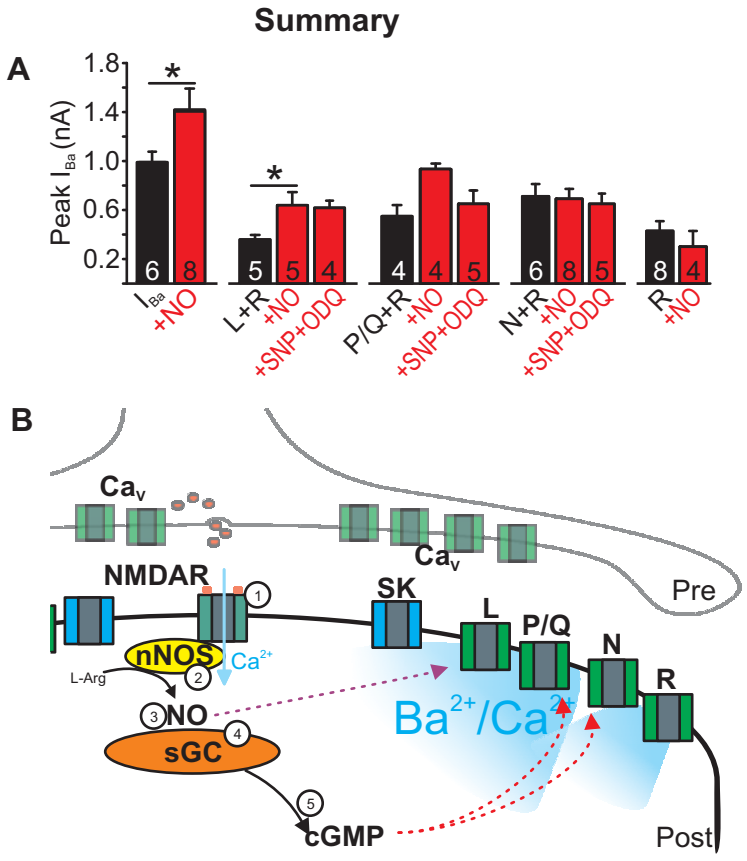

(Adapted from Tozer *et al.* 2012)

Figure 3.13. NO modulates L, P/Q and N-type channels by distinct pathways.

A. Summary bar graphs showing the effect of NO and NO+ODQ on the mean±SEM peak amplitudes of whole cell I_{Ba}, and the isolated currents. *p<0.05, one-way ANOVA with Tukey's post-hoc test.

B. Schematic illustration showing differential NO signalling to L- (direct NO effects), P/Q- and N- type (sGC-mediated effects) Ca^{2+} channels, resulting in augmented Ca^{2+} influx following nitrergic activation. **1.** Activation of NMDAR and Ca2+ influx activates nNOS. **2.** nNOS produces a molecule of NO from the breakdown of L-Arginine to L-Citrulline.**3.** NO is diffusible and could directly modulate L-type channels. **4.** Soluble Guanylyl Cyclase is activated by NO **5.** This produces cGMP which can then have other downstream effects which lead to the observed modulation of P/Q and N-type channels.

Different cell types express different channels with different auxiliary subunits. These are fast becoming recognised as important players in the world of Ca_V channel modulation (Dolphin, 2009). So my observations in the MNTB could be completely opposite to the effects observed in cells in other nuclei or organisms, and this is the case, as I will explain. Previous studies in native neurons, dissociated hair cells from frog and rat (Almanza *et al.*, 2007; Lv *et al.*, 2010), found that nitrergic activation reduced L-type and whole-cell I_{Ca} in a cGMP-dependent manner, suggesting that NO regulation differs greatly between cellular systems. Different studies in rat cultured hippocampal (Jian *et al.*, 2007) or cortical neurons (Petzold *et al.*, 2005) agree with my findings and suggest a NO-mediated increase in L-type currents. N-type currents are suppressed following activation of the classical NO-cGMP pathway in neuroblastoma IMR32 cells due to a reduction in single channel open probability (D'Ascenzo *et al.*, 2002), whereas my findings suggest more channels will be available to open at more negative voltages. In contrast, P/Q-type channels, which are found throughout the brain and are known to participate in transmitter release, are augmented by NO in BHK cells (Arikkath *et al.*, 2002; Chen *et al.*, 2002).

Many of the differences reported above could be accounted for by the differing signalling cascades initiated by NO, but also by the wealth of different isoforms of the proteins within the cascade, and the regulation that could exist to affect or tone the signalling pathway. At the measurable end, the channels, there could be a host of different subunit isoforms that can associate with the channels and affect their behaviour, and they could also interact with the signalling cascade to shape the channels response to NO.

If the potentiation in I_{Ba} that I see translates as an increase in Ca^{2+} concentration in the cell then this could have a big effect on cellular behaviour. Intracellular Ca^{2+} is critically involved in many aspects of the neuronal "life cycle", including communication, plasticity, development, differentiation, migration and cell death. And unregulated intracellular Ca^{2+} signalling pathways have been implicated in neurological diseases, such as migraine, epilepsy, ischemia, cerebral hemorrhage and Alzheimer's disease (Lipton *et al.*, 1994). NO has a ubiquitous role in health and disease of the central nervous system (Steinert *et al.*, 2010) and, perhaps not surprisingly, NO is fundamentally involved in many aspects of Ca^{2+} signalling in the neuron-glial network (Garthwaite, 1995; Willmott *et al.*, 2000; Li *et al.*, 2003).

Although Ca^{2+}entry into principal MNTB neurons occurs primarily via activation of postsynaptic AMPAR and NMDAR (Youssoufian *et al.*, 2005; Steinert *et al.*, 2008; Steinert *et al.*, 2011a), and secondarily via depolarisation-induced activation of Ca_V, my observations could imply that NO-induced enhanced Ca^{2+} influx could have important downstream signalling effects. Ca_V channel subtypes have been linked to multiple downstream signalling pathways leading to gene expression through CREB (Ca^{2+} response element binding protein), CaRF (the Ca^{2+} response factor) and NFAT (the nuclear factor of activated T-cells) (West *et al.*, 2001; Tao *et al.*, 2002), and it is important to understand how nitrergic activity might influence these Ca^{2+}-mediated pathways. Among these transcription factors, CREB is closely coupled with Ca^{2+} elevation via Ca_V channels and ligand-gated ion channels (Brosenitsch & Katz, 2001; Hardingham *et al.*, 2001; West *et al.*, 2001; Zhao *et al.*, 2007). Ultimately, Ca^{2+}-induced

gene expression has been linked to changes in intrinsic excitability mediated by L-type Ca^{2+} channels, as reported in primary hippocampal cultures (O'Leary *et al.*, 2010) or organotypic cultures of the auditory brainstem (Tong *et al.*, 2010). Ca^{2+} influx through L-type Ca^{2+} channels triggers sustained phosphorylation through mitogen-activated protein kinase (MAPK) pathways (West *et al.*, 2001; Wu *et al.*, 2001), whereas N-type Ca^{2+} channel activation leads to gene induction through PKA and PKC pathways.

This could mean that that differential modulation of Ca^{2+} entry, as reported in my observations, would lead to specific NO-dependent downstream signalling. Elevation of intracellular Ca^{2+} and specific modulation of Ca^{2+} entry pathways provide versatile mechanisms for regulating short-term events such as adaptation of excitability, or long-term effects such as gene expression, and depending on the influx pathway, this will determine neuronal communications and information transmission.

In summary, NO's differential modulation of high-voltage-activated (HVA) channels in these neurons could have big implications for the cell. As NO is produced during high frequency activity, does this mean that the channel modulation I have shown only happens at high levels of excitability? Also does NO modulate low-voltage-activated LVA channels? These are two questions that I have tried to answer and will describe in the following chapters.

4. Nitric oxide (NO)-dependent inhibition of T-type (Ca_V3) channels in the Superior Paraolivary Nucleus (SPN).

In light of NO's differential modulation of HVA currents natively expressed in the MNTB, I wondered if NO modulates low-voltage-activated (LVA) calcium currents, classically known as T-type (Catterall *et al.*, 2005). The MNTB does not express T-type channels and so the downstream superparaolivary nucleus was chosen as the model. This nucleus is proximal to, and receives strong glycinergic input from, the MNTB (Banks *et al.*, 1993). The glycine receptor mediated inhibitory postsynaptic potentials (IPSPs) silence the SPN cells which subsequently fire on relief of the inhibition in a rebound fashion, a firing phenotype known to be partly dependent on T-type channels in other neurons (Russier *et al.*, 2003). In collaboration with Conny Kopp-Scheinpflug, we investigated the native ionic conductances in the SPN of P13-P16 CBA mice in an effort to understand the ionic basis of this firing phenotype and the nuclei's role in audiology. Here I present my findings from that body of work, and show that T-type current (I_{TCa}) is present in neurons of the (SPN), contributes to the rebound firing phenotype and is inhibited by nitric oxide. A portion of this work has been published in Kopp-Scheinpflug *et al.* 2011.

4.1 Low-voltage-activated (LVA) T-type channels are expressed in superparaolivary nucleus (SPN), and contribute to rebound spiking.

4.1.1 Characterisation of T-type current.

SPN neurons were visually identified in slices from animals aged P13-16, the cells were harder to visualise than MNTB principal neurons and sparser in number. The targeting of the correct cell type was confirmed by the occurrence of rebound firing activity following hyperpolarisation, as I will describe.

T-type current (I_{TCa}) activates at voltages around -80mV. It's a transient current and rapidly activates and inactivates. The voltage step protocol used to activate I_{TCa} employed a hyperpolarising pre pulse to -100mV from a holding potential of -50mV (400ms), prior to 5mV step depolarisations from -100mV to 40mV. This enabled recruitment of I_{TCa} as excluding the pre pulse prevented activation of the LVA inward current. These experiments were done in the presence of TTx (0.5µM) and TEA (30mM), to block Na_V and K_V channels, as described in the previous chapter. The internal CsCl pipette solution was also the same as that used in the MNTB experiments. In this chapter, data presented in the figures is corrected for a junction potential of -4mV.

Ca^{2+} currents in the SPN were much larger (>1nA) than those observed in the MNTB (~400pA), and so it was possible to record the currents in aCSF containing physiological calcium (2mM), as opposed to barium (5mM) used in the MNTB investigation.

Cells were subjected to the voltage command IV protocol described above. Without the hyperpolarising pre-pulse, only HVA Ca^{2+} current was observed in the IV, identified as a bell shaped curve with a single peak at ~-10mV (gray trace and data points, Figure

4.1. A and B). Inclusion of the 400ms hyperpolarising pre-pulse to -100mV reveals a large LVA Ca_V current on a step to -50mV, introducing a second peak to the IV at ~-50mV (Figure 4.1. A and B). The current generated by this step to -50mV had a fast time course of activation, measured as the time to peak, which was 5.7±0.7ms (n=7). The current also had a fast inactivation time course, measured as the single exponential decay, of 11.5±1.4ms (n=7) (Figure 4.1. C), this was much faster than the currents recorded in the MNTB. The transient nature of this current and large amplitude at hyperpolarised potentials suggest it must be conducted through T-type Ca_V channels. This is confirmed by the partial block of this current with mibefradil (2μM), which is known to block LVA Ca_V channels at low concentrations (Martin *et al.*, 2000) (Figure 4.1. D and E). In this experiment the cells were treated with mibefradil prior to patching and a pre-pulse was included in the protocol to remove inactivation of the T-type channels, mibefradil blocked the current by ~79% (Figure 4.1. F).

Interestingly a slight hump in the inactivation phase of the I_{TCa} was observed, and removed by mibefradil. Although an example for only one cell is shown, this phenomenon was also observed in other recorded cells, and suggests a second component to the current, another LVA subtype perhaps, as it is present at more negative potentials? But this was not investigated further.

The voltage dependence of activation of I_{TCa} was calculated by plotting the normalised conductance (G/G_{max}, see methods) of the current between -100mV and -40mV as this was the $V_{command}$ that generated the first peak in the IV. This plot was fitted with a Boltzmann function and showed I_{TCa} had an activation range that was half activated at -51±0.3mV (black circles, Figure 4.1. H). To understand the percentage of the channels

available to open, i.e. not inactivated, at the different potentials in this voltage range, the cells were subjected to a protocol that generated an inactivation curve. 400ms 5mV pre-step depolarisations from -100mV were given prior to a step to -45mV command potential. The currents generated on the step to command V_m were relative to the number of channels available to open i.e. not inactivated during the pre-step. These currents were converted to conductance (G) and normalised (G/G_{max}, see methods) for plotting against pre-step V_m in Figure 4.1. H (grey circles), the plot is fitted with a Boltzmann function. The channels were half inactivated -72.8±0.4mV (Figure 4.1. H). The hump observed in the raw current traces is more obvious in the tail currents generated by the inactivation curve protocol.

The more negative voltage dependence of this current adds further evidence in support of it being mediated by LVA T-type Ca_V channels, but what is the role of this current in the SPN and does it contribute to the rebound firing phenotype of these cells?

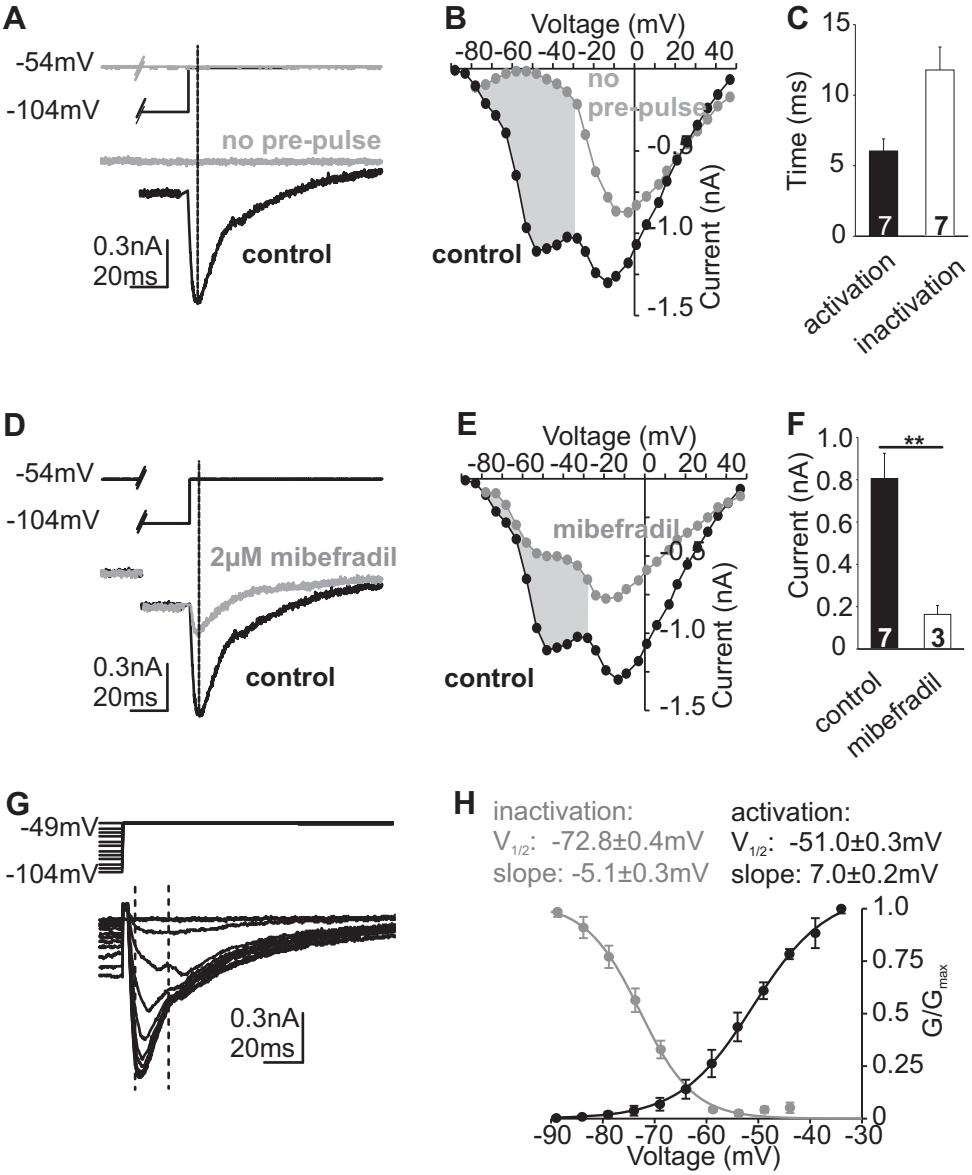

Fig 4.1. I_{TCa} is present in SPN neurones.

A. Raw traces of currents generated on a step depolarisation to -54mV from -104mV in the absence (grey trace) and presence (black trace) of a pre-pulse (400ms). **B.** IV relationship of currents generated following (black circles) or not following (grey circles) a pre-pulse to -104mV (400ms). **C.** summary bar graph of time course of activation (black bar) and inactivation (grey bar) of I_{TCa}. **D.** Raw trace of currents generated on a step to -54mV in the absence (black trace) and presence (grey trace) of mibefradil (2μM). **E.** IV relationships of currents measured in the absence (black circles) and presence (grey circles) of mibefradil. **F.** Summary bar graph to show effect of mibefradil (white bar) on on I_{TCa} (black bar, **p<0.01). **G.** Tail currents generated on a step to -49mV from different pre-pulse voltages. Peak current measured between dashed lines. **H.** Inactivation (grey circles) and activation (black circles) curves to show voltage dependence of I_{TCa}. Error bars are ±SEM.

4.2 T-type channels contribute to rebound burst firing.

It has been shown *in vivo* that the SPN fires on cessation of a sound, whilst the MNTB fires during a sound (Figure 4.2. A and B) in both rats (Kadner *et al.*, 2006) and mice (Kopp-Scheinpflug *et al.*, 2011). The downstream inhibitory glycinergic projections of the MNTB to the SPN mean that the SPN is switched off by MNTB activity during the sound. Relief of inhibition produces a rapid firing response or rebound burst in the SPN. Given the large amplitude I_{TCa} present in the SPN, and the fact that T-type channels are known to contribute to rebound burst firing in other areas of the brain (Huguenard & Prince, 1992; Russier *et al.*, 2003), we investigated its role in the SPN.

In vivo experiments by Conny Kopp-Scheinpflug, who recorded field potentials in the MNTB and SPN in anaesthetised mice during a sound stimulus of differing intensities, reveal the different responses of the communicating nuclei to sound. The MNTB shows a direct increase in firing frequency during a sound which increased with sound stimulus intensity. Following cessation of the sound the MNTB is silenced in a sound correlated way, such that higher frequency firing produces a longer period of silencing (Figure 4.2. A). In contrast the SPN shows a reciprocal response, and is silenced during sound stimuli, but fires on cessation of the sound. The duration of the response is matched to the silencing of the MNTB, such that higher frequency MNTB firing produces an increased duration of SPN firing on cessation of the sound. The firing activity in the SPN appears to be more ordered than in the MNTB, and could be said to be rhythmic (Figure 4.2. B).

To investigate the ionic basis of the rebound firing phenotype, SPN neurons were patched in the whole-cell configuration and a current clamp approach was used. The

cell resting potential was adjusted to -60mV and a step current command (-400pA, 200ms) was given to hyperpolarise the cell (Figure 4.2. C.) The initial hyperpolarisation was quickly followed by a relaxation or sag in the membrane potential (V_m) reducing the hyperpolarisation by ~50%. Following the termination of the current step, a fast depolarising rebound spiking response was generated (enlarged in the inset). This sag is characteristic of activation of I_h (Pape, 1996).

I_h and I_{TCa} have previously been shown to induce oscillatory and rebound firing activity in thalamic neurons (McCormick & Pape, 1990). Given the observed sag on hyperpolarisation and characterised T-type conductance there was good evidence for their expression in SPN neurons. By repeating the hyperpolarising current command in the presence of the I_h blocker ZD7288 (20μM), the membrane sag was removed and only a single rebound spike observed (Figure 4.2. D). The I_h block also slowed the membrane time constant (τ). Addition of the T-type blocker mibefradil (2μM) on top of I_h block prevented rebound firing, although a sub threshold depolarisation is still observed following current step termination, and did not further affect membrane τ (Figure 4.2. E),

ZD7288 alone did not significantly reduce the number of rebound APs firing following termination of the current step. The addition of mibefradil in the presence of I_h blocker ZD7288 significantly reduced the number of rebound APs, suggesting both I_h and I_{Tca} are necessary for rebound firing. However, block of HCN and T-type channels did not completely remove rebound AP firing from all cells in the data set. This could mean rebound APs are not solely dependent on LVA Ca_V channels for their initiation, or that mibefradil did not completely block the channels. This is summarised in the bar graph

in Figure 4.2. F. One-way ANOVA reveals very significant variance between the means within the group, p=0.002, and Tukey's post-hoc test was used for pair-wise comparison. Control cells produced 3.34±0.39 rebound APs (n=69, black bar), whereas ZD7288 treated cells produced 2±0.6 APs (n=6, blue bar, p>0.05). ZD7288 +mibefradil treated cells produced 0.45±0.3 APs (n=11, p<0.05). Excluding all Ca_V conductances by adding cadmium (Cd^{2+}, 0.5µM, light blue bar) on top of the ZD7288 and mibefradil reduced the average number of rebound AP firing further but did not prevent it, as one cell produced a single rebound AP in the presence of the blockers: ZD7288 +mibefradil +Cd^{2+} produced 0.14±0.14 APs (n=7, p<0.05, Tukey's post-hoc test, control vs ZD7288+mibefradil+Cd^{2+}). This suggests that the APs are not solely dependent on either LVA or HVA Ca_V channels, and could still be initiated by Na_V channels as long as threshold activation is reached on the rebound depolarisation.

Block of I_h removed the observed membrane sag, increased R_m and slowed membrane τ. This slowed the rebound response but did not affect the number of rebound APs fired. Block of I_{TCa} in addition to I_h block did not affect the membrane τ further, but did reduce the number of APs generated. However, the rebound APs were not solely dependent on Ca^{2+} influx as Cd^{2+} application did not fully remove them. Taken together we have a situation where glycinergic inhibition from the MNTB generates an IPSP with a negative peak amplitude of -88mV (Kopp-Scheinpflug *et al.* 2011) which: activates I_h, removes T-type Ca_V inactivation, and facilitates the rebound firing response by allowing a large Ca^{2+} dependent depolarisation at hyperpolarised potentials, which drives the membrane to threshold for AP firing.

Principal neurons of the MNTB do not express LVA T-type Ca_Vs, but the HVA channels present do show a differential modulation by NO, such that: L-type and P/Q-type channels are potentiated, N-type channel activation is leftward shifted and no effect on R-type channels is observed (Tozer *et al.*, 2012). In light of this HVA Ca_V modulation in MNTB neurons, NO-dependent modulation of the LVA T-type channels expressed in SPN neurons, and the subsequent effect on rebound AP firing, was investigated.

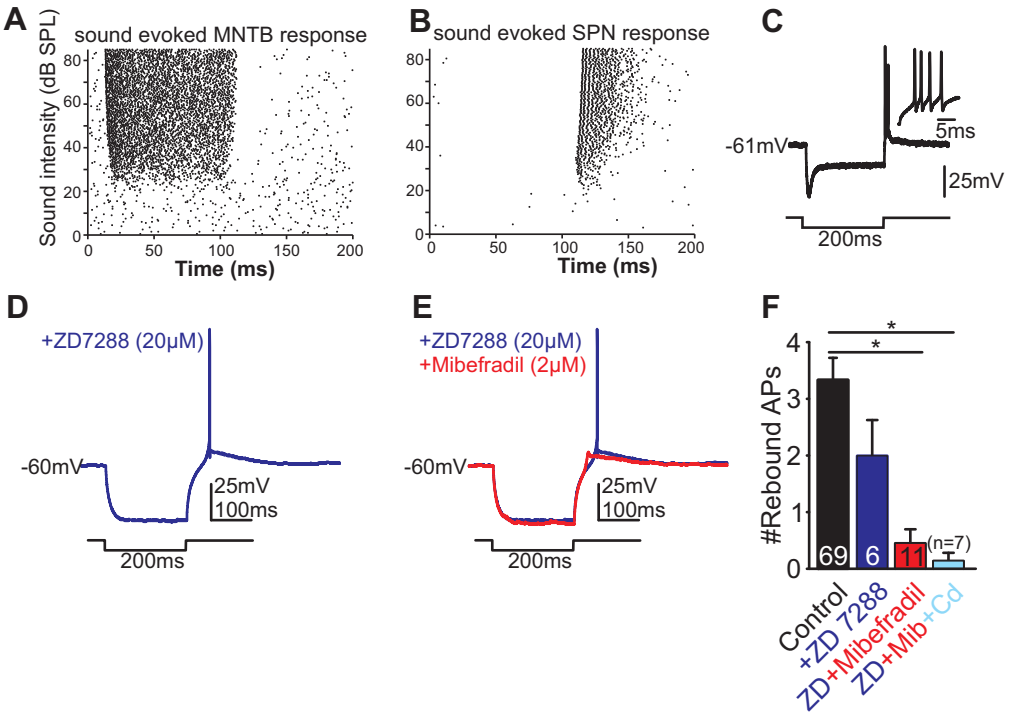

Figure 4.2. I_{TCa} contributes to rebound firing.
A. *In vivo* single unit AP recordings measured at different sound intensities in the MNTB. **B.** In vivo single unit AP recordings measured at different sound intensities in the SPN (Kopp-Scheinpflug et al., 2011). **C.** Iclamp raw trace observed on -400pA current injection (I_{inj}). *inset* enlargement of rebound spikes following completion of the current step. **D.** Iclamp raw trace in presence of I_H blocker ZD7288 (20μM, blue trace). **E.** Iclamp raw trace +ZD7288+mibefradil (2μM, red trace). **F.** Summary bar graph of number of rebound APs generated following the end of the hyperpolarising current step measured in control cells (black bar) and cells treated with ZD7288 (blue), ZD7288+Mibefradil (red) and ZD7288+Mibefradil+Cadmium (light blue). *p<0.05, Tukey's post-hoc test. Error bars are ±SEM.

4.3 T-type channels are inhibited by NO.

To investigate NO-dependent modulation of I_{TCa} amplitude, voltage dependence and kinetics, a voltage clamp approach was used. 7-NI incubated slices were perfused with normal aCSF containing 10mM TEA to block K_v channels, and 0.5µM TTx to block Na_V channels, and maintained at 37˚C. SPN neurons were visually identified and patched in the whole cell configuration.

The voltage step protocol included a hyperpolarising pre pulse to -100mV (400ms) to ensure removal of voltage-dependent inactivation of T-Type channels and activation of I_{TCa} on 5mV step depolarisations from -100mV to 40mV.

The effect of NO on T-type Ca_Vs was observed by recording from cells in slices treated with the NO donor SNP (100µM), this was done in an unpaired fashion as described in earlier sections of this thesis.

The raw traces in Figure 4.3. A reveal an NO-dependent reduction in the amplitude of the T-type current by ~50%. The inhibition of I_{TCa} was significant and observed in all cells: 7-NI peak I_{TCa} amplitude was 653±85pA (n=4, black bar), and 7-NI+SNP treated was 322±54pA (n=4, red bar, $p<0.05$, unpaired t-test) (Figure 4.3. B). The IV curves, drawn from the two unpaired cells in Fig A, show LVA and HVA I_{Ca} components as two peaks and, as the 50% reduction caused by NO (Figure 4.3. C) is mirrored in the HVA currents, this could suggest the HVA channel amplitudes are not affected by NO in this nucleus.

NO did not affect the voltage dependence of activation of I_{TCa} as no shift was observed in the activation curves, plotted as G/G_{max} on steps from -100 to -50mV: I_{TCa} +7-NI $V_{1/2}$

was -57±2.0mV (n=4, black circles), I_{TCa} +7-NI+SNP treated I_{TCa} $V_{1/2}$ was -55.25±3.1mV (n=4, red circles, p>0.05, unpaired t-test), fitted with a Boltzmann function. Voltage dependence of inactivation was also unaffected by NO, again plotted as the peak of the tail current generated on steps to -50mV from pre-pulse steps between -100 and -50mV (400ms): I_{TCa} +7-NI $V_{1/2}$ was -70±2.3mV (n=4, black circles), and I_{TCa} +7-NI +SNP treated $V_{1/2}$ was -72±2mV (n=4, red circles, p>0.05, unpaired t-test) (Figure 4.3. D).

As NO reduced I_{TCa} by ~50%, without affecting the voltage dependence of the current, we next sought to understand how this may affect rebound firing activity in these cells. As described earlier, we used a current clamp approach to hyperpolarise cells and observe their behaviour on relief of the hyperpolarisation. Cells were whole cell patched and given a hyperpolarising current command (-400pA) which induced a rebound firing response following its termination. In control conditions the cell showed the characteristic membrane sag and multiple rebound spikes following the termination of the step current injection (Figure 4.3. E). In NO treated cells the sag is slowed and does not return to as positive a potential as the control, with the membrane potential remaining more negative. Following the end of the stimulus, the cell fires only a single AP (Figure 4.3. E). The NO induced reduction, albeit not significant, in the number of rebound APs fired was observed in all cells from NO-treated slices and is summarised in the bar graph in Figure 4.3. F: control rebound APs 3.34±0.39 (n=69), SNP treated rebound APs 1.16±0.40 (n=6, p>0.05, Tukey's post-hoc test, control vs SNP-treated comparison).

From these data we can conclude NO inhibits I_{TCa} by ~50% and so reduces the number of rebound APs elicited following cessation of the hyperpolarising current step by

about 60%, although any effect of NO on I_h and it's contribution to rebound firing has not been accounted for in this scenario.

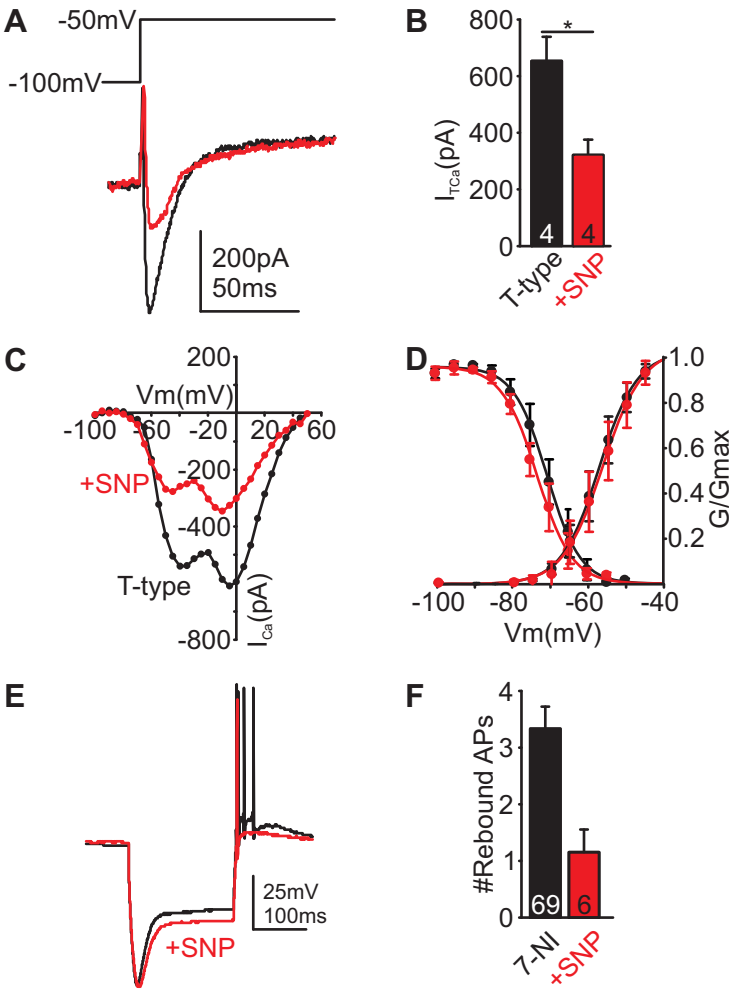

Figure 4.3 . I_{TCa} is inhibited by NO.
A. Raw traces generated on a step depolarisation to -50mV from -90mV in 7-NI (black trace) and 7-NI+SNP (100µM, red trace) treated conditions. **B.** Summary bar graph to show peak amplitude of I_{TCa} generated on a step to -50mV in 7-NI (black bar) and 7-NI+SNP treated (red bar) cells (*p<0.05, unpaired t-test). **C.** IV relationship of I_{Ca} in 7-NI (black circles) and 7-NI+SNP treated (red circles) cells. **D.** Inactivation and activation curves of 7-NI (black circles) and 7-NI+SNP treated (red circles) cells. **E.** Iclamp raw traces in 7-NI (black trace) and 7-NI+SNP treated (red trace) cells. **F.** Summary bar graph to show the number of APs generated following a hyperpolarising current step in 7-NI (black bar) and 7-NI+SNP treated (red bar) cells. Error bars are ±SEM.

4.4 Discussion of NO modulation of LVA channels expressed in the SPN.

Including a hyperpolarising pre-pulse in voltage clamp protocols recruited a LVA current that was transient in nature, characteristic of T-type current (I_{TCa}) (Randall, 1998; Catterall *et al.*, 2005), and ~79% blocked by mibefradil, a known T-type antagonist (Martin *et al.*, 2000). Other T-type blockers could also have been used to add further evidence in support the LVA current being I_{TCa}, such as nickel (Lee *et al.*, 1999) and NNC 55-0396 (Huang *et al.*, 2004).

The low voltage half activation ($V_{1/2}$) of -51mV was similar to that of T-type currents in cerebellar purkinje cell dendrites (Mouginot *et al.*, 1997), and more positive than that described in rat thalamic neurons (-63mV) (Coulter *et al.*, 1989), which also show a rebound firing phenotype (Huguenard & Prince, 1992) similar to SPN neurons. The negative $V_{1/2}$ of inactivation of -73mV was within the known range for T-type currents (Randall, 1998), but again more positive than the $V_{1/2}$ of -83.5mV in rat thalamic neurons (Coulter *et al.*, 1989).

However, the kinetics of activation between mice SPN and rat thalamus were similar: 5.7±0.7ms in this investigation and between 2 and 8ms in rat thalamic neurons. Although inactivation kinetics of the current were faster in this study than in that of the rat thalamic neurons: 11.5±1.4ms vs 20-50ms (Coulter *et al.*, 1989) and the inactivation rates suggested in the literature (τ ~20ms) (Randall, 1998; Catterall *et al.*, 2005). Interestingly, the voltage dependence of inactivation of I_{TCa} in rat SPON (analogous to mouse SPN) was found to be -92.1mV (Felix *et al.*, 2011), ~20mV more hyperpolarised, suggesting a species difference in voltage dependence.

The first peak at -54mV in the IV in Figure 4.1. A. is of large amplitude (~1nA) and mediated by T-type, and the second peak at -14mV by the HVA component (1.3nA). LVA channels would be maximally activated at -14mV, as shown by the activation curve in Figure 4.1. E., and the HVA current influx additive to the LVA. One could expect a much larger peak than the one observed and this suggests that the majority of voltage-dependent Ca^{2+} influx in these cells occurs through the T-type current.

The raw traces suggested there may be more than one Ca_V3 subtype present due to the second smaller 'hump' observed in the inactivating stage of the current traces. And $Ca_V3.3$ channels are known to inactivate slower than $Ca_V3.1$ or 3.2 channels in neurons (Chemin *et al.*, 2002). The hump was also sensitive to mibefradil, further supporting its possible identity as a slower activating T-type Ca_V (Ca_V3) channel.

T-type channels are known to contribute to a multitude of different functions in different cells, their LVA activation means they contribute as much to driving cellular depolarisation as they do to allowing Ca^{2+} influx. Their window current, caused by an overlap in the channels availability and voltage dependence of activation (Figure 4.1. E), means there is a portion of channels open at RMP, trying to drive the cell to depolarise. Because of their constant activation/fast inactivation kinetics the channels are suited to their roles in thalamic neurons where they generate oscillatory behaviour in thalamic neurons (Huguenard, 1996) controlling fast and slow rhythm generations, and underlying sleep oscillations (Astori *et al.*, 2011). They are also important for synaptic integration at dendrites in thalamic reticular neurons, and help to counter the attenuation of signals due to cable properties (Destexhe *et al.*, 1996) (Crandall *et al.*, 2010). In the auditory brainstem they are known to exist in axon initial

segments of Cartwheel cells in the dorsal cochlea nucleus and contribute to AP firing, and depolarisations underlying complex spikes (Bender & Trussell, 2009; Bender *et al.*, 2012). Their cellular location in SPN neurons is unknown but they function to initiate rebound spiking on relief of inhibitory innervation from the MNTB. This is achieved in conjunction with I_h, the hyperpolarisation activated non-specific cation current.

The current clamp experiments reveal the extent to which I_h and I_{TCa} contribute to the firing phenotype of these cells, both during inhibitory suppression of the cells and on release from this inhibition. An IPSP will hyperpolarise the cell activating I_h, and deinactivating T-type channels. On relief of the inhibition I_h facilitates a swift recovery from the hyperpolarisation, speeding up the membrane tau, by reducing R_m. This enables I_{TCa} activation, driving the membrane to threshold for AP firing before the I_{TCa} has a chance to inactivate. The APs themselves are not Ca^{2+} dependent, and so may be generated by Na_V channels which sit on top a low threshold spike or sustained depolarisation until the membrane returns to RMP due to inactivation of the Ca_V3 channels or activation of a K_{Ca} channel (McCormick & Pape, 1990; Cain & Snutch, 2010). This means the role of I_h and I_{TCa} is to rapidly depolarise the membrane to the threshold of activation of Na_V channels. This synergistic relationship is very effective in producing short latency responses on relief of inhibition (Engbers *et al.*, 2011), and would make it a good ionic mechanism for generating an 'off'-response, which would be useful in auditory perception of gaps in sound stimuli, such as when interpreting speech, for example (Kadner & Berrebi, 2008; Kopp-Scheinpflug *et al.*, 2011).

Voltage clamp investigation of T-type current following exposure of cells to NO revealed a ~50% decrease in current amplitude (Figure 4.3. A), which translates into a

reduction in rebound AP firing following the end of the hyperpolarising current command (Figure 4.3. F.). This inhibitory action of NO, delivered by S-nitrosothiol compounds, has been seen before in the thalamus (Joksovic *et al.*, 2007), and reduced spike firing frequency.

The inhibition here in the SPN is in contrast to potentiation of the HVA currents expressed in the upstream MNTB nucleus. NO is also known to inhibit rebound spiking in the deep nuclei of the cerebellum by apparent potentiation of I_h (Wilson & Garthwaite, 2010), although the striking finding is the reduction in the number of rebound APs following NO exposure in these cells, but NO effects on T-type current, which is known to work with I_h in these neurons (Engbers *et al.*, 2011), was not investigated.

nNOS is not known to be expressed in the SPN, but the close apposition of the nucleus to the MNTB could mean that NO reaches the SPN, when generated at high concentrations, by the volume diffusion principle, and would work in an anterograde fashion (Park *et al.*, 1998). The consequence of NO modulating the SPN *in vivo* would be to negate gap detection in sounds, shortening the offset rebound response.

Here we show the functional importance of Ca_V3 and I_h in producing a firing phenotype, and show its physiological relevance to the organism, which has since been confirmed in the rat (Felix *et al.*, 2011). T-type channels are known to interact with other potassium channels *in vitro*, such as Ca_v3 and K_v4 in cerebellar stellate cells (Anderson *et al.*, 2011), and it would be interesting to know if other conductances interact with T-type channels in these SPN neurons. We also show how NO can change

the firing properties of these cells by inhibition of the T-type channels, and by affecting the voltage dependence of the I_h, although this is not discussed here.

In the next chapter I investigate the role NO-dependent modulation of Ca_Vs has in controlling cellular excitability in the MNTB.

5. Nitric oxide (NO) potentiates an SK-mediated after hyperpolarising potential (AHP) in mouse MNTB neurons.

In the auditory brainstem NO modulates the different families of Ca_V channels in different ways, potentiating members of the Ca_V1 and Ca_V2 families in the MNTB, but inhibiting members of the Ca_V3 family in the SPN. This differential NO→Ca_V signalling could have many interesting consequences for cell behaviour in response to nitric oxide. Thinking in terms of the neurophysiology and electrophysiology of MNTB neurons it would be interesting to know how these characterised pathways could affect their excitability. Potassium channels restrict the excitability of neurons, and several different suites of voltage-gated potassium (K_V) channels are expressed in the MNTB (Schneggenburger & Forsythe, 2006; Johnston *et al.*, 2011). NO-dependent inhibition of native $K_V3.1$ and upregulated expression K_V2 channels has already been characterised in this nucleus (Steinert *et al.*, 2008; Steinert *et al.*, 2011b)and, whilst there is evidence in other neurons that Ca^{2+} influx can lead to modulation of K_V currents (K_V4) via interacting proteins (An *et al.*, 2000), there is a family of K^+ channels that are directly gated by intracellular Ca^{2+} and are known to contribute to neuronal excitability (Wei *et al.*, 2005). However, not much is known about the presence of these calcium activated potassium channels (K_{Ca}) in MNTB neurons, and I wondered if this could be because no one has looked for their existence before, or if they simply weren't there?

Grouped loosely into three families based on the amplitude of their conductance, three types of K_{Ca} channels are known to exist: big/large conductance (BK), medium/intermediate conductance (IK) and small conductance (SK) channels (Wei *et*

al., 2005). This chapter describes the investigations made to elucidate the presence of one type of K_{Ca} channels, the small conductance (SK) family, in MNTB principal neurons. It then goes on to investigate their presence in relation to the potentiated Ca^{2+} influx in these cells caused by NO signalling, and finally aims to understand the importance of this in regard to the bigger picture of NO-dependent modulation of pre and post synaptic neuronal excitability in the MNTB.

5.1 I_{SK} is present in MNTB neurons and is potentiated by NO via the NO-cGMP pathway.

To confirm the presence or absence of SK channels in the MNTB I used a three pronged approach: utilising quantitative polymerase chain reaction (qPCR) analysis, to understand if the genes for any of the three SK subunit isoforms (SK1-3) were transcribed into mRNA in MNTB neurons; immunohistochemistry, to enquire if the mRNA was translated into an SK channel protein, and if this was expressed in these neurons; and electrophysiology, to determine if the SK channel protein was functionally expressed in the cell membrane.

The qPCR and immunohistochemistry experiments were done in collaboration with Sue Robinson. For the qPCR, MNTB tissue from 3 P14 CBA mice was sectioned from brain slices by laser micro-dissection (PALM laser system, Zeiss) and RNA was then extracted from the tissue and examined for the presence of mRNA for the SK subunits, SK1-3, by qPCR using targeted SK primers designed using the Universal Probe Library (Roche). Expression levels were normalised to the house keeping ribosomal protein RPL44 gene. The results, analysed using the Pfaffl method (Nucleic Acids Reseach,

2001), are displayed as a summary bar graph in Figure 5.1. A, and show the SK2 subunit isoform to be the dominantly expressed subunit, with negligible expression of SK1 and SK3.

The immunohistochemistry experiment aimed to see if the mature SK2 channel protein was expressed in MNTB neurons. 12µm brain slice sections were incubated with a primary rabbit anti-mouse antibody to SK2 (1:200 dilution, Alomone), and finally incubated with a fluorescent secondary goat anti-rabbit antibody (Invitrogen, Molecular Probes). Figure 5.1. B reveals a fluorescent signal in the MNTB, suggesting the presence of SK2 protein in these cells.

To understand if functional SK2 channels were expressed in MNTB neurons, and activated by voltage-gated Ca^{2+} entry, I used a voltage clamp approach and exploited the channel's selective sensitivity to low concentrations of the honey bee venom, apamin (100nM)(Ngo-Anh *et al.*, 2005). Cells were voltage clamped in the whole cell configuration and held at -60mV. They were then stepped to -90mV to remove any voltage-dependent inactivation of the calcium channels for 300ms before stepping to -10mV for 200ms. This step aimed to maximise the voltage-dependent Ca^{2+} entry, as -10mV is the peak potential for I_{Ca} in these cells, as shown in Chapter 3. Tail currents were then observed on a step back down to -40mV for 50ms (black arrow). These tail currents could be investigated for apamin sensitivity so understand if SK channels were functional in these cells.

Slices were incubated with 7-NI to inhibit NOS activity, and 1mM TEA was included in the physiological bath solution. TEA was included to block $K_V3.1$ channels as it is already known that this channel is inhibited by nitrergic signalling, and we wanted to exclude this effect from our tail current measurements. Experiments were unpaired, meaning slices were exposed to the different test conditions prior to patching.

Raw traces of the tail currents from 3 cells are shown in Fig 5.1. C, it is clear that apamin reduces the tail current amplitude, whereas NO potentiates it compared to 7-NI. The summary bar graph in Fig 5.1. D shows the mean±SEM tail current data from the different groups analysed using one-way ANOVA with a Tukey's post-hoc test. 7-NI tail current amplitude was 0.9±0.15nA (n=10), and 7-NI+apamin reduced it by ~60% to 0.35±0.12nA (n=5, $p<0.01$). 7-NI+SNP potentiated the tail current amplitude by ~90% compared to 7-NI, and was 1.796±0.173nA (n=9, $p<0.01$). This potentiation was apamin sensitive as the SK blocker reduced the current back down to 7-NI+apamin levels, 7-NI+SNP+apamin was 0.482±0.13nA (n=5, $p<0.001$). Interestingly the apamin sensitive current was also sensitive to Ca_V block, as the tail currents measured in the presence of NO and P/Q and N-type channel blockers, ω-agatoxin IVA (200nM) and ω-conotoxin GVIA (2μM) respectively, were also significantly reduced compared to the NO treated cells, 7-NI+SNP+agatoxin and conotoxin-treated tail current amplitude was 0.78±0.15nA (n=4, $p<0.01$)

The three-pronged approach has confirmed the presence of a small conductance potassium (SK) channel in the MNTB. The qPCR findings show that SK2 is the dominant isoform in these animals (aged P13-16), and the punctate anti-SK2 antibody immunoflourescence signal suggests that there is expression in the MNTB, although its exact position in the cell cannot be discerned. The electrophysiological approach of

assessing the apamin sensitivity of the postsynaptic MNTB neurons provides evidence for SK channel expression, and based on the qPCR and immuno data, we can say that the apamin sensitive current (I_{SK}) is most likely through SK2 containing SK channels.

It was interesting to see that the apamin sensitive current is potentiated by NO, and is also sensitive to P/Q and N-type Ca_V block. This could mean that NO-dependent potentiation of the Ca_V channels described in the first results chapter could lead to increased Ca^{2+} influx and activation of SK channels.

As nNOS activation is dependent on NMDAR activation, which classically needs a high level of membrane depolarisation, achieved by high frequency stimulation, it might be reasonable to postulate that high frequency activity leads to nNOS activation, which potentiates Ca^{2+} influx, recruiting SK channels. By using the voltage clamp approach we artificially depolarise the membrane, driving Ca^{2+} influx and activating SK channels. The next step was to test if this NO→Ca_V→SK pathway operates in a more physiological scenario.

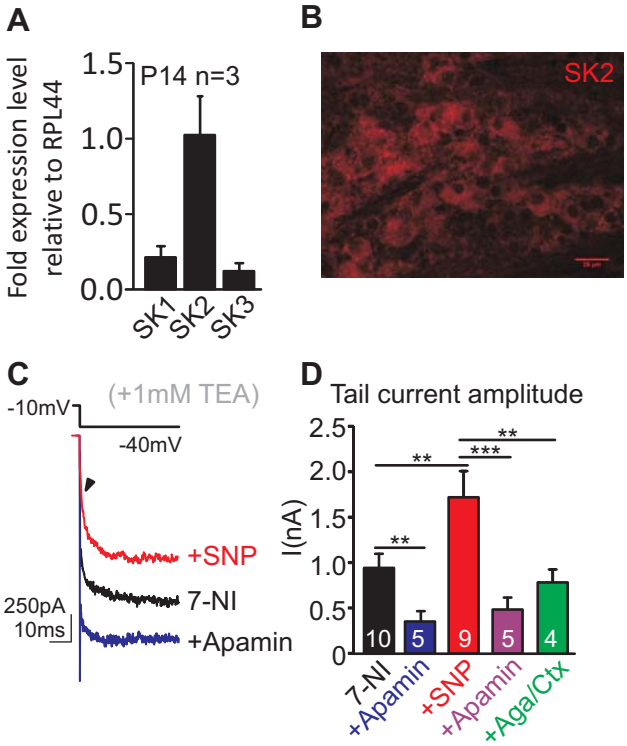

Figure 5.1. ISK is present in MNTB and potentiated by NO via P/Q and N-type CaV.

A. qPCR reveals SK2 is the dominantly expressed subunit isoform in the MNTB, relative to housekeeping RPL44 gene. **B.** Anti SK2 antibody (red) confirms immunofluorescence for protein in the MNTB. **C.** Raw traces of tail currents measured in the presence of 1mM TEA. Arrow indicates point of measurement. Tail currents generated on step to -40mV following 200ms depolarisation to -10mV, in 7-NI(black trace),7-NI+Apamin-treated (blue trace) and 7-NI+SNP-treated (red trace) cells. **D.** Summary bar graph to show mean±SEM tail current amplitudes in: 7-NI (black bar), 7-NI+Apamin-treated (100nM, blue bar), 7-NI+SNP exposed cells (red bar); and 7-NI+SNP+Apamin (mauve bar),7-NI+SNP+Agatoxin (200nM) +Conotoxin (2μM, green bar) treated cells. **p<0.01, ***p<0.001, one-way ANOVA with Tukey's post-hoc test.

5.2 SK channels do not contribute to the action potential waveform.

The functional output of neuronal excitability is the action potential (AP). The biphasic AP is an all-or-nothing phenomenon dependent on the rapid flux of ions through channels in the membrane. Classically dependent on Na^+ influx for the rising/depolarising phase and K^+ efflux for the decline/repolarising phase (Hodgkin *et al.*, 1952), different suites and isoforms of contributory ion channels can affect the waveform shape, as can modulation of these channels. As already mentioned, NO inhibits $K_V3.1$ channels, the main K^+ channels underlying the repolarisation or delayed rectification of the membrane potential during the AP, this has the effect of broadening the AP waveform (Steinert *et al.*, 2008).

To test whether SK channels contribute to AP waveform in these neurons a whole cell current clamp approach was used. The cell was held at -60mV and given a 500pA current injection pulse for 0.8ms to initiate an AP. This was done in an unpaired fashion, such that slices were treated prior to recording. Raw traces of the APs generated in a 7-NI cell (black trace) and 7-NI+apamin treated cell (blue trace) are shown overlaid in Figure 5.2. A, the AP waveforms are very similar in shape. The APs generated in 7-NI+SNP-treated (red trace) and 7-NI+SNP+apamin treated (mauve trace) cells are shown in Figure 5.2. B. The APs in the NO treated scenario are noticeably broader than the 7-NI cells, but again the apamin treated waveform shows no dramatic difference in shape to the non-apamin treated. However, in both 7-NI and apamin 7-NI+SNP-treated scenarios the overlay suggests that the apamin treated cells reach threshold faster than their overlaid counterparts, and their AP waveforms looked to peak earlier.

To see if blocking SK channels affected input resistance which might explain the subtle differences in the APs, I calculated the input resistances of cells treated with the different conditions by calculating the reciprocal of the IV leak conductance gradient and presented the findings in the summary bar graph in Figure 5.2 C. Mean±SEM input resistance R_{in} in 7-NI cells was 83.2±14MΩ (n=7), and in 7-NI + apamin treated cells R_{in} was 106.2±19MΩ (n=7). NO-treated mean±SEM R_{in} was 74.6±5MΩ (n=5), and NO+apamin R_{in} was 107±19MΩ (n=5). Although in both 7-NI and NO-treated scenarios apamin produced an increase in input resistance, this was not significant.

To understand if blocking SK current affected the AP waveform halfwidth, I measured the ½ amplitude of the AP, between threshold and peak, and then calculated the time it took the AP to peak and repolarise to the measured ½ amplitude. The mean±SEM halfwidths measured in the different treatment scenarios are displayed in the summary bar graph in Figure 5.2 D. Data analysed using one-way ANOVA with Tukey's post-hoc test. 7-NI treated AP halfwidth was 0.22±0.01ms (n=5), 7-NI+apamin treated was 0.23±0.01ms (n=5), 7-NI+SNP-treated was 0.26±0.01ms (n=5), and 7-NI+SNP+apamin AP halfwidth was 0.26±0.02ms (n=4). As expected, NO broadened the AP halfwidth, although this was not quite statistically significant (p=0.07), but apamin had no effect on the AP halfwidths in either 7-NI or 7-NI+SNP-treated conditions.

These data suggest that there is no contribution of SK channels to the single AP, and this was as expected. I_{Ca} activation in these neurons is in the millisecond range, which is much slower than the rapid APs exhibited by these neurons, this would mean negligible I_{Ca} would be activated during a single AP. Nor was there any effect of SK block on the NO-treated cells, and one might expect a broadened AP would allow

some I_{Ca} activation leading to recruitment of I_{SK}. Perhaps the APs in this test were still too fast?

Classically SK channels are not thought to contribute to the rapid upstroke and downstroke of the AP waveforms, but to the after hyperpolarisation following the biphasic deflections (Lancaster & Nicoll, 1987). Specifically SK channels are thought to contribute to the intermediate phase as the membrane potential returns to rest (Sah, 1996).

This gives us two parameters in which to explore the contribution of I_{SK} in these cells. Firstly, to look at SK contribution during trains of APs, which would be more physiologically relevant when again considering that nNOS is activated during high levels of activity. And secondly, to look for any contribution of I_{SK} to an afterhyperpolarisation following these trains of APs.

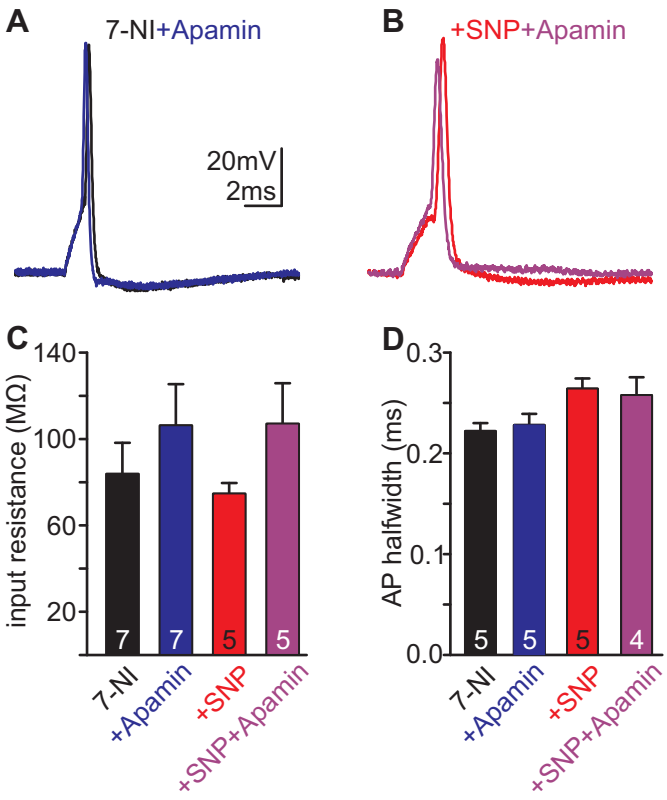

Figure 5.2. SK block does not affect AP waveform.
A. APs elicited in 7-NI (black trace) and 7-NI+Apamin (100nM, blue trace) treated cells. **B.** APs elicited in 7-NI+SNP-treated (red trace) and 7-NI+SNP+Apamin treated(mauve trace) cells **C.** Summary bar graph to show the mean±SEM input resistance in 7-NI (black bar), 7-NI+Apamin treated (blue bar), 7-NI+SNP-treated (red bar), and 7-NI+SNP+Apamin treated cells (mauve bar). **D.** Summary bar graph to show mean±SEM of AP halfwidth in 7-NI (black bar), 7-NI+Apamin treated (blue bar), 7-NI+SNP-treated (red bar), and 7-NI+SNP+Apamin treated cells (mauve bar).

5.3 AP trains are followed by an AHP.

MNTB principal neurons will only fire a single fast AP during sustained depolarisation due to the presence of a large LVA K_V1 current restricting depolarisation to threshold, and HVA $K_V3.1$ current rapidly repolarising the AP to negative potentials. To initiate trains of APs postsynaptically it is necessary to pulse the cells with depolarising current. This was achieved in the whole-cell patch configuration in current clamp mode, and adjusting membrane potential to -60mV before injecting 0.8ms pulses of 2nA current at a frequency of 400Hz, for increasing durations in 200ms steps, from 200ms to 1s. This was done unpaired, in normal aCSF (methods), so slices were treated with the different pharmacology prior to patching.

The raw traces from four cells, one each from the different conditions, are displayed in Figure 5.3. All the traces: 7-NI (black trace), 7-NI+apamin (blue trace), NO-treated (red trace) and NO+apamin (mauve trace), show the first 200ms as a solid trace with the subsequent extended duration trains as lighter-shaded traces. The after hyperpolarisation (AHP) following the trains is clearly visible in all scenarios.

It is clear from these AP trains that there are differences between these examples, both in the trains themselves and also in the AHP shapes and amplitudes. This suggests that SK channels could be recruited during a train and could contribute to the AHP in these cells.

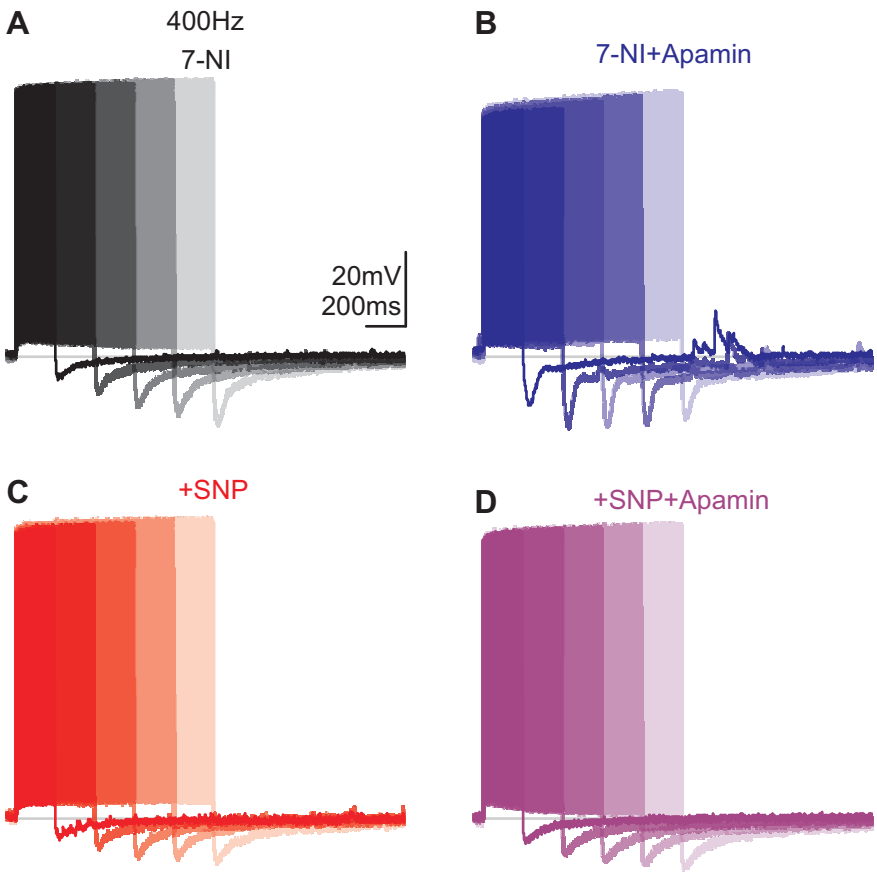

Figure 5.3. Afterhyperpolarising potential (AHP) amplitude and kinetics are dependent on the preceding cellular activity.
A. Raw trace from 7-NI cell (black trace) subjected to 0.8ms 2nA current injections at a frequency of 400Hz for increasing durations. **B**. Raw trace from 7-NI+Apamin cell (blue trace) subjected to 0.8ms 2nA current injections at a frequency of 400Hz for increasing durations. **C**. Raw trace from 7-NI+SNP treated cell (red trace) subjected to 0.8ms 2nA current injections at a frequency of 400Hz for increasing durations. **D**. Raw trace from 7-NI+SNP+Apamin treated cell (mauve bar) subjected to 0.8ms 2nA current injections at a frequency of 400Hz for increasing durations.

5.4 Increasing train duration broadens AP halfwidth and increases AHP amplitude, but does not affect AHP time to half decay.

Analysing the mean±SEM data for the trains generated using the protocol described above it is possible to look at the activity dependent changes in these cells during AP trains and understand SK contribution to the train waveforms. In Figure 5.4. A, the AP halfwidths of the first and last APs in a 200ms and 1s train are shown for each scenario. In all conditions the trend is for the APs to become significantly broader over the course of the train, ~20% broader over the 200ms train, and by ~30% over the 1s train. In the 200ms train the mean±SEM AP broadening in the 7-NI cells is significant from 0.27±0.01ms to 0.34±0.02ms (black circles, n=5, $p<0.01$, paired t-test), 7-NI+apamin AP broadens from 0.27±0.01ms to 0.3±0.02ms (blue circles, n=5, $p<0.05$, paired t-test), NO-treated AP broadens from 0.31±0.2ms to 0.37±0.04ms (red circles, n=7, $p<0.001$, paired t-test), and NO+apamin significantly broadens from 0.29±0.01ms to 0.36±0.02ms (mauve circles, n=6, $p<0.001$, paired t-test). In the 1s train, the mean±SEM AP broadening is very significant in all scenarios: 7-NI AP broadens from 0.29±0.01ms to 0.39±0.02ms (black circles, n=5, $p<0.001$, paired t-test); 7-NI+apamin APs broaden from 0.28±0.02ms to 0.36±0.02ms (blue circles, n=5, $p<0.01$, paired t-test); NO-treated APs broaden from 0.33±0.02ms to 0.43±0.03ms (red circles, n=7, $p<0.001$, paired t-test); NO+apamin APs broaden from 0.31±0.01ms to 0.41±0.02ms (mauve circles, n=6, $p<0.001$, paired t-test).

The membrane potential (V_m) between the APs can change during a train. Measuring the V_m before the last AP in the train gives a measurement of this V_m change (ΔV_m) compared to the adjusted pre train potential (V_h, -60mV), and gives a readout of the

accumulating depolarisation/hyperpolarisation during a train. In Figure 5.4. B, the mean±SEM ΔV_m for each treatment scenario is plotted against the train duration at which it was recorded and analysed using one-way ANOVA with Tukey's post-hoc test. Across the increasing 400Hz train durations the 7-NI treated cells did not accrue any significant changes in ΔV_m (n=5, p=0.5). This is also true for 7-NI+apamin treated cells which do not accrue any significant changes in ΔV_m (n=5, p=0.12). The different train durations consistently depolarised the 7-NI+SNP treated cells (n=5, p=0.0001), whereas 7-NI+SNP+apamin treated cells showed a variable ΔV_m response to the increasing train durations, being hyperpolarised over the 400ms train and depolarised over the 1s train (n=4, p=0.017, 400ms vs 1000ms comparison p<0.05).

apaminapaminThese data suggest that during 400Hz frequency trains, AP halfwidth broadens, and this broadening is dependent on train duration, and independent of NO exposure and SK block. These data also suggest that with NO-treatment cells accumulate a more depolarised interspike potential during a train, whereas 7-NI, 7-NI+apamin and 7-NI+SNP+apamin treated cells do not. This evidence could imply that NO-dependent depolarisation requires SK activation.

Following the trains, AHPs are generated in all the treatment scenarios. In Figure 5.4. C, the mean±SEM AHP peak amplitude is plotted against the train duration after which it is generated. At 200ms up to 600ms the block of I_{SK} with apamin significantly increases the AHP amplitude compared to 7-NI-treated, 7-NI+SNP-treated and 7-NI+SNP+apamin-treated cells. Following a 600ms 400Hz train, 7-NI peak AHP was -11.1±1.3mV (black circles, n=6), whereas in 7-NI+apamin treated cells peak AHP was -16.8±2.3mV (blue circles, n=5, p<0.05). In the 7-NI+SNP-treated group, the AHP was -

8.6±5mV (n=5) and in the 7-NI+SNP+apamin-treated group, AHP was -7.7±3mV (n=4). 7-NI+SNP-treated cells (red circles) tended to produce a smaller peak AHP in comparison to control cells, as did 7-NI+SNP+apamin-treated cells (mauve circles, n=4). apamin

These results are difficult to explain as they suggest that removing the SK conductance potentiates AHP peak amplitude compared to 7-NI cells. However, in the presence of NO, apamin has no effect on AHP amplitude. As NO broadens AP halfwidth, and increases depolarisation within the train, one would think more Ca^{2+} would move into the cell activating SK channels, and more of an effect of SK block would be observed in the NO-treated cells.

However, as previously stated, SK channels are known to contribute more to the intermediate repolarising phase of the AHP, and not the peak, so to investigate this the time to half decay of the AHP following the trains was investigated.

In Figure 5.4. D, the mean±SEM time to half decay of the AHP is plotted for each treatment scenario against the stimulus duration after which they were generated. This was calculated by measuring the time taken for the AHP to repolarise halfway to -60mV from the peak. One-way ANOVA with Tukey's post-hoc test reveals a significant variance between the group's AHP times to half decay following a 1s stimulus ($p=0.0038$); the trend is for SK block to reduce the AHP time to half decay and for NO exposure to increase AHP time to half decay. 7-NI-treated time to half decay was 76±12ms (black circles, n=6), and 7-NI+apamin was 50±4ms (blue circles, n=5), 7-NI+SNP-treated was 165±33ms (red circles, n=5) and 7-NI+SNP+apamin was 122±21ms (mauve circles, n=4, $p<0.05$, 7-NI vs 7-NI+SNP comparison,).

NO significantly increased the AHP time to half decay compared to 7-NI-treated following a 1s stimulus train, and 7-NI+apamin reduced the time to half decay, albeit not with statistical significance.

Interestingly, SK block in the presence of NO did not significantly affect the time to half decay of the AHP following any of the stimulus trains, although the data does suggest a reduction in decay time towards control levels. This could mean that the AHP prolongation by NO is not via SK channels, or that the influx of Ca^{2+} during these trains was not sufficient to maximally activate the SK channels and that is why only a small effect was observed.

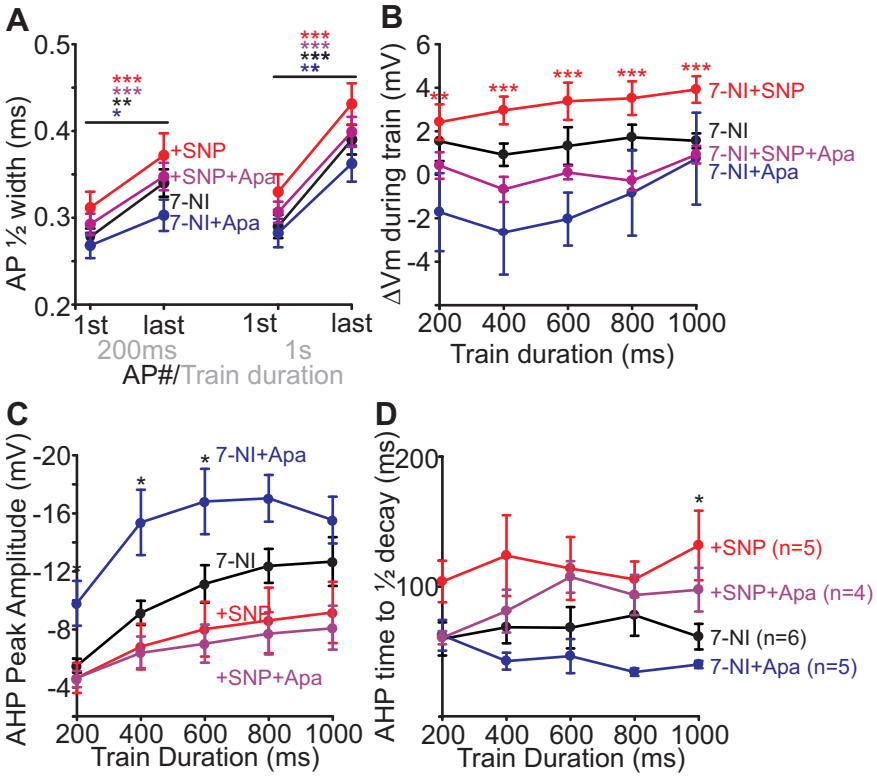

Figure 5.4. Increasing train duration broadens AP halfwidth and increases AHP amplitude, but does not affect AHP time to half decay.
A. Plot to show mean±SEM halfwidths of first and last AP in the train (paired t-test). **B.** Plot to show change in membrane potential (ΔVm) during trains of increasing duration, measured as the difference between the mean±SEM last inter spike potential and the holding potential (-60mV) (one-way ANOVA with Tukey's post-hoc test). **C.** Plot to show the mean±SEM peak AHP amplitudes generated following the increasing duration stimulus trains (one-way ANOVA with Tukey's post-hoc test). **D.** Plot to show AHP time to ½ decay following increasing duration stimulus trains (one-way ANOVA with Tukey's post-hoc test). *p<0.05, **p<0.01, ***p<0.001. Error bars are ±SEM.

5.5 AHP is calcium dependent, but stimulus trains in the presence of TEA, to promote Ca^{2+} influx during train, does not affect AHPs.

I next investigated if the reason for the lack of a significant apamin effect on the train stimuli and AHPs in the previous experiments was due to sub-maximal activation of SK channels.

To improve the I_{SK} recruitment, and therefore resolution of any apamin dependent effect, I tried to maximise the amount of Ca^{2+} entering the cells during the train stimuli, by repeating the postsynaptic current injection trains in the presence of the $K_V3.1$ blocker tri-ethyl ammonium (TEA, 1mM). This broadened the AP, facilitating depolarisation during a train, increasing Ca^{2+} influx, and also precluded any variability in the NO-dependent effect on the $K_V3.1$ channels.

Figure 5.5 Ai and Aii show raw traces recorded from a control 7-NI treated cell (black trace) and 7-NI+SNP-treated cell (red trace) respectively. In Figure 5.5 Aiii, the 7-NI+SNP-treated raw trace is overlaid with a 7-NI+SNP+apamin treated raw trace (mauve trace). To investigate any calcium dependence to the trains or AHP I also blocked P/Q- and L-type Ca_V channels, with ω-agatoxin IVA (200nM) and nifedipine (10μM) respectively, in NO-treated cells, and a raw trace for 7-NI+SNP+agatoxin+nifedipine treated cells (green trace) is overlayed with that of an 7-NI+SNP-treated cell in Figure 5.5. Aiv.

I_{SK} contributes to the repolarising phase of AHPs, and Figure 5.5. B shows enlarged AHPs taken from the raw traces in A. Displayed are the AHPs generated following 200ms and 1s 400Hz trains. It is clear from the figure that the largest and longest duration AHPs are generated following the 1s train stimuli in all conditions. Looking at

the raw trace overlays it is clear that the biggest effect on the AHP is caused by the P/Q and L-type Ca_V block following a 1s train, and this is confirmed by the averaged data plotted in Figure 5.5. C and D.

Figure 5.5. C plots the mean±SEM peak AHP amplitudes generated following the different duration trains compared using one-way ANOVA with Tukey's post-hoc test. There is no difference in peak AHP amplitude between 7-NI-treated (black circles), 7-NI+SNP-treated (red circles) and 7-NI+SNP+apamin treated (mauve circles) cells. However, block of P/Q and L-type Ca_V channels in the 7-NI+SNP+agatoxin+nifedipine cells (green circles) reduces the peak AHP amplitude compared to 7-NI and 7-NI+SNP-treated cells following train durations greater than 400ms, with the greatest magnitude reduction observed following the 1s train: 7-NI peak AHP was -23.98±2.6 (n=5), 7-NI+SNP-treated peak AHP was -24.5±2.2mV (n=8), 7-NI+SNP+apamin was -22.12±1.9mV (n=5) and 7-NI+SNP+aga+nif was -14.5±1.2mV (n=7, $p<0.01$).

Figure 5.5. D plots the mean±SEM AHP time to half decay against the stimulus train after which it was generated. The trend is for time to half decays to decrease following increasing stimulus durations. Following a 1s stimulus train AHP time to half decays generated in: 7-NI-treated cells were 40.98±5.7ms (n=5, black circles); 7-NI+SNP-treated cells were 49.78±5.1ms (n=8, red circles); 7-NI+SNP+apamin treated cells were 46.2±4.1ms (n=5, mauve circles); and 7-NI+SNP+aga+nif-treated cells were 73.18±11.9ms (n=7, green circles). One-way ANOVA reveals significant variance between the group means, $p=0.04$, but no significant difference is observed following pair-wise comparisons with Tukey's post-hoc test.

This set of experiments suggests that inclusion of TEA may still not guarantee enough Ca^{2+} influx to recruit SK activation, and therefore contribution of I_{SK} to the AHP. That said, AHPs are still generated and, in 7-NI+TEA conditions are ~2 fold greater in amplitude than those generated without TEA (Figure 5.4.), and their half decay time is also ~30% faster. The AHP generated in NO-treated cells following a 400Hz stimulus train of 1s duration is sensitive to P/Q and L-type Ca_V channel block as removal of these conductances significantly reduces the amplitude of the following AHP. So there is a Ca^{2+} dependence to the stimulus trains and the AHP.

The lack of apamin sensitivity in these cells under these stimulus conditions suggests that the SK channels are not well coupled to the Ca^{2+} influx during these trains, and perhaps this could be due to spatial separation within the cell? Without the availability of good antibodies to observe channel locations it is difficult to test this.

The question of whether I_{SK} can ever be recruited during a train can be answered by increasing the train durations beyond 1s, further increasing Ca^{2+} entry and boosting the chance of SK activation.

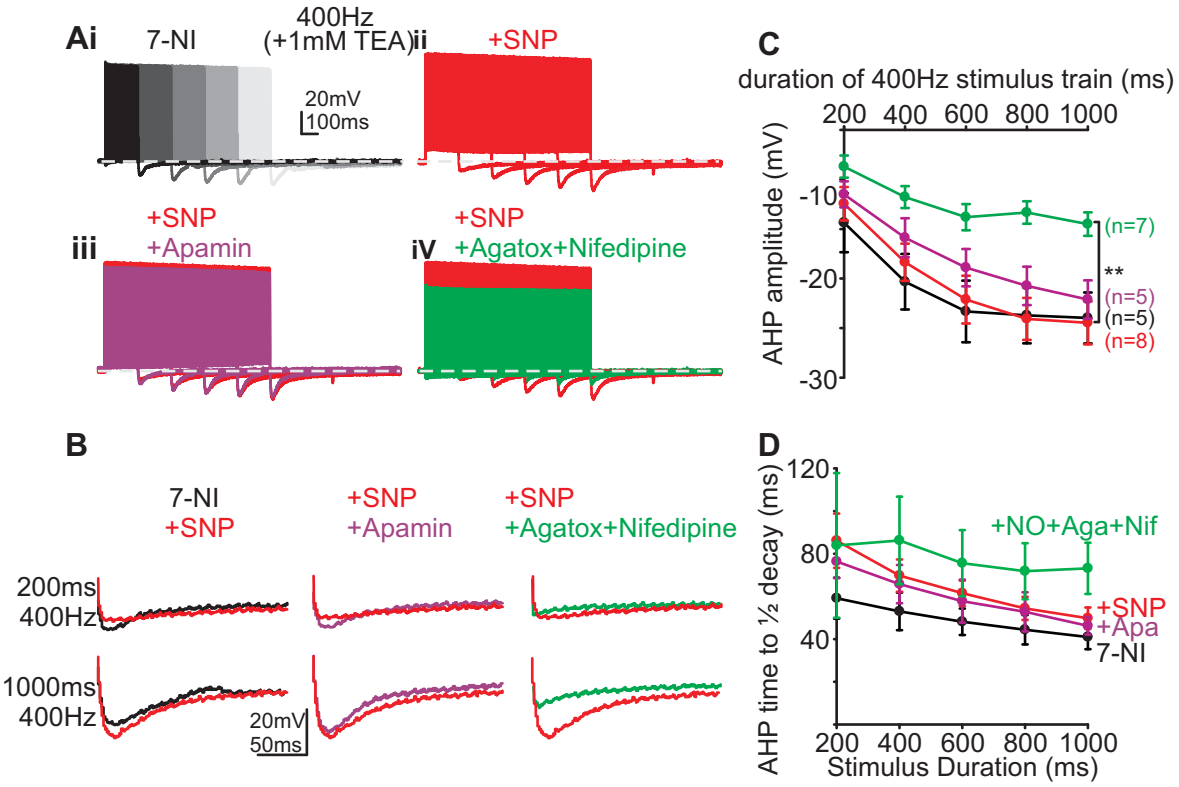

Figure 5.5. AHP is calcium dependent, but stimulus trains in the presence of TEA to broaden APs and increase Ca^{2+} influx during train does not affect AHPs.
Ai. Raw trace from 7-NI (black trace) subjected to 0.8ms 2nA current injections at a frequency of 400Hz for increasing durations in the presence of 1mM TEA. **Aii.** Raw trace from 7-NI+SNP-treated cell (red trace) subjected to 0.8ms 2nA current injections at a frequency of 400Hz for increasing durations in the presence of 1mM TEA. **Aiii.** Raw trace from an 7-NI+SNP+Apamin treated cell (mauve trace) overlaid with a raw trace from an SNP-treated cell (red trace), both having been subjected to 0.8ms 2nA current injections at a frequency of 400Hz for increasing durations in the presence of 1mM TEA. **Aiv.** overlay of raw traces from a 7-NI+SNP (red trace) treated cell and a 7-NI+SNP+Agatoxin and Nifedipine treated cell (green trace), generated by 0.8ms 2nA current injections at a frequency of 400Hz for increasing durations in the presence of 1mM TEA. **B.** Enlarged AHPs from 200ms and100ms trains as shown in A. AHPs from 7-NI+SNP treated cells are overlaid with AHPs from 7-NI, 7-NI+SNP+Apamin and 7-NI+SNP+Agatoxin and Nifedipine treated cells, as described at top of panel. **C.** Plot to show mean±SEM AHP amplitude generated following 400Hz stimulus trains of increasing duration. **D.** AHP time to half decay following 400Hz stimulus trains of increasing duration. **p<0.01, one-way ANOVA with Tukey's post-hoc test.

5.6 Prolonged stimulus trains recruit I_{SK} to the AHP.

By prolonging the stimulus protocol to 4s of 400Hz 0.8ms 2nA pulse current injections in the presence of 1mM TEA, we can push the Ca^{2+} influx during the train, maximising the chances of SK activation. Looking at the raw traces from a control 7-NI cell (black trace), 7-NI+SNP-treated cell (red trace) and 7-NI+SNP+apamin treated (mauve trace) shown in Figure 5.6 Ai-iii, it is clear that there are differences within the trains and that large AHPs are generated following the trains. Figure 5.6. B plots the mean±SEM ΔV_m accrued during the train: 7-NI was -7±1.5mV (n=6), 7-NI+SNP-treated was -5.8±1.7mV (n=6), and 7-NI+SNP+apamin was -3±0.8mV (n=9) (p=0.08, one-way ANOVA).

With $K_V3.1$ blocked by the presence of 1mM TEA the APs were already broader than those measured in section 5.4. However, a very significant broadening of the APs took place within the train, and the mean±SEM AP halfwidths are plotted in Figure 5.6. C: 7-NI AP halfwidth increased from 0.38±0.04ms to 0.5±0.04ms (black circles, n=6, $p<0.05$, paired t-test); 7-NI+SNP-treated cells (red circles) broadened from 0.29±0.01ms to 0.43±0.02ms ($p<0.001$, n=6, paired t-test); and 7-NI+SNP+apamin cells broadened from 0.28±0.02ms to 0.42±0.02ms ($p<0.001$, n=9, paired t-test).

As expected, there was no significant difference between the peak AHP amplitudes of the 7-NI, 7-NI+SNP and 7-NI+SNP+apamin treated cells. The mean±SEM peak amplitudes compared using one-way ANOVA with Tukey's post-hoc test are plotted in the summary bar graph in Figure 5.6. D: 7-NI amplitude was -18.4±1.7mV (black bar, n=6, $p>0.05$), 7-NI+SNP-treated peak amplitude was -21±1.8mV (red bar, n=6, $p>0.05$), and 7-NI+SNP+apamin treated peak amplitude was -22.1±3.8 (mauve bar, n=9, $p>0.05$).

Interestingly, this longer duration stimulus does recruit I_{SK} to the AHP, and block by apamin in NO-treated cells reduced the time to half decay, compared using one-way ANOVA with Tukey's post-hoc test, as summarised in the bar graph in Figure 5.6. E: 7-NI-treated cells time to half decay was 66.5±6.6ms (black bar, n=4), 7-NI+SNP-treated was 72.4±7.6ms (red bar, n=6) and 7-NI+SNP+apamin-treated time to half decay was 43.4±5.9ms (mauve bar, n=9, $p<0.05$)

These longer duration stimuli induced apamin-sensitive AHPs that apaminwere therefore partially dependent on SK channels. The 4s 400Hz stimuli in the presence of NO+TEA must have facilitated enough Ca^{2+} entry to activate the SK channels, which are known to contribute to the repolarising phase of the AHP (Lancaster & Adams, 1986), slowing membrane return to RMP(/V_h), as cells treated with NO+apamin (and TEA) generated AHP time to half decays that were 30% faster than NO-treated alone.

However, long duration protocols and need for presence of $K_V3.1$ inhibitor TEA to ensure enough Ca^{2+} enters the cell during the train to activate I_{SK}, is not physiologically relevant, neither is injecting current postsynaptically. As SK channels are known to associate with NMDARs in hippocampal pyramidal neurons (Ngo-Anh *et al.*, 2005) and, as the same glutamate receptors are expressed at the postsynaptic face of the MNTB neurons, I next asked if SK channels could be activated on synaptic stimulation.

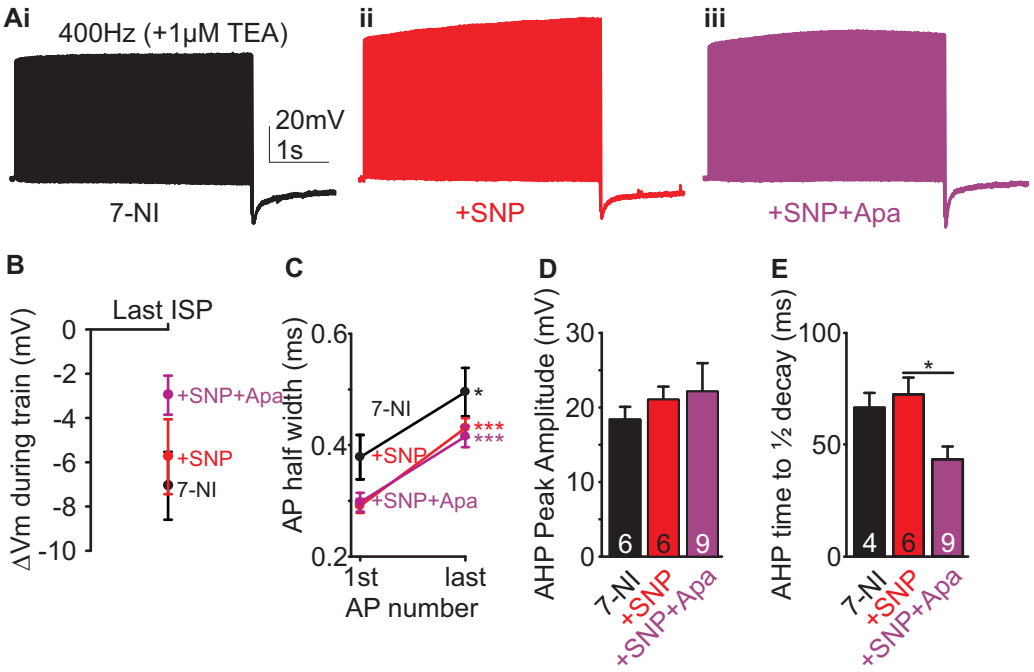

Figure 5.6. 4s stimulus trains recruit SK channels to contribute to AHP. **Ai.**7-NI cell stimulated at 400Hz for 4s with 0.8ms 2nA current injections (black trace). **Aii.** 7NI+SNP-treated cell stimulated at 400Hz for 4s with 0.8ms 2nA current injections (red trace). **Aiii.**7-NI+SNP+apamin treated cell stimulated at 400Hz for 4s with 0.8ms 2nA current injections (mauve trace). **B.** Plot to show change in membrane potential (ΔVm) during the 4s stimulus train, measured as the difference between the mean±SEM last inter spike potential and the holding potential (-60mV) **C.** Plot to show mean±SEM halfwidths of first and last AP in the train. *p<0.05,***p<0.001, paired t-test. **D.** Summary bar graph of mean±SEM peak AHP amplitude in 7-NI (black bar),7-NI+SNP (red bar) and 7-NI+SNP+Apamin (mauve bar) treated cells. **E.** Summary bar graph of mean±SEM AHP time to half decay for 7-NI (black bar), 7-NI+SNP (red bar) and 7-NI+SNP+apamin (mauve bar) treated cells. *p<0.05, one-way ANOVA with Tukey's post-hoc test.

5.7 I_{SK} induces an after hyperpolarisation in the presence of NO following synaptic stimulation.

Inducing trains of excitation by synaptic innervation of MNTB neurons is more physiological than the postsynaptic current injection scenario used in the previous sections. Working in collaboration with Joern Steinert, a bipolar electrode was placed across the midline of the brainstem slice to stimulate the fibres that innervated the postsynaptic MNTB principal neurons (Figure 5.7. A). When a presynaptic fibre is stimulated, glutamate is released into the synapse which activates postsynaptic glutamate receptors, depolarising the postsynaptic cell and inducing an AP. When a connected principal neuron was found it was possible to stimulate the presynaptic fibre and record the postsynaptic response by patching the postsynaptic cell, and observing its activity in current clamp mode.

On finding a connected cell, 150ms burst stimuli were given at frequencies of 100, 300 or 400Hz. Example raw traces from 7-NI (black trace), NO-treated (red trace) and NO+apamin treated cells are shown in Figure 5.7. B. It is evident from these example traces that an AHP is generated following the train in the NO-treated cell, and this is absent in the NO+apamin treated cell. Measuring the amplitude of the afterpotential at a 50ms latency following the train (Stocker, 2004) reveals effects of both stimulus frequency and NO exposure on these cells. The summary bar graphs in Figure 5.7. C shows the mean±SEM afterpotential generated following a 100, 300 and 400Hz stimuli (150ms), data are analysed using a one-way ANOVA with Tukey's post-hoc tests. No afterhyperpolarisation is generated following a 100Hz stimulus in all treatment conditions: 7-NI, 1.3±0.7mV (black bar, n=6); 7-NI+apamin, 3.5±1.8mV (blue bar, n=4);

7-NI+SNP, 1.2±1.3mV (red bar, n=4); or 7-NI+SNP+apamin, 4.6±1.3mV (mauve bar, n=3). In the presence of NO, a 300Hz stimulus train tends to induce an afterhyperpolarisation, which is almost significant when compared with 7-NI-treated cells (p=0.056). 7-NI mean±SEM was 0.9±1.0mV (black bar, n=6), 7-NI+apamin was 4.0±1.9mV (blue bar, n=4), 7-NI+SNP mean±SEM was -1.7±1.1mV (n=4), 7-NI+SNP+apamin was 2.3±0.8mV (mauve bar, n=6). In both 7-NI and 7-NI+SNP-treated conditions the 300Hz stimulus train ainduces an after depolarisation in the presence of apamin. Following a 400Hz train the afterpotential amplitudes produced by the different treatment conditions were: 7-NI-treated AHP, 1.5±0.8mV (n=4, black bar); 7-NI+apamin, 5.9±1.6mV (blue bar, n=3, $p<0.05$ vs 7-NI+SNP); 7-NI+SNP, -3.6±1.2mV (n=3, red bar, $p<0.05$, vs 7-NI+SNP+apamin); 7-NI+SNP+apamin, 5.9±1.6mV (blue bar, n=3). The stimulus train in the presence of apamin again induced an afterdepolarising potential in control and NO-treated conditions following the 400Hz stimulus.

Using presynaptic stimulation instead of postsynaptic current injections is a more physiologically relevant scenario, and induced an AHP after just 150ms in the 400Hz frequency NO-treated test. The AHP following the 400Hz stimulus was apamin sensitive, suggesting an SK dependency. This suggests that postsynaptic SK channels are more readily activated by synaptic induction, and possibly therefore Ca^{2+} influx through glutamate receptors, such as the NMDA receptor.

At all frequencies and in all conditions SK block induced an afterdepolarising potential following the synaptic stimulus trains. This could be explained by an increased postsynaptic response to the synaptically evoked depolarisation, maintaining the

induced depolarisation following the train, or by a presynaptic mechanism increasing the evoked depolarisation.

This was answered by investigating the amplitudes of the evoked excitatory post synaptic currents (EPSCs) and their sensitivity to NO-treatment and SK block.

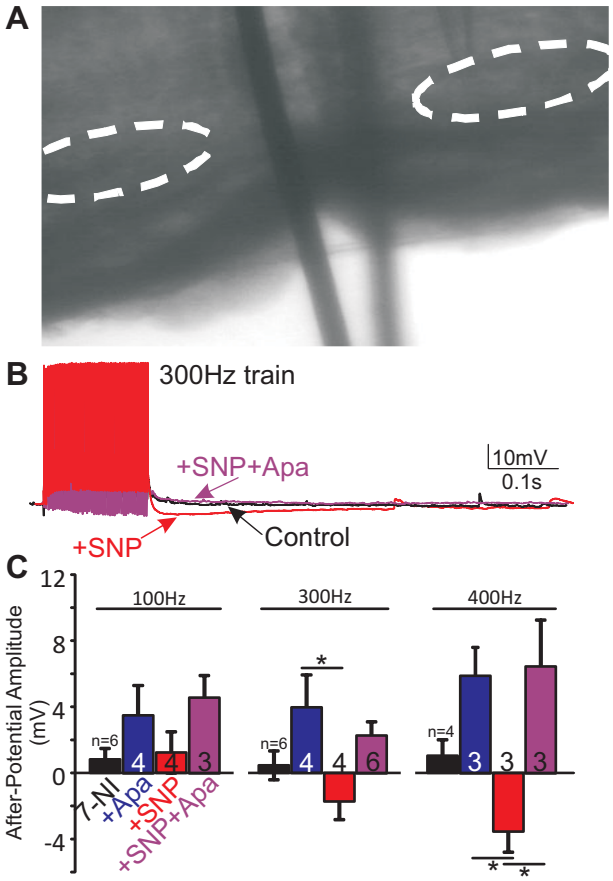

Figure 5.7. I_{sK} induces an after hyperpolarisation in the presence of NO following synaptic stimulation.
A. Photograph shows a bipolar electrode being placed across the midline of the slice. The dashed elipses show the position of the MNTB in the slice. **B.** Raw traces from three cells in 7-NI (black trace), 7-NI+SNP (red trace) and 7-NI+SNP+Apamin (mauve trace). **C.** Summary bar graph of mean±SEM after potential amplitudes in 7-NI control (black bar), 7-NI+Apamin (blue bar), 7-NI+SNP (red bar) and 7-NI+SNP+apamin (mauve bar) treated cells, following 200ms train of different stimulus frequencies. *p<0.05, one-way ANOVA with Tukey's post-hoc test.

5.8 SK block increases release probability at the calyx.

To investigate EPSC amplitudes I repeated the synaptic stimulation, and held the postsynaptic cell under voltage clamp control. By holding the cell at -40mV it was possible to observe the fast depolarising AMPA receptor current. Figure 5.8. Ai shows an overlay of single raw EPSC traces from 7-NI (black trace) and 7-NI+apamin treated (blue trace) cells. It is clear that treating the slice with 7-NI+apamin increases the EPSC amplitude in these cells. Glutamate receptor activation and therefore EPSC amplitude is dependent on glutamate binding. Increased amplitude EPSCs is indicative of increased glutamate release at the synapse. Figure 5.8. Aii shows overlayed raw traces of control and apamin treated EPSCs during a 300Hz 200ms stimulus train, the EPSC potentiation in Ai is not as obvious in the train. This may be the result of the experimental design as the single EPSCs were generated from a single test pulse, whereas the 300Hz stimuli were carried out after 100Hz test pulses, and it is possible that the synapse was not given enough time to recover before the 300Hz test.

Figure 5.8. Bi shows a 7-NI+SNP-treated raw trace EPSC (red trace) overlaid with an 7-NI+SNP+apaminApamin EPSC raw trace (mauve trace). ApaminApamin also increases EPSC amplitude in NO-treated cells. Figure 5.8. Bii shows an overlay of 7-NI+SNP -treated and 7-NI+SNP +apamin raw traces during a 300Hz 200ms train. From the raw data in Figures 5.8. A and B, it looks as if NO reduces the amplitude of the evoked EPSC compared to control, and in doing so reduces synaptic depression during a train. SK block increases the evoked EPSC amplitude in both control and NO-treated conditions, and causes a similar amount of synaptic depression during the train in both. This is best observed in Figures 5.8. Ci and Cii which show the mean+SEM EPSC amplitudes

during a 300Hz train in 7-NI (black circles), 7-NI+apamin treated (blue circles), 7-NI+SNP-treated (red circles) and 7-NI+SNP+apamin treated (mauve circles) cells. The effect of apamin on the evoked mean±SEM EPSC amplitudes illicited by a single stimulus are summarised in the bar graph in Figure 5.8. D, and data are analysed using one-way ANOVA with Tukey's post-hoc test: 7-NI amplitude was 9.7±0.3nA (black bar, n=4), and 7-NI+apamin doubled the I_{EPSC} amplitude to 20.1±2nA (blue bar, n=4, $p<0.01$); treatment of cells with 7-NI+SNP reduced the I_{EPSC} amplitude by ~30% compared to 7-NI to 7.5±0.6nA (red bar, n=6), and 7-NI+SNP+apamin significantly potentiated the I_{EPSC} to 16.4±3nA (mauve bar, n=4, $p<0.01$, vs 7-NI+SNP). To understand if the potentiation caused by apamin is different between control and NO-treated conditions I normalised to the parent condition, and the summary data is displayed in the bar graph in figure 5.8. E. NO reduced the EPSC amplitude by ~30% compared to control, whereas apamin potentiates the evoked EPSC by ~110%. NO+apamin potentiates the EPSC amplitude by ~120% compared to the normalised NO-treated amplitude. This suggests that SK block increases the 7-NI and NO-treated EPSC amplitudes by similar amounts.

NO reduces the EPSC amplitude by ~30% but also reduces synaptic depression during a train. The summary bar graph in Figure 5.8. F shows the normalised mean±SEM depression, calculated as the percentage difference between the 1st EPSC ($EPSC_1$) in the 300Hz train and the last ($EPSC_{60}$) across the data set: 7-NI EPSCs depressed by 65±13% (black bar, n=4); 7-NI+apamin by 64±9% (blue bar, n=4); 7-NI+SNP-treated by 37±11% (red bar, n=5); and 7-NI+SNP +apamin EPSCs by 70±5% (mauve bar, n=4). Although the variation between the group means was not significant ($p=0.11$, one-way

ANOVA), the trends suggest that NO reduction in synaptic depression during a train is dependent on SK activation, or that SK block increases the release probability of the presynaptic terminal which counteracts the apparent NO-dependent reduction in synaptic depression.

Given the larger evoked EPSCs generated on SK channel block it made sense to test any effect of apamin on release probability. For this it was more intuitive to look at miniature, non-evoked EPSCs, as any change in the mini frequency could suggest a change in release probability.

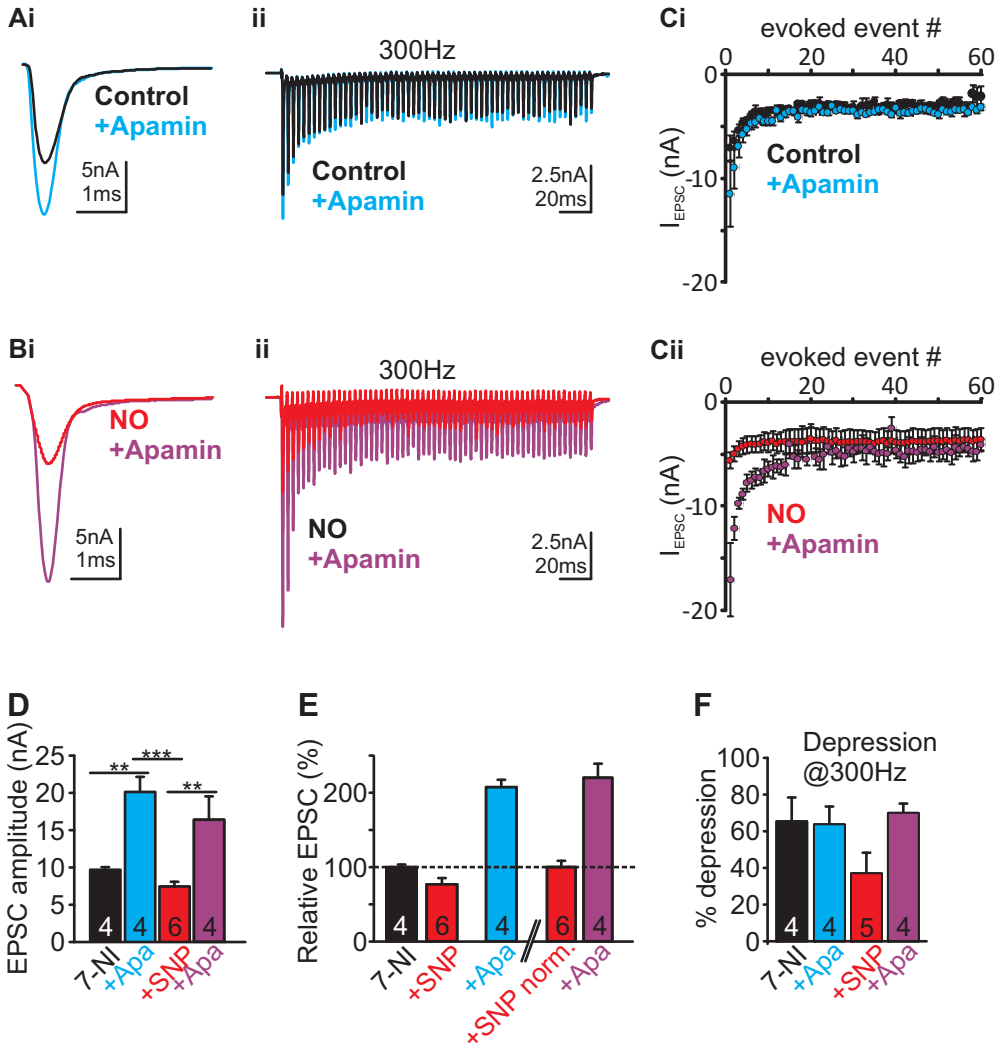

Figure 5.8. SK block increases evoked release at the Calyx.
Ai. Overlay of single evoked EPSCs recorded in 7-NI (black trace) and 7-NI+Apamin (blue trace) cell. **Aii.** Overlay of 300Hz 200ms train recorded in a control (black trace) and apamin treated (blue trace) cell. **Bi.** Overlay of single evoked EPSCs recorded in an NO-treated cell (red trace) and NO+apamin treated (mauve trace) cell. **Bii**. Overlay of 300Hz 200ms train recorded in an NO-treated cell (red trace) and NO+apamin treated (mauve trace) cell. **Ci.** Mean±SEM peak I_{EPSC} recorded at each stimulus in a 300Hz 200ms synaptic train for 7-NI control (black circles) and apamin treated (blue circles) cells. **Cii.** Mean±SEM peak I_{EPSC} recorded at each stimulus in a 300Hz 200ms synaptic train for NO-treated (red circles) and NO+apamin treated (mauve circles) cells. **D.** Summary bar graph of mean±SEM evoked EPSC amplitudes in 7-NI control (black bar), 7-NI+apamin (blue bar), NO (red bar) and NO+apamin (mauve bar) treated cells. **E.** Summary bar graph of mean±SEM %EPSC amplitude of NO-treated (red bar) and apamin treated (blue bar) normalised primarily to amplitude of 7-NI control (black bar) cells, and secondly of NO+apamin treated (mauve bar) to amplitude of NO-treated (red bar after dash) cells. **F.** Summary bar graph of mean±SEM EPSC depression for the differently treated cells within the 300Hz train, shown as the difference in amplitude between the first $EPSC_1$ and last $EPSC_{60}$, data is normalised to $EPSC_1$. *p<0.05,**p<0.01, ***p<0.001, one-way ANOVA with Tukey's post-hoc test.

5.9 There is a trend for an NO-dependent reduction in mEPSC amplitude at the calyx.

Miniature EPSCs (mEPSCS) or minis are the currents generated by the random release of quanta from synaptic vesicles at the pre synaptic terminal (Fatt & Katz, 1952). They differ from the evoked EPSCs in that they are usually from single vesicles, and they are random events, not evoked by active depolarisation of the terminal following an AP.

To measure mEPSCs at the calyx synapse, 7-NI incubated slices were perfused with normal aCSF containing 0.5µM TTx, to block Na_V channels, and AP firing. MNTB principal neurons were whole cell patched and voltage clamped at -80mV. The mEPSCs were then recorded over 60 seconds, and the findings are presented in Figure 5.9.

Figure 5.9. A, shows a frequency histogram detailing the distribution of mEPSC amplitudes binned in 5pA lots and the frequency of mEPSCs at those amplitudes in 7-NI (black bars, n=4) and 7-NI+apamin treated cells (blue bars, n=2). 7-NI+apamin treatment seems to increase the number of larger amplitude events, causing a rightward shift in the frequency histogram, compared to control, but this data is only from two cells.

Figure 5.9. B, shows a frequency histogram of the mEPSC amplitudes recorded from 7-NI+SNP treated (red bars, n=3) and 7-NI+SNP+apamin treated (pink bars, n=3) cells. NO seems to reduce the frequency of larger amplitude mEPSCs compared to control, but the frequency of smaller mEPSCs is unaffected. 7-NI+SNP+apamin looks to cause a leftward shift in the frequency histogram compared to NO-treated, increasing the frequency of smaller mEPSCs.

When analysing the mean±SEM mEPSC amplitude from across the data set this apparent NO-induced increased frequency of smaller amplitude events is lost, and mEPSCs have a similar mean amplitude. 7-NI mean±SEM amplitude was 43±7pA (n=4, black bar), 7-NI+apamin-treated amplitude was 80pA (n=2, blue bar), 7-NI+SNP treated mini amplitude was 45±18pA (n=3, red bar), 7-NI+SNP+apamin amplitude was 56±23pA (n=3, mauve bar) (Figure 5.9. C). A change in mEPSC amplitude could be explained by a change in quantal size, i.e. the amount of glutamate released per vesicle, or a change in the postsynaptic receptors' response to glutamate binding. The 7-NI+apamin mean amplitude is taken from only two cells and so is difficult to interpret. These data go against previous findings (Steinert *et al.*, 2008) which suggest an NO-dependent decrease in mEPSC amplitude and decay tau. This is hard to explain, and could be due to the low n numbers in this experiment. More repeats in all conditions will improve the resolution of any NO-dependent or apamin-dependent effects on mEPSCs and may reveal smaller amplitude mEPSCs in the NO-treated conditions consistent with the findings of Steinert *et al* (2008).

Any changes in mEPSC decay time will reflect a change in glutamate receptor sensitivity to glutamate, and so indicate a post synaptic effect. Analysing the mean±SEM decay times measured using clampfit software reveals no significant effect of NO or apamin, but there is a trend for a slowing in decay τ compared to 7-NI: 7-NI mEPSC decay time was 0.25±0.07ms (n=4, black bar); 7-NI+apamin treated was 0.3ms (n=2, blue bar); 7-NI+SNP-treated was 0.34±0.02ms (n=3, red bar); 7-NI+SNP+apamin was 0.35±0.06ms (n=3, mauve bar). This is in contrast to previous findings of NO's effect in slowing mEPSC decay by 30% (Steinert *et al.*, 2008).

The number of mEPSCs generated per second, or frequency of mEPSCs, is governed by the release probability of the vesicles. For a single docked vesicle, the induced mEPSC is a product of the quantal volume, and the probability of its release into the synapse. A high frequency of mEPSC events suggests a high release probability of vesicles. The summary bar graph in figure 5.9. E. shows the mean±SEM mEPSC frequency at the treated synapses: 7-NI was 4.9±2.9 events s^{-1} (n=4, black bar), 7-NI+apamin treated was 6.3 events s^{-1} (n=2, blue bar); 7-NI+SNP-treated was 1.9±0.9 events s^{-1} (n=3, red bar), and 7-NI+SNP+apamin treated was 2.1±0.3 events s^{-1} (n=3, mauve bar).

This reduction in mEPSC frequency in the NO-treated conditions is not significant (p=0.47, one-way ANOVA) but suggests a reduction in release probability of vesicles at this synapse. apamin has no effect on the mEPSC frequencies measured at control or NO-treated synapses.

Taken together these results suggest that NO is having an effect on the mEPSCs, with the frequency distribution data suggesting a reduction in larger amplitude events. This is not significant when comparing the mean mEPSC amplitudes. However, the low n numbers could restrict the interpretation of this data. In either control or NO-treated cases, apamin and therefore SK block does not have an effect on mEPSC amplitude or frequency, but again the lack of repeats could limit this interpretation.

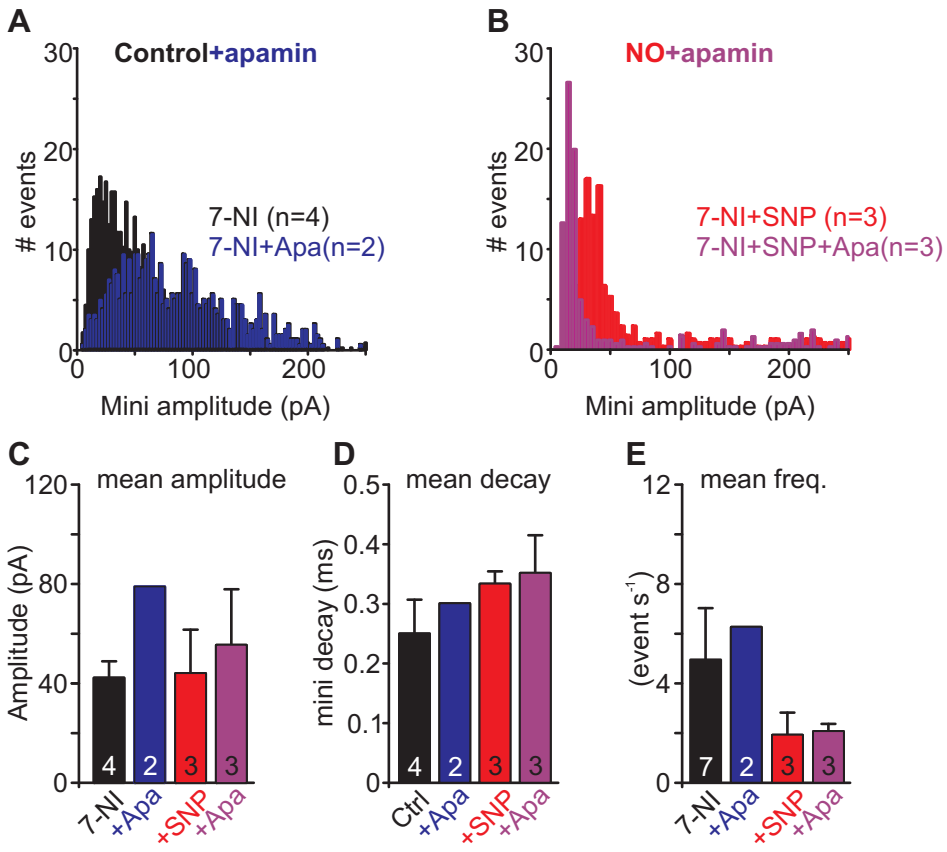

Figure 5.9. SK block does not affect mini amplitudes or frequency in control or NO-treated cells

A. Frequency histogram for mini EPSC amplitudes recorded in 7-NI (black bars) and 7-NI+Apamin (blue bars) conditions. **B.** Frequency histogram for mini EPSC amplitudes in 7-NI+SNP-treated (red bars) and 7-NI+SNP+Apamin treated conditions (mauve bars). **C-E.** Bar graphs to show mean±SEM amplitude (**C**), time course of decay (**D**), and frequency (**E**) of mini EPSCs generated in 7-NI (black bars), Apamin (blue bars), 7-NI+SNP (red bars) and 7-NI+SNP+apamin treated (mauve bars) cells.

5.10 Discussion

The three pronged approach of qPCR, immunohistochemistry and electrophysiology confirms the presence of SK channels, composed of the dominantly expressed SK2 subunit, in MNTB principal neurons. The apamin sensitivity of the tail currents measured in Figure 5.1. infer the amplitude of the SK current, and are plotted as the absolute peak. Other groups calculate the integral of the tail current or induced I_{AHP} before and after apamin to calculate the amplitude of the current (Buchanan *et al.*, 2011; Petrovic *et al.*, 2012), but as our recordings are unpaired, this was not possible. Either way it is clear that there is a significant apamin sensitive current in these neurons and this is potententiated by NO. More strikingly, block of P/Q and N-type channels, the channels modulated via the NO-cGMP pathway, reduces the NO-potentiated apamin sensitive current back to control+apamin levels. This suggests that NO-potentiation of the Ca_V channels underlies the potentiation of the apamin sensitive current as well. This could be indicative of NO→Ca_V→SK coupling, and SK channels are known to couple to Ca_V channels, L-type and SK couple in the hippocampus (Marrion & Tavalin, 1998) and P/Q and SK couple in the cerebellum (Womack & Khodakhah, 2004). Coupling could have been investigated here by increasing EGTA concentration in the patch pipette and seeing if increased intracellular Ca^{2+} buffering occluded SK activation. This is an experiment for the future.

Despite the voltage clamp evidence it was difficult to activate SK channels in more physiological scenarios. No striking effect of SK block on single APs in control and NO-treated cells was observed, although NO AP-broadening was present. SK block did hint

at an increase in input resistance, consistent with increases in membrane tau seen in other investigations (Buchanan *et al.*, 2011), but this was not significant.

Due to MNTB neurons propensity to only fire single APs on depolarisation, AP trains were induced by postsynaptic current injection, and the AHPs observed following these trains. However, variable apamin sensitivity was observed in the AHPs following the trains. This could be due to not enough Ca^{2+} entering the cell to activate SK channels during the train in control or NO-treated conditions, or to inefficient coupling between Ca_Vs and SK channels. In addition, the experimental design was not optimised to robustly measure Ca_V→SK activation during a train. This is because synaptic current blockers were not included in the bath solution, and random activation of glutamate receptors during the postsynaptic train could increase Ca^{2+} influx, or lead to increased release of Ca^{2+} from internal stores via alternative pathways to the somatic AP firing, which would influence SK activation, and hence the relevant apamin sensitivity observed.

There are technical issues with the approach taken to elucidate the physiological relevance of the NO→Ca_V→SK pathway as well. The Axopatch 200B amplifier is not the most suitable amplifier for making current clamp recordings or measuring high frequency activity in neurons (Magistretti *et al.*, 1996). Also the protocol of injecting postsynaptic current is not as relevant as synaptically induced depolarisation. However, presynaptic stimulation would also include any presynaptic effects of the pharmacology, and so cannot be used in this case. A better solution would have been to measure the EPSC following evoked presynaptic release, and convert this into conductance which can then be injected into the post synaptic cell as a voltage

waveform, termed simulated synaptic conductance (SSG) (Johnston *et al.*, 2009). An improved solution would be to use dynamic clamp to inject the AP waveform, and then remove or add Ca_V or SK conductances electrophysiologically to understand their contribution to waveform shape in control and NO conditions.

Despite these confounding issues, changes in waveform shape were observed throughout and following the trains. AP halfwidth broadened during the train, and AHP amplitude also increased. This is consistent with inactivation of $K_V3.1$ channels.

Block of SK channels did not induce depolarised interspike potentials, as might have been expected based on evidence from cerebellar purkinje cells (Raman & Bean, 1999), instead hyperpolarisation was observed during the train, and a potentiated AHP was generated with a faster time to half decay following high frequency trains. The hyperpolarisation during the train could be explained by an increase in input resistance, but is difficult to explain otherwise. The increase amplitude AHP could also be explained by increased input resistance, and the reduced time to half decay of the AHP is an expected observation in the presence of apamin, although this was not potentiated in the presence of NO. Due to the multitude of channel contributions in the current clamp scenario it is difficult to draw conclusions from the data, but one striking observation was the effect of blocking L-type and P/Q-type calcium currents, which dramatically reduced AHP amplitude, but slowed rather than sped up the AHP time to half decay. If Ca^{2+} through these channels activated SK channels then one would expect a faster AHP in their absence.

Pushing the physiological boundaries of the current clamp scenario to maximise Ca^{2+} influx during the train by including TEA (1mM) to broaden the APs, prolonging the high

frequency (400) stimulus to 4s, did recruit SK channels to contribute to the AHP. This evidence may support a lack of coupling between the Ca_V and SK channels, and argues against an NO→ Ca_V → SK pathway.

Synaptic stimulation reveals an AHP that is NO and SK dependent. In the nNOS silent, control condition, no AHPs are induced after a 150ms synaptic trains of 100, 300 and 400Hz frequencies. However, in the presence of NO, an AHP is induced at higher frequencies, suggesting a frequency dependent generation of AHP. This conveniently fits with the model that nNOS is activated during high frequency innervations. The AHP induced in the presence of NO was removed by the co-application of apamin.

As described above, synaptic trains measured postsynaptically are confounded by any presynaptic effects. As NO is a diffusible messenger presynaptic modulation of transmitter release by NO or apamin was investigated. Interestingly, apamin significantly increased the amplitude of the EPSC in control conditions without affecting the degree of synaptic depression during a 300Hz train. In the averaged plot of I_{EPSC} evoked during the 300Hz train the potentiation is not as pronounced. This could be due to a technical reason because experimentally I may not have allowed enough recovery time between stimulus trains, and as such the 300Hz train was given when the synapse was still recovering.

In the NO treated cells, the EPSC is reduced by 30% as seen previously (Steinert *et al.*, 2008), but apamin potentiates the evoked response to a similar amplitude seen in the control test. These data suggest that SK channels act to suppress transmitter release at this synapse.

NO is thought to act postsynaptically on AMPARs, altering their response to glutamate binding by reducing current amplitude and slowing their deactivation kinetics (Steinert *et al.*, 2008). These changes in EPSC amplitude underlie the reduction in synaptic depression seen in NO-treated cells. Over the 150ms 300Hz train, the synapse depresses by 40%, whereas in control, apamin, and NO+apamin-treated conditions the synapse depresses by ~70%. SK block increases EPSC amplitude by a similar proportion in control and NO treated cells, suggesting SK channel action may be independent of NO's modulatory effect at the synapse, but as SK block increased synaptic depression in NO-treated cells to control levels, we can conclude that SK action is fundamentally important for NO's effects.

At the calyx, the number of vesicles that will be released per evoked response, or AP invading the synaptic terminal, is dependent on how many active zones are activated (N), how many vesicles are docked and primed for release (q) in these active zones, and the probability that they will be released (p): EPSC=Nqp

In a very simple model, with the same release probability for each active zone, and the same number of vesicles ready for release per active zone, then the evoked release is entirely dependent on how many active zones can be recruited, EPSC=N.

In reality the picture is further complicated by the fact that each active zone has its own release probability, and number of vesicles, with a range of glutamate concentrations per vesicle.

Release probability is governed by activation of presynaptic Ca^{2+} influx through Ca_V channels, which in the calyx of P13-P16 mice are P/Q-type (Forsythe, 1994; Iwasaki &

Takahashi, 1998). An invading AP will depolarise the terminal, activating P/Q channels allowing Ca^{2+} influx which will initiate transmitter release (Neher & Sakaba, 2008). This Ca^{2+} will also stimulate endocytosis, modulate the P/Q-type channels (Forsythe *et al.*, 1998), and contribute to short term facilitation if the next depolarisation arrives before intracellular buffering (Borst & Soria van Hoeve, 2011), or it could activate K_{Ca} channels like BK (Nakamura & Takahashi, 2007) or SK.

The amount of Ca^{2+} influx per invading AP is dependent on the number of channels available to open, and the driving force acting on those channels. This Ca^{2+} influx is closely coupled to transmitter release, such that it has recently been shown that the Ca^{2+} channel density directly corresponds to release probability at active zones (Sheng *et al.*, 2012).

If SK channels are located in or close to active zones, then they will be activated during synaptic depolarisation and Ca^{2+} influx, and theoretically would contribute to hyperpolarisation of the membrane, restricting Ca^{2+} influx, but also maintaining the driving force for further depolarisations. This would mean blocking them would drive the active zone to depletion quickly, with successive depolarisations, as $Ca^{2+}$and sustained depolarisation would facilitate release probability.

This goes against what is seen in my data. Although the trains are relatively short (150ms) they are quite high frequency, and although we see large EPSCs with 70% depression throughout the train, we do not see EPSC failures.

This brings me to postulate that the SK channels do not act solely to restrict release probability in the calyx, but also to restrict spike invasion along the fenestrated

terminal, and restrict the number of active zones recruited per terminal AP by reducing input resistance, acting as a calcium dependent leak.

To further test my hypothesis, one could stimulate the calyx in the presence of an SK activator to see if this lowered release probability, generating smaller EPSCs.

To confirm that apamin did not have a direct effect on vesicular release machinery at the calyx, I attempted to investigate mini events at the synapse. The data set is incomplete, but in summary suggests that apamin and SK block does not cause any significant differences in mini amplitude or frequency in control or NO-treated conditions. However the frequency histogram in the presence of NO suggests it might increase the frequency of lower amplitude events. This needs further testing.

In conclusion, these data suggest SK channels are expressed in the MNTB and in the calyx of Held, and they contribute to the AHP generated in these neurons. Their expression fits with the accepted synaptic model of the calyx as a high fidelity auditory relay synapse, facilitated by its large number of release sites and low release probability (Borst & Soria van Hoeve, 2011).

6. Discussion of findings and future work.

Nitric oxide is a diffusible messenger generated in neurons on Ca^{2+} activation of nNOS (Garthwaite, 2008). In the hippocampus glutamatergic activation of NMDA receptors, and Ca^{2+} influx through these channels, activates the NOS1α isoform which associates with NMDARs at the post synaptic density (Rameau *et al.*, 2007). NO directly interacts with cellular proteins, like soluble guanylyl cyclase which activates the NO-cGMP pathway. As a feedback messenger NO can diffuse back across the synapse to modulate signalling in the presynaptic terminal in a volume limited way (Garthwaite, 2005; Steinert *et al.*, 2008). In the hippocampus this can induce presynaptic mechanisms of plasticity (Arancio *et al.*, 1996), and in the MNTB it is known to increase exoendocytic coupling at the calyx, speeding up endocytosis via increased activation of PIP_2 (Eguchi *et al.* 2012).

NMDARs, and hence nNOS, is only activated during sustained or high frequency periods of activity and postsynaptic activation, this means NO exerts its modulatory actions in an activity dependent manner (Steinert *et al.*, 2011b).

In NO we have a signalling molecule that is generated on high frequency activation, is membrane permeable and can therefore signal over small distances to inform proximal neurons of the activity in a local network. An accumulating body of evidence in the MNTB suggests that NO's action at this highfidelity synapse is to: broaden AP halfwidth by inhibition of K_V3 (Steinert *et al.*, 2008), upregulate K_V2 activity (Steinert *et al.*, 2011b), reduce postsynaptic sensitivity to glutamate, whilst decreasing release

probability of the synapse (Steinert *et al.*, 2008), at the same time as pre synaptically increasing the rate of endocytosis (Eguchi *et al.*, 2012).

Here I have tried to add to this body of evidence by exploring NO-dependent modulation of Ca_V channels, and the effect this might have on cellular excitability (Figure 6.1). Using a voltage clamp approach I have characterised NO-dependent modulation of the four high-voltage-activated (HVA) Ca_V channels present in the MNTB principal neurons such that, L-type and P/Q-type channels are potentiated by NO, but by different pathways, and N-type channel voltage dependence is leftward shifted by NO-cGMP signalling, whilst R-type channels are unaffected (Figure 6.1. A). I have shown that this modulation is maintained over time, and functionally changes the contribution of Ca_V channels to the whole cell voltage-dependent Ca^{2+} entry in these neurons, shifting the bias of influx from R and N-type, to L and P/Q-type. This work is published (Tozer *et al.* 2012).

Future experiments would hope to further delineate the steps in the pathway that lead to this modulatory change, such as whether it is by S-nitrosylation or phosphorylation that the NO-dependent effects are taking place, and this could be furthered by proving which amino acid residues on the Ca_V channels or their associated subunits are modulated by NO signalling. This could be achieved by biochemical assays looking for sites of phosphorylation/S-nitrosylation combined with a recombinant channel expression system occluding these proposed sites of interaction, and the effect of those occlusions on channel current.

Having shown NO-dependent modulation of HVA I_{Ca}, I then looked at NO-dependent modulation of low-voltage-activated (LVA) T-type channels in the SPN. Firstly, I

characterised the T-type conductance (or possibly multiple conductances) revealing its large amplitude and transient kinetics. Secondly, I investigated its contribution, in cooperation with I_h, to the rebound spike firing phenotype of SPN neurons. And thirdly I showed that LVA T-type channels are inhibited by NO (~50% inhibition). NO dampens the rebound response by shifting the voltage activation of I_h more negative and inhibiting T-type current amplitude, hence reducing depolarising drive at more negative potentials. Part of this work is published (Kopp-Scheinpflug *et al.* 2011), and the NO-dependent modulation work is in preparation.

Future work will aim to identify the NO-dependent pathway by which this modulation is taking place. Applying NO-donors in the presence of the cyclase blocker ODQ will broadly separate the modulation as direct or cGMP dependent, and it would be interesting to know if I_h and I_{TCa} are modulated by the same pathway.

By trying to link the observed NO-dependent increase in voltage-dependent Ca^{2+} influx to excitability I investigated the possibility of K_{Ca} channel expression in the MNTB. BK channels were already known to be expressed (Nakamura *et al.* 2007) in the calyx of Held, but nothing was known of SK expression in the MNTB. Here we show for the first time that SK channels are expressed in the MNTB, and that the SK2 subunit is the dominantly expressed isoform in P14 mice. The channel contribution in the MNTB principal neurons was inferred as a measure of apamin sensitivity, and apamin sensitive tail currents were potentiated by NO, but sensitive to P/Q and N-type channel block suggesting an NO→ Ca_V → SK modulatory pathway.

An overlooked experiment in this situation would have been to repeat the voltage clamp tail current investigation with an increased EGTA concentration in the pipette.

The effect of increased cellular Ca^{2+} buffering might occlude SK activation, and tell us something about coupling between Ca_V Ca^{2+} entry and SK activation.

SK channels partially contributed to an after hyperpolarising potential (AHP) following trains of APs in the principal neurons, but this required long duration high frequency trains of broad APs. To further improve the resolution of these experiments, it would be necessary to repeat them in the presence of synaptic current blockers, i.e. MK801 and CNQX, as Ca^{2+} influx through synaptic currents could activate SK channels, affecting results.

Apamin sensitive SK-mediated AHPs were induced by synaptic stimulation in the presence of NO. Shorter duration synaptic trains induced robust AHPs, which showed apamin sensitivity, suggesting that SK channels may be closely coupled to Ca^{2+} influx during synaptic current depolarisation, either mediated through glutamate receptors or via activation of Ca_Vs.

The data hinted at a frequency dependency of AHP induction, higher frequency activity generated larger and broader AHPs. It would have been interesting to further develop this concept, testing the synapse at higher frequencies. Future work should also aim to explain the function of the AHP following the stimulus train input, does it facilitate fast latency responses to the following input? Does it facilitate relief of inhibition downstream in the SPN? These could be tested by giving a sequential train shortly after the first, and assessing firing behaviour in the different conditions, and by looking at IPSPs in the SPN in NO and apamin treated conditions.

In the thesis I tried to link NO-dependent modulation of Ca_V mediated Ca^{2+} influx to SK channel activation, however it might be more intuitive to separate them:

- NO potentiates P/Q-tye current postsynaptically. Presynaptically only P/Q-type current is present, and Ca^{2+} influx through these channels activates vesicular release. If NO potentiates the presynaptic channel, then you might expect a larger evoked EPSC. However, a 30% smaller and longer duration EPSC is observed (Figure 6.1. B).
- SK channels contribute to hyperpolarising the membrane on Ca^{2+} influx postsynaptically. Presynaptically, nothing is known about their expression but you might expect that as Ca_V channels open, SK channels act to hyperpolarise the membrane inactivating the Ca_V channels, restricting Ca^{2+} influx, reducing vesicular release, but maintaining the driving force for the next incoming AP. However, a larger EPSC is observed (Figure 6.1. B) and this is also the case in the presence of NO.

The calyx is not a classic synapse, it is a fenestrated giant synapse (Ford *et al.*, 2009; Grande & Wang, 2011), that has between 700 and 5000 active zones containing the release sites of a multitude of vesicles (Schneggenburger *et al.*, 1999). These fenestrations contain boutoun-like bumps and thinner diameter cables between them, like thin bony fingers. Any effect on the cable properties of these fenestrations will greatly influence the invasion of the depolarising waveform into the fingers, affecting recruitment of active zones, and vesicular release. I_{SK} current is effectively a Ca^{2+}-dependent leak conductance. A large Ca^{2+} current would activate a large SK current, reducing the input resistance of the calyceal fenestration, preventing the excitatory

presynaptic potential from propagating to the tips of the bony fingers and releasing a larger number of vesicles. Hence SK block allows a greater recruitment of active zones and more synaptic release resulting in a bigger EPSC compared to control and NO-treated conditions.

This postulate could be further tested in this experimental scenario by recording EPSC amplitude in the presence of an SK activator, EBIO or CyPPa.

Presynaptic capacitance measurements could also be made, and a greater increase in capacitance following terminal stimulation in the presence of apamin would confirm this hypothesis.

The MNTB principal neurons receive large EPSCs. In the absence of nNOS activity an after depolarising potential (ADP) is observed following a train of synaptic inputs. Replacing NO in the system causes the synaptic train to induce an AHP in these cells at higher frequencies (Figure 6.1. C). This could suggest that in control conditions a basal level of NO is constantly produced in these neurons and, together with SK channels, helps to regulate presynaptic release, and the postsynaptic response to innervations, maintaining functional excitability and high-fidelity firing in this nucleus.

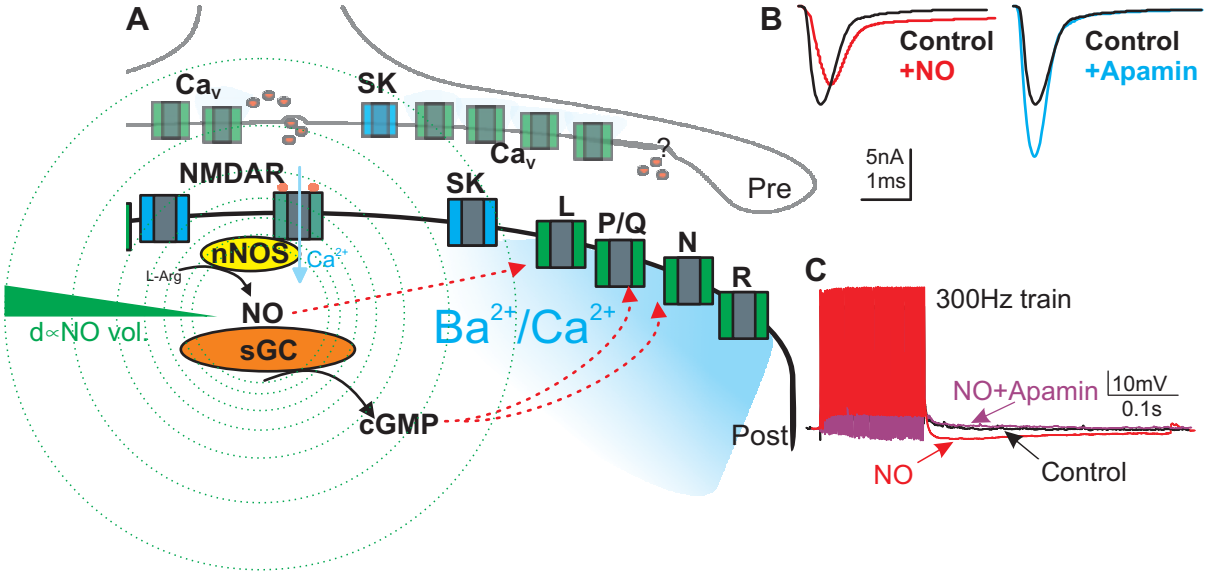

Figure 6.1. NO is a diffusible regulator of neuronal and synaptic excitability. **A.** NO is a volume diffusion dependent messenger molecule that can augment L-type and P/Q-type channels via different mechanistic pathways. N-type activation is leftward shifted and R-type is not affected. **B.** NO is a feedback messenger that can modulate synaptic release and modulate post-synaptic receptor sensitivity to glutamate, generating smaller EPSCs than control. Apamin is a selective SK antagonist that increases EPSC amplitude suggesting SK channels restrict release probability at the synapse. **C.** NO induces an Apamin sensitive AHP following synaptic stimulus trains.

7. Appendix

7.1 Methods

7.1.1 Immunohistochemistry

Brains were frozen in Lamb OCT compound (Thermo Fisher Scientific) and cryostat sectioned at 12 m in the transverse plane. Sections were fixed in 4% paraformaldehyde at 4^{o}C followed by antigen retrieval in 10mM citrate buffer(pH6) at 95^{0}C for 20 minutes and subsequently incubated for 30min at room temperature with PBS containing 0.1% Triton X-100 (PBS-T), 1% BSA and 10% normal goat serum (NGS) to reduce non-specific binding of secondary antibody. Sections were incubated with primary antibody to SK2 (1:200, Alomone) diluted in PBS-T containing 1% BSA and 10% NGS overnight at 4^{o}C. After three washes in PBS-T, sections were incubated with secondary antibody (Invitrogen; Molecular Probes AlexaFluor goat anti-rabbit 546 (1:1000)) diluted in PBS-T, 1% BSA and 10% NGS for 2 hours at room temperature. After rinsing in PBS-T, sections were stained with DAPI, rinsed again in PBS-T then cover-slipped with Vectashield Hard Set Mounting Medium (Vector Laboratories). Images were acquired with a Zeiss laser-scanning confocal microscope (LSM 510, Carl Zeiss International) or Leica DM2500 fluorescence microscope. As negative controls for specificity, sections incubated with the omission of the primary antibody showed no specific immunostaining (data not shown) and pre-incubation with antigenic peptide (where available) also blocked specific staining.

7.1.2 Quantitative PCR

MNTB tissue samples were excised from P14 CBA frozen cryostat sections using laser micro-dissection (PALM laser system, Zeiss). Total RNA extraction was performed using RNeasy tissue mini kit (Qiagen) and RNA was reverse-transcribed with SuperScript III (Invitrogen) using random hexamer primers (Promega). PCR primers were designed using the Universal Probe Library (Roche).Primers were designed to cross exon-exon regions and the gene of interest normalised against a housekeeping gene (RPL44).

Primer sequences:

SK1 L- **ggtgtgtgtctgctcactgg** R- **caacttccgagccacgac**

SK2 L- **gaaattcttgcaagctattcatca** R- **gggtatttgcttggtcattca**

SK3 L- **tgtgcgagtctgtgaaaggt** R- **cacatggcacccagaaagtt**

RPL44 L-**ggccggtctctcgttctca** R- **ttacagaaagtccttcgggttttt**

qPCR was performed using SYBR Green PCR Master Mix in the ABI PRISM 7700 Sequence Detection System, the thermal-cycler protocol was: stage one, 50 °C for 2 minutes; stage two, 95 °C for 10 minutes; stage three, 40cycles at 95 °C for 15 seconds and 60 °C for 1 minute. Each sample was run in triplicate. PCR results were analysed using the Pfaffl model for relative quantitation (Nucleic Acids Research, 2001)

References.

Adelman JP, Maylie J & Sah P. (2011). Small-conductance Ca2+-activated K+ channels: form and function. *Annu Rev Physiol* **74,** 245-269.

Ahern GP, Hsu SF & Jackson MB. (1999). Direct actions of nitric oxide on rat neurohypophysial K+ channels. *J Physiol* **520 Pt 1,** 165-176.

Ahern GP, Klyachko VA & Jackson MB. (2002). cGMP and S-nitrosylation: two routes for modulation of neuronal excitability by NO. *Trends Neurosci* **25,** 510-517.

Ahlijanian MK, Westenbroek RE & Catterall WA. (1990). Subunit structure and localization of dihydropyridine-sensitive calcium channels in mammalian brain, spinal cord, and retina. *Neuron* **4,** 819-832.

Alderton WK, Cooper CE & Knowles RG. (2001). Nitric oxide synthases: structure, function and inhibition. *Biochem J* **357,** 593-615.

Allen D, Fakler B, Maylie J & Adelman JP. (2007). Organization and regulation of small conductance Ca2+-activated K+ channel multiprotein complexes. *J Neurosci* **27,** 2369-2376.

Allen RD, David GB & Nomarski G. (1969). The zeiss-Nomarski differential interference equipment for transmitted-light microscopy. *Z Wiss Mikrosk* **69,** 193-221.

Almanza A, Navarrete F, Vega R & Soto E. (2007). Modulation of voltage-gated Ca2+ current in vestibular hair cells by nitric oxide. *J Neurophysiol* **97,** 1188-1195.

An WF, Bowlby MR, Betty M, Cao J, Ling HP, Mendoza G, Hinson JW, Mattsson KI, Strassle BW, Trimmer JS & Rhodes KJ. (2000). Modulation of A-type potassium channels by a family of calcium sensors. *Nature* **403,** 553-556.

Anderson D, Mehaffey WH, Iftinca M, Rehak R, Engbers JD, Hameed S, Zamponi GW & Turner RW. (2011). Regulation of neuronal activity by Cav3-Kv4 channel signaling complexes. *Nat Neurosci* **13,** 333-337.

Arancio O, Kiebler M, Lee CJ, Lev-Ram V, Tsien RY, Kandel ER & Hawkins RD. (1996). Nitric oxide acts directly in the presynaptic neuron to produce long-term potentiation in cultured hippocampal neurons. *Cell* **87,** 1025-1035.

Arikkath J, Felix R, Ahern C, Chen CC, Mori Y, Song I, Shin HS, Coronado R & Campbell KP. (2002). Molecular characterization of a two-domain form of the neuronal voltage-gated P/Q-type calcium channel alpha(1)2.1 subunit. *FEBS Lett* **532,** 300-308.

Armstrong CM. (1969). Inactivation of the potassium conductance and related phenomena caused by quaternary ammonium ion injection in squid axons. *J Gen Physiol* **54,** 553-575.

Arnold WP, Mittal CK, Katsuki S & Murad F. (1977). Nitric oxide activates guanylate cyclase and increases guanosine 3':5'-cyclic monophosphate levels in various tissue preparations. *Proc Natl Acad Sci U S A* **74,** 3203-3207.

Artinian L, Tornieri K, Zhong L, Baro D & Rehder V. (2010). Nitric oxide acts as a volume transmitter to modulate electrical properties of spontaneously firing neurons via apamin-sensitive potassium channels. *J Neurosci* **30,** 1699-1711.

Astori S, Wimmer RD, Prosser HM, Corti C, Corsi M, Liaudet N, Volterra A, Franken P, Adelman JP & Luthi A. (2011). The Ca(V)3.3 calcium channel is the major sleep spindle pacemaker in thalamus. *Proc Natl Acad Sci U S A* **108,** 13823-13828.

Atochin DN & Huang PL. (2011). Role of endothelial nitric oxide in cerebrovascular regulation. *Curr Pharm Biotechnol* **12,** 1334-1342.

Awatramani GB, Price GD & Trussell LO. (2005). Modulation of transmitter release by presynaptic resting potential and background calcium levels. *Neuron* **48,** 109-121.

Banks MI, Pearce RA & Smith PH. (1993). Hyperpolarization-activated cation current (Ih) in neurons of the medial nucleus of the trapezoid body: voltage-clamp analysis and enhancement by norepinephrine and cAMP suggest a modulatory mechanism in the auditory brain stem. *J Neurophysiol* **70,** 1420-1432.

Banks MI & Smith PH. (1992). Intracellular recordings from neurobiotin-labeled cells in brain slices of the rat medial nucleus of the trapezoid body. *J Neurosci* **12,** 2819-2837.

Barnes-Davies M & Forsythe ID. (1995). Pre- and postsynaptic glutamate receptors at a giant excitatory synapse in rat auditory brainstem slices. *J Physiol* **488 (Pt 2),** 387-406.

Barnes-Davies M, Owens S & Forsythe ID. (2001). Calcium channels triggering transmitter release in the rat medial superior olive. In *Hear Res*, pp. 134-145.

Bean BP. (1989). Classes of calcium channels in vertebrate cells. *Annu Rev Physiol* **51,** 367-384.

Bechade C, Pascual O, Triller A & Bessis A. (2011). Nitric oxide regulates astrocyte maturation in the hippocampus: involvement of NOS2. *Mol Cell Neurosci* **46,** 762-769.

Behnisch T & Reymann KG. (1998). Inhibition of apamin-sensitive calcium dependent potassium channels facilitate the induction of long-term potentiation in the CA1 region of rat hippocampus in vitro. *Neurosci Lett* **253,** 91-94.

Bellamy TC, Wood J & Garthwaite J. (2002). On the activation of soluble guanylyl cyclase by nitric oxide. *Proc Natl Acad Sci U S A* **99,** 507-510.

Bendahhou S, Cummins TR, Tawil R, Waxman SG & Ptacek LJ. (1999). Activation and inactivation of the voltage-gated sodium channel: role of segment S5 revealed by a novel hyperkalaemic periodic paralysis mutation. *J Neurosci* **19,** 4762-4771.

Bender KJ & Trussell LO. (2009). Axon initial segment Ca2+ channels influence action potential generation and timing. *Neuron* **61,** 259-271.

Bender KJ, Uebele VN, Renger JJ & Trussell LO. (2012). Control of firing patterns through modulation of axon initial segment T-type calcium channels. *J Physiol* **590,** 109-118.

Bichet D, Cornet V, Geib S, Carlier E, Volsen S, Hoshi T, Mori Y & De Waard M. (2000). The I-II loop of the Ca2+ channel alpha1 subunit contains an endoplasmic reticulum retention signal antagonized by the beta subunit. *Neuron* **25,** 177-190.

Biel M, Wahl-Schott C, Michalakis S & Zong X. (2009). Hyperpolarization-activated cation channels: from genes to function. *Physiol Rev* **89,** 847-885.

Billups B & Forsythe ID. (2002). Presynaptic mitochondrial calcium sequestration influences transmission at mammalian central synapses. *J Neurosci* **22,** 5840-5847.

Bliss TV & Collingridge GL. (1993). A synaptic model of memory: long-term potentiation in the hippocampus. *Nature* **361,** 31-39.

Boland LM, Morrill JA & Bean BP. (1994). omega-Conotoxin block of N-type calcium channels in frog and rat sympathetic neurons. *J Neurosci* **14,** 5011-5027.

Borst JG & Soria van Hoeve J. (2011). The calyx of held synapse: from model synapse to auditory relay. *Annu Rev Physiol* **74,** 199-224.

BoSmith RE, Briggs I & Sturgess NC. (1993). Inhibitory actions of ZENECA ZD7288 on whole-cell hyperpolarization activated inward current (If) in guinea-pig dissociated sinoatrial node cells. *Br J Pharmacol* **110,** 343-349.

Bourinet E, Soong TW, Sutton K, Slaymaker S, Mathews E, Monteil A, Zamponi GW, Nargeot J & Snutch TP. (1999). Splicing of alpha 1A subunit gene generates

phenotypic variants of P- and Q-type calcium channels. *Nat Neurosci* **2,** 407-415.

Bowden SE, Fletcher S, Loane DJ & Marrion NV. (2001). Somatic colocalization of rat SK1 and D class (Ca(v)1.2) L-type calcium channels in rat CA1 hippocampal pyramidal neurons. *J Neurosci* **21,** RC175.

Brackenbury WJ, Calhoun JD, Chen C, Miyazaki H, Nukina N, Oyama F, Ranscht B & Isom LL. (2010). Functional reciprocity between Na+ channel Nav1.6 and beta1 subunits in the coordinated regulation of excitability and neurite outgrowth. *Proc Natl Acad Sci U S A* **107,** 2283-2288.

Bredt DS, Hwang PM, Glatt CE, Lowenstein C, Reed RR & Snyder SH. (1991). Cloned and expressed nitric oxide synthase structurally resembles cytochrome P-450 reductase. *Nature* **351,** 714-718.

Brew HM & Forsythe ID. (1995). Two voltage-dependent K+ conductances with complementary functions in postsynaptic integration at a central auditory synapse. *J Neurosci* **15,** 8011-8022.

Brosenitsch TA & Katz DM. (2001). Physiological patterns of electrical stimulation can induce neuronal gene expression by activating N-type calcium channels. *J Neurosci* **21,** 2571-2579.

Buchanan KA, Petrovic MM, Chamberlain SE, Marrion NV & Mellor JR. (2011). Facilitation of long-term potentiation by muscarinic M(1) receptors is mediated by inhibition of SK channels. *Neuron* **68,** 948-963.

Buraei Z & Yang J. (2010). The ss subunit of voltage-gated Ca2+ channels. *Physiol Rev* **90,** 1461-1506.

Cain SM & Snutch TP. (2010). Contributions of T-type calcium channel isoforms to neuronal firing. *Channels (Austin)* **4,** 475-482.

Cao XJ & Oertel D. (2010). Auditory nerve fibers excite targets through synapses that vary in convergence, strength, and short-term plasticity. *J Neurophysiol* **104,** 2308-2320.

Catterall WA. (2012). Voltage-gated sodium channels at 60: structure, function and pathophysiology. *J Physiol* **590,** 2577-2589.

Catterall WA, Goldin AL & Waxman SG. (2003). International Union of Pharmacology. XXXIX. Compendium of voltage-gated ion channels: sodium channels. *Pharmacol Rev* **55,** 575-578.

Catterall WA, Perez-Reyes E, Snutch TP & Striessnig J. (2005). International Union of Pharmacology. XLVIII. Nomenclature and structure-function relationships of voltage-gated calcium channels. *Pharmacol Rev* **57,** 411-425.

Cens T, Rousset M, Leyris JP, Fesquet P & Charnet P. (2006). Voltage- and calcium-dependent inactivation in high voltage-gated Ca(2+) channels. *Prog Biophys Mol Biol* **90,** 104-117.

Chartrain NA, Geller DA, Koty PP, Sitrin NF, Nussler AK, Hoffman EP, Billiar TR, Hutchinson NI & Mudgett JS. (1994). Molecular cloning, structure, and chromosomal localization of the human inducible nitric oxide synthase gene. *J Biol Chem* **269,** 6765-6772.

Chavis P, Fagni L, Lansman JB & Bockaert J. (1996). Functional coupling between ryanodine receptors and L-type calcium channels in neurons. *Nature* **382,** 719-722.

Chemin J, Monteil A, Perez-Reyes E, Bourinet E, Nargeot J & Lory P. (2002). Specific contribution of human T-type calcium channel isotypes (alpha(1G), alpha(1H) and alpha(1I)) to neuronal excitability. *J Physiol* **540,** 3-14.

Chen J, Daggett H, De Waard M, Heinemann SH & Hoshi T. (2002). Nitric oxide augments voltage-gated P/Q-type Ca(2+) channels constituting a putative positive feedback loop. *Free Radic Biol Med* **32,** 638-649.

Cho DH, Nakamura T, Fang J, Cieplak P, Godzik A, Gu Z & Lipton SA. (2009). S-nitrosylation of Drp1 mediates beta-amyloid-related mitochondrial fission and neuronal injury. *Science* **324,** 102-105.

Coetzee WA, Amarillo Y, Chiu J, Chow A, Lau D, McCormack T, Moreno H, Nadal MS, Ozaita A, Pountney D, Saganich M, Vega-Saenz de Miera E & Rudy B. (1999). Molecular diversity of K+ channels. *Ann N Y Acad Sci* **868,** 233-285.

Cole KS. (1949). Dynamic electrical characteristics of the squid axon membrane. *Arch Sci Physiol* **3,** 253-258.

Cole RL, Lechner SM, Williams ME, Prodanovich P, Bleicher L, Varney MA & Gu G. (2005). Differential distribution of voltage-gated calcium channel alpha-2 delta (alpha2delta) subunit mRNA-containing cells in the rat central nervous system and the dorsal root ganglia. *J Comp Neurol* **491,** 246-269.

Coulter DA, Huguenard JR & Prince DA. (1989). Calcium currents in rat thalamocortical relay neurones: kinetic properties of the transient, low-threshold current. *J Physiol* **414,** 587-604.

Crandall SR, Govindaiah G & Cox CL. (2010). Low-threshold Ca2+ current amplifies distal dendritic signaling in thalamic reticular neurons. *J Neurosci* **30,** 15419-15429.

Cui J, Cox DH & Aldrich RW. (1997). Intrinsic voltage dependence and Ca2+ regulation of mslo large conductance Ca-activated K+ channels. *J Gen Physiol* **109,** 647-673.

Cull-Candy S, Brickley S & Farrant M. (2001). NMDA receptor subunits: diversity, development and disease. *Curr Opin Neurobiol* **11,** 327-335.

Cuttle MF, Rusznak Z, Wong AY, Owens S & Forsythe ID. (2001). Modulation of a presynaptic hyperpolarization-activated cationic current (I(h)) at an excitatory synaptic terminal in the rat auditory brainstem. *J Physiol* **534,** 733-744.

Cuttle MF, Tsujimoto T, Forsythe ID & Takahashi T. (1998). Facilitation of the presynaptic calcium current at an auditory synapse in rat brainstem. *J Physiol* **512 (Pt 3),** 723-729.

D'Ascenzo M, Martinotti G, Azzena GB & Grassi C. (2002). cGMP/protein kinase G-dependent inhibition of N-type Ca2+ channels induced by nitric oxide in human neuroblastoma IMR32 cells. *J Neurosci* **22,** 7485-7492.

Davies A, Douglas L, Hendrich J, Wratten J, Tran Van Minh A, Foucault I, Koch D, Pratt WS, Saibil HR & Dolphin AC. (2006). The calcium channel alpha2delta-2 subunit partitions with CaV2.1 into lipid rafts in cerebellum: implications for localization and function. *J Neurosci* **26,** 8748-8757.

Davies A, Hendrich J, Van Minh AT, Wratten J, Douglas L & Dolphin AC. (2007). Functional biology of the alpha(2)delta subunits of voltage-gated calcium channels. *Trends Pharmacol Sci* **28,** 220-228.

Destexhe A, Contreras D, Steriade M, Sejnowski TJ & Huguenard JR. (1996). In vivo, in vitro, and computational analysis of dendritic calcium currents in thalamic reticular neurons. *J Neurosci* **16,** 169-185.

Dierickx PJ. (1989). Cytotoxicity testing of 114 compounds by the determination of the protein content in Hep G2 cell cultures. *Toxicol In Vitro* **3,** 189-193.

Dodson PD & Forsythe ID. (2004). Presynaptic K+ channels: electrifying regulators of synaptic terminal excitability. *Trends Neurosci* **27,** 210-217.

Dolmetsch RE, Pajvani U, Fife K, Spotts JM & Greenberg ME. (2001). Signaling to the nucleus by an L-type calcium channel-calmodulin complex through the MAP kinase pathway. *Science* **294,** 333-339.

Dolphin AC. (2009). Calcium channel diversity: multiple roles of calcium channel subunits. *Curr Opin Neurobiol* **19,** 237-244.

Doughty JM, Barnes-Davies M, Rusznak Z, Harasztosi C & Forsythe ID. (1998). Contrasting Ca2+ channel subtypes at cell bodies and synaptic terminals of rat anterioventral cochlear bushy neurones. *J Physiol* **512 (Pt 2),** 365-376.

Edwards FA, Konnerth A, Sakmann B & Takahashi T. (1989). A thin slice preparation for patch clamp recordings from neurones of the mammalian central nervous system. *Pflugers Arch* **414,** 600-612.

Eguchi K, Nakanishi S, Takagi H, Taoufiq Z & Takahashi T. (2012). Maturation of a PKG-dependent retrograde mechanism for exoendocytic coupling of synaptic vesicles. *Neuron* **74,** 517-529.

Elezgarai I, Diez J, Puente N, Azkue JJ, Benitez R, Bilbao A, Knopfel T, Donate-Oliver F & Grandes P. (2003). Subcellular localization of the voltage-dependent potassium channel Kv3.1b in postnatal and adult rat medial nucleus of the trapezoid body. *Neuroscience* **118,** 889-898.

Engbers JD, Anderson D, Asmara H, Rehak R, Mehaffey WH, Hameed S, McKay BE, Kruskic M, Zamponi GW & Turner RW. (2012). Intermediate conductance calcium-activated potassium channels modulate summation of parallel fiber input in cerebellar Purkinje cells. *Proc Natl Acad Sci U S A* **109,** 2601-2606.

Engbers JD, Anderson D, Tadayonnejad R, Mehaffey WH, Molineux ML & Turner RW. (2011). Distinct roles for I(T) and I(H) in controlling the frequency and timing of rebound spike responses. *J Physiol* **589,** 5391-5413.

Ertel EA, Campbell KP, Harpold MM, Hofmann F, Mori Y, Perez-Reyes E, Schwartz A, Snutch TP, Tanabe T, Birnbaumer L, Tsien RW & Catterall WA. (2000). Nomenclature of voltage-gated calcium channels. *Neuron* **25,** 533-535.

Faber ES, Delaney AJ & Sah P. (2005). SK channels regulate excitatory synaptic transmission and plasticity in the lateral amygdala. *Nat Neurosci* **8,** 635-641.

Faber ES & Sah P. (2003). Ca2+-activated K+ (BK) channel inactivation contributes to spike broadening during repetitive firing in the rat lateral amygdala. *J Physiol* **552,** 483-497.

Faber ES & Sah P. (2007). Functions of SK channels in central neurons. *Clin Exp Pharmacol Physiol* **34,** 1077-1083.

Fakler B & Adelman JP. (2008). Control of K(Ca) channels by calcium nano/microdomains. *Neuron* **59,** 873-881.

Fatt P & Katz B. (1952). Spontaneous subthreshold activity at motor nerve endings. *J Physiol* **117,** 109-128.

Felix RA, 2nd, Fridberger A, Leijon S, Berrebi AS & Magnusson AK. (2011). Sound rhythms are encoded by postinhibitory rebound spiking in the superior paraolivary nucleus. *J Neurosci* **31,** 12566-12578.

Fessenden JD, Altschuler RA, Seasholtz AF & Schacht J. (1999). Nitric oxide/cyclic guanosine monophosphate pathway in the peripheral and central auditory system of the rat. *J Comp Neurol* **404,** 52-63.

Ford MC, Grothe B & Klug A. (2009). Fenestration of the calyx of Held occurs sequentially along the tonotopic axis, is influenced by afferent activity, and facilitates glutamate clearance. *J Comp Neurol* **514,** 92-106.

Forsythe ID. (1994). Direct patch recording from identified presynaptic terminals mediating glutamatergic EPSCs in the rat CNS, in vitro. *J Physiol* **479 (Pt 3),** 381-387.

Forsythe ID. (2001). auditory processing. In *encyclopaedia of life science*.

Forsythe ID & Barnes-Davies M. (1993). The binaural auditory pathway: excitatory amino acid receptors mediate dual timecourse excitatory postsynaptic currents in the rat medial nucleus of the trapezoid body. *Proc Biol Sci* **251,** 151-157.

Forsythe ID, Tsujimoto T, Barnes-Davies M, Cuttle MF & Takahashi T. (1998). Inactivation of presynaptic calcium current contributes to synaptic depression at a fast central synapse. *Neuron* **20,** 797-807.

Fox AP, Nowycky MC & Tsien RW. (1987). Kinetic and pharmacological properties distinguishing three types of calcium currents in chick sensory neurones. *J Physiol* **394,** 149-172.

Fozzard HA. (1991). Excitation-contraction coupling in the heart. *Adv Exp Med Biol* **308,** 135-142.

Furchgott RF & Zawadzki JV. (1980). The obligatory role of endothelial cells in the relaxation of arterial smooth muscle by acetylcholine. *Nature* **288,** 373-376.

Galvez A, Gimenez-Gallego G, Reuben JP, Roy-Contancin L, Feigenbaum P, Kaczorowski GJ & Garcia ML. (1990). Purification and characterization of a unique, potent, peptidyl probe for the high conductance calcium-activated potassium channel from venom of the scorpion Buthus tamulus. *J Biol Chem* **265,** 11083-11090.

Garcia-Pino E, Caminos E & Juiz JM. (2010). KCNQ5 reaches synaptic endings in the auditory brainstem at hearing onset and targeting maintenance is activity-dependent. *J Comp Neurol* **518,** 1301-1314.

Garthwaite J. (1995). Neural nitric oxide signalling. *Trends Neurosci* **18,** 51-52.

Garthwaite J. (2005). Dynamics of cellular NO-cGMP signaling. *Front Biosci* **10,** 1868-1880.

Garthwaite J. (2008). Concepts of neural nitric oxide-mediated transmission. *Eur J Neurosci* **27,** 2783-2802.

Garthwaite J, Charles SL & Chess-Williams R. (1988). Endothelium-derived relaxing factor release on activation of NMDA receptors suggests role as intercellular messenger in the brain. *Nature* **336,** 385-388.

Goldin AL, Snutch T, Lubbert H, Dowsett A, Marshall J, Auld V, Downey W, Fritz LC, Lester HA, Dunn R & et al. (1986). Messenger RNA coding for only the alpha subunit of the rat brain Na channel is sufficient for expression of functional channels in Xenopus oocytes. *Proc Natl Acad Sci U S A* **83,** 7503-7507.

Gomez-Ospina N, Tsuruta F, Barreto-Chang O, Hu L & Dolmetsch R. (2006). The C terminus of the L-type voltage-gated calcium channel Ca(V)1.2 encodes a transcription factor. *Cell* **127,** 591-606.

Grande G & Wang LY. (2011). Morphological and functional continuum underlying heterogeneity in the spiking fidelity at the calyx of Held synapse in vitro. *J Neurosci* **31,** 13386-13399.

Gutman GA, Chandy KG, Grissmer S, Lazdunski M, McKinnon D, Pardo LA, Robertson GA, Rudy B, Sanguinetti MC, Stuhmer W & Wang X. (2005). International Union of Pharmacology. LIII. Nomenclature and molecular relationships of voltage-gated potassium channels. *Pharmacol Rev* **57,** 473-508.

Habets RL & Borst JG. (2005). Post-tetanic potentiation in the rat calyx of Held synapse. *J Physiol* **564,** 173-187.

Hamann M, Billups B & Forsythe ID. (2003). Non-calyceal excitatory inputs mediate low fidelity synaptic transmission in rat auditory brainstem slices. *Eur J Neurosci* **18,** 2899-2902.

Hamill OP, Marty A, Neher E, Sakmann B & Sigworth FJ. (1981). Improved patch-clamp techniques for high-resolution current recording from cells and cell-free membrane patches. *Pflugers Arch* **391,** 85-100.

Hardingham GE, Arnold FJ & Bading H. (2001). Nuclear calcium signaling controls CREB-mediated gene expression triggered by synaptic activity. *Nat Neurosci* **4,** 261-267.

Hardman RM & Forsythe ID. (2009). Ether-a-go-go-related gene K+ channels contribute to threshold excitability of mouse auditory brainstem neurons. *J Physiol* **587,** 2487-2497.

Haustein MD, Read DJ, Steinert JR, Pilati N, Dinsdale D & Forsythe ID. (2011). Acute hyperbilirubinaemia induces presynaptic neurodegeneration at a central glutamatergic synapse. *J Physiol*.

Held H. (1893). Die zentrale Gehörleitung. *Archiv für Anatomie und Physiologie* **17,** 201-248.

Herlitze S, Garcia DE, Mackie K, Hille B, Scheuer T & Catterall WA. (1996). Modulation of Ca2+ channels by G-protein beta gamma subunits. *Nature* **380,** 258-262.

Hille B. (1968). Pharmacological modifications of the sodium channels of frog nerve. *J Gen Physiol* **51,** 199-219.

Hille B. (2001). *Ion channels of excitable membranes.* Sinauer Associates.

Hodgkin AL, Huxley AF & Katz B. (1952). Measurement of current-voltage relations in the membrane of the giant axon of Loligo. *J Physiol* **116,** 424-448.

Honore T, Davies SN, Drejer J, Fletcher EJ, Jacobsen P, Lodge D & Nielsen FE. (1988). Quinoxalinediones: potent competitive non-NMDA glutamate receptor antagonists. *Science* **241,** 701-703.

Hoppa MB, Lana B, Margas W, Dolphin AC & Ryan TA. (2012). alpha2delta expression sets presynaptic calcium channel abundance and release probability. *Nature* **486,** 122-125.

Hu H, Shao LR, Chavoshy S, Gu N, Trieb M, Behrens R, Laake P, Pongs O, Knaus HG, Ottersen OP & Storm JF. (2001). Presynaptic Ca2+-activated K+ channels in glutamatergic hippocampal terminals and their role in spike repolarization and regulation of transmitter release. *J Neurosci* **21,** 9585-9597.

Huang H & Trussell LO. (2008). Control of presynaptic function by a persistent Na(+) current. *Neuron* **60,** 975-979.

Huang H & Trussell LO. (2011). KCNQ5 channels control resting properties and release probability of a synapse. *Nat Neurosci* **14,** 840-847.

Huang L, Keyser BM, Tagmose TM, Hansen JB, Taylor JT, Zhuang H, Zhang M, Ragsdale DS & Li M. (2004). NNC 55-0396 [(1S,2S)-2-(2-(N-[(3-benzimidazol-2-yl)propyl]-N-methylamino)ethyl)-6-fluoro-1,2, 3,4-tetrahydro-1-isopropyl-2-naphtyl cyclopropanecarboxylate dihydrochloride]: a new selective inhibitor of T-type calcium channels. *J Pharmacol Exp Ther* **309,** 193-199.

Huguenard JR. (1996). Low-threshold calcium currents in central nervous system neurons. *Annu Rev Physiol* **58,** 329-348.

Huguenard JR & Prince DA. (1992). A novel T-type current underlies prolonged Ca(2+)-dependent burst firing in GABAergic neurons of rat thalamic reticular nucleus. *J Neurosci* **12,** 3804-3817.

Ignarro LJ, Buga GM, Wood KS, Byrns RE & Chaudhuri G. (1987). Endothelium-derived relaxing factor produced and released from artery and vein is nitric oxide. *Proc Natl Acad Sci U S A* **84,** 9265-9269.

Imredy JP & Yue DT. (1992). Submicroscopic Ca2+ diffusion mediates inhibitory coupling between individual Ca2+ channels. *Neuron* **9,** 197-207.

Inchauspe CG, Forsythe ID & Uchitel OD. (2007). Changes in synaptic transmission properties due to the expression of N-type calcium channels at the calyx of Held synapse of mice lacking P/Q-type calcium channels. *J Physiol* **584,** 835-851.

Inchauspe CG, Martini FJ, Forsythe ID & Uchitel OD. (2004). Functional compensation of P/Q by N-type channels blocks short-term plasticity at the calyx of held presynaptic terminal. *J Neurosci* **24,** 10379-10383.

Ishii TM, Silvia C, Hirschberg B, Bond CT, Adelman JP & Maylie J. (1997). A human intermediate conductance calcium-activated potassium channel. *Proc Natl Acad Sci U S A* **94,** 11651-11656.

Ishikawa T, Nakamura Y, Saitoh N, Li WB, Iwasaki S & Takahashi T. (2003). Distinct roles of Kv1 and Kv3 potassium channels at the calyx of Held presynaptic terminal. *J Neurosci* **23,** 10445-10453.

Isom LL, De Jongh KS & Catterall WA. (1994). Auxiliary subunits of voltage-gated ion channels. *Neuron* **12,** 1183-1194.

Isom LL, De Jongh KS, Patton DE, Reber BF, Offord J, Charbonneau H, Walsh K, Goldin AL & Catterall WA. (1992). Primary structure and functional expression of the beta 1 subunit of the rat brain sodium channel. *Science* **256,** 839-842.

Iwasaki S & Takahashi T. (1998). Developmental changes in calcium channel types mediating synaptic transmission in rat auditory brainstem. *J Physiol* **509 (Pt 2),** 419-423.

Jacoby S, Sims RE & Hartell NA. (2001). Nitric oxide is required for the induction and heterosynaptic spread of long-term potentiation in rat cerebellar slices. *J Physiol* **535,** 825-839.

Jensen BS, Hertz M, Christophersen P & Madsen LS. (2002). The Ca2+-activated K+ channel of intermediate conductance:a possible target for immune suppression. *Expert Opin Ther Targets* **6,** 623-636.

Jian K, Chen M, Cao X, Zhu XH, Fung ML & Gao TM. (2007). Nitric oxide modulation of voltage-gated calcium current by S-nitrosylation and cGMP pathway in cultured rat hippocampal neurons. *Biochem Biophys Res Commun* **359,** 481-485.

Jiang LH, Kim M, Spelta V, Bo X, Surprenant A & North RA. (2003). Subunit arrangement in P2X receptors. *J Neurosci* **23,** 8903-8910.

Johnston J, Forsythe ID & Kopp-Scheinpflug C. (2011). Going native: voltage-gated potassium channels controlling neuronal excitability. *J Physiol* **588,** 3187-3200.

Johnston J, Griffin SJ, Baker C & Forsythe ID. (2008a). Kv4 (A-type) potassium currents in the mouse medial nucleus of the trapezoid body. *Eur J Neurosci* **27,** 1391-1399.

Johnston J, Griffin SJ, Baker C, Skrzypiec A, Chernova T & Forsythe ID. (2008b). Initial segment Kv2.2 channels mediate a slow delayed rectifier and maintain high frequency action potential firing in medial nucleus of the trapezoid body neurons. *J Physiol* **586,** 3493-3509.

Johnston J, Postlethwaite M & Forsythe ID. (2009). The impact of synaptic conductance on action potential waveform: evoking realistic action potentials with a simulated synaptic conductance. *J Neurosci Methods* **183,** 158-164.

Joksovic PM, Doctor A, Gaston B & Todorovic SM. (2007). Functional regulation of T-type calcium channels by s-nitrosothiols in the rat thalamus. *J Neurophysiol* **97,** 2712-2721.

Kadner A & Berrebi AS. (2008). Encoding of temporal features of auditory stimuli in the medial nucleus of the trapezoid body and superior paraolivary nucleus of the rat. *Neuroscience* **151,** 868-887.

Kadner A, Kulesza RJ, Jr. & Berrebi AS. (2006). Neurons in the medial nucleus of the trapezoid body and superior paraolivary nucleus of the rat may play a role in sound duration coding. *J Neurophysiol* **95,** 1499-1508.

Kandler K, Clause A & Noh J. (2009). Tonotopic reorganization of developing auditory brainstem circuits. *Nat Neurosci* **12,** 711-717.

Keefer LK, Nims RW, Davies KM & Wink DA. (1996). "NONOates" (1-substituted diazen-1-ium-1,2-diolates) as nitric oxide donors: convenient nitric oxide dosage forms. *Methods Enzymol* **268,** 281-293.

Kemenes I, Kemenes G, Andrew RJ, Benjamin PR & O'Shea M. (2002). Critical time-window for NO-cGMP-dependent long-term memory formation after one-trial appetitive conditioning. *J Neurosci* **22,** 1414-1425.

Koch U, Braun M, Kapfer C & Grothe B. (2004). Distribution of HCN1 and HCN2 in rat auditory brainstem nuclei. *Eur J Neurosci* **20,** 79-91.

Kohler M, Hirschberg B, Bond CT, Kinzie JM, Marrion NV, Maylie J & Adelman JP. (1996). Small-conductance, calcium-activated potassium channels from mammalian brain. *Science* **273,** 1709-1714.

Kopp-Scheinpflug C, Fuchs K, Lippe WR, Tempel BL & Rubsamen R. (2003). Decreased temporal precision of auditory signaling in Kcna1-null mice: an electrophysiological study in vivo. *J Neurosci* **23,** 9199-9207.

Kopp-Scheinpflug C, Tozer AJ, Robinson SW, Tempel BL, Hennig MH & Forsythe ID. (2011). The sound of silence: ionic mechanisms encoding sound termination. *Neuron* **71,** 911-925.

Koshland DE, Jr. (1992). The molecule of the year. *Science* **258,** 1861.

Lancaster B & Adams PR. (1986). Calcium-dependent current generating the afterhyperpolarization of hippocampal neurons. *J Neurophysiol* **55,** 1268-1282.

Lancaster B & Nicoll RA. (1987). Properties of two calcium-activated hyperpolarizations in rat hippocampal neurones. *J Physiol* **389,** 187-203.

Leao KE, Leao RN, Sun H, Fyffe RE & Walmsley B. (2006a). Hyperpolarization-activated currents are differentially expressed in mice brainstem auditory nuclei. *J Physiol* **576,** 849-864.

Leao RM, Kushmerick C, Pinaud R, Renden R, Li GL, Taschenberger H, Spirou G, Levinson SR & von Gersdorff H. (2005a). Presynaptic Na+ channels: locus, development, and recovery from inactivation at a high-fidelity synapse. *J Neurosci* **25,** 3724-3738.

Leao RN, Berntson A, Forsythe ID & Walmsley B. (2004). Reduced low-voltage activated K+ conductances and enhanced central excitability in a congenitally deaf (dn/dn) mouse. *J Physiol* **559,** 25-33.

Leao RN, Naves MM, Leao KE & Walmsley B. (2006b). Altered sodium currents in auditory neurons of congenitally deaf mice. *Eur J Neurosci* **24,** 1137-1146.

Leao RN, Svahn K, Berntson A & Walmsley B. (2005b). Hyperpolarization-activated (I) currents in auditory brainstem neurons of normal and congenitally deaf mice. *Eur J Neurosci* **22,** 147-157.

Lee JH, Gomora JC, Cribbs LL & Perez-Reyes E. (1999). Nickel block of three cloned T-type calcium channels: low concentrations selectively block alpha1H. *Biophys J* **77,** 3034-3042.

Letts VA, Felix R, Biddlecome GH, Arikkath J, Mahaffey CL, Valenzuela A, Bartlett FS, 2nd, Mori Y, Campbell KP & Frankel WN. (1998). The mouse stargazer gene encodes a neuronal Ca2+-channel gamma subunit. *Nat Genet* **19,** 340-347.

Li N, Sul JY & Haydon PG. (2003). A calcium-induced calcium influx factor, nitric oxide, modulates the refilling of calcium stores in astrocytes. *J Neurosci* **23,** 10302-10310.

Liberatore GT, Jackson-Lewis V, Vukosavic S, Mandir AS, Vila M, McAuliffe WG, Dawson VL, Dawson TM & Przedborski S. (1999). Inducible nitric oxide synthase stimulates dopaminergic neurodegeneration in the MPTP model of Parkinson disease. *Nat Med* **5,** 1403-1409.

Lin KH, Oleskevich S & Taschenberger H. (2011). Presynaptic Ca2+ influx and vesicle exocytosis at the mouse endbulb of Held: a comparison of two auditory nerve terminals. *J Physiol* **589,** 4301-4320.

Lin MT, Lujan R, Watanabe M, Frerking M, Maylie J & Adelman JP. (2010). Coupled activity-dependent trafficking of synaptic SK2 channels and AMPA receptors. *J Neurosci* **30,** 11726-11734.

Lipton SA, Singel DJ & Stamler JS. (1994). Neuroprotective and neurodestructive effects of nitric oxide and redox congeners. *Ann N Y Acad Sci* **738,** 382-387.

Liu X, Srinivasan P, Collard E, Grajdeanu P, Zweier JL & Friedman A. (2008). Nitric oxide diffusion rate is reduced in the aortic wall. *Biophys J* **94,** 1880-1889.

Llinas RR. (1988). The intrinsic electrophysiological properties of mammalian neurons: insights into central nervous system function. *Science* **242,** 1654-1664.

Lu W, Shi Y, Jackson AC, Bjorgan K, During MJ, Sprengel R, Seeburg PH & Nicoll RA. (2009). Subunit composition of synaptic AMPA receptors revealed by a single-cell genetic approach. *Neuron* **62,** 254-268.

Lv P, Rodriguez-Contreras A, Kim HJ, Zhu J, Wei D, Choong-Ryoul S, Eastwood E, Mu K, Levic S, Song H, Yevgeniy PY, Smith PJ & Yamoah EN. (2010). Release and elementary mechanisms of nitric oxide in hair cells. *J Neurophysiol* **103,** 2494-2505.

Ma H, Groth RD, Wheeler DG, Barrett CF & Tsien RW. (2011). Excitation-transcription coupling in sympathetic neurons and the molecular mechanism of its initiation. *Neurosci Res*.

Magistretti J, Mantegazza M, Guatteo E & Wanke E. (1996). Action potentials recorded with patch-clamp amplifiers: are they genuine? *Trends Neurosci* **19,** 530-534.

Malenka RC & Nicoll RA. (1999). Long-term potentiation--a decade of progress? *Science* **285,** 1870-1874.

Marionneau C, Carrasquillo Y, Norris AJ, Townsend RR, Isom LL, Link AJ & Nerbonne JM. (2012). The sodium channel accessory subunit Navbeta1 regulates neuronal excitability through modulation of repolarizing voltage-gated K(+) channels. *J Neurosci* **32,** 5716-5727.

Marrion NV & Tavalin SJ. (1998). Selective activation of Ca2+-activated K+ channels by co-localized Ca2+ channels in hippocampal neurons. *Nature* **395,** 900-905.

Marsden PA, Schappert KT, Chen HS, Flowers M, Sundell CL, Wilcox JN, Lamas S & Michel T. (1992). Molecular cloning and characterization of human endothelial nitric oxide synthase. *FEBS Lett* **307,** 287-293.

Martin E, Berka V, Sharina I & Tsai AL. (2012). Mechanism of binding of NO to soluble guanylyl cyclase: implication for the second NO binding to the heme proximal site. *Biochemistry* **51,** 2737-2746.

Martin RL, Lee JH, Cribbs LL, Perez-Reyes E & Hanck DA. (2000). Mibefradil block of cloned T-type calcium channels. *J Pharmacol Exp Ther* **295,** 302-308.

McCormick DA & Pape HC. (1990). Properties of a hyperpolarization-activated cation current and its role in rhythmic oscillation in thalamic relay neurones. *J Physiol* **431,** 291-318.

McGehee DS & Role LW. (1995). Physiological diversity of nicotinic acetylcholine receptors expressed by vertebrate neurons. *Annu Rev Physiol* **57,** 521-546.

Meredith FL, Li GQ & Rennie KJ. (2011). Postnatal expression of an apamin-sensitive k(ca) current in vestibular calyx terminals. *J Membr Biol* **244,** 81-91.

Michel T & Lamas S. (1992). Molecular cloning of constitutive endothelial nitric oxide synthase: evidence for a family of related genes. *J Cardiovasc Pharmacol* **20 Suppl 12,** S45-49.

Miki N, Kawabe Y & Kuriyama K. (1977). Activation of cerebral guanylate cyclase by nitric oxide. *Biochem Biophys Res Commun* **75,** 851-856.

Ming G & Wang LY. (2003). Properties of voltage-gated sodium channels in developing auditory neurons of the mouse in vitro. *Chin Med Sci J* **18,** 67-74.

Mintz IM, Venema VJ, Swiderek KM, Lee TD, Bean BP & Adams ME. (1992). P-type calcium channels blocked by the spider toxin omega-Aga-IVA. *Nature* **355,** 827-829.

Mouginot D, Bossu JL & Gahwiler BH. (1997). Low-threshold Ca2+ currents in dendritic recordings from Purkinje cells in rat cerebellar slice cultures. *J Neurosci* **17,** 160-170.

Mulle C, Sailer A, Swanson GT, Brana C, O'Gorman S, Bettler B & Heinemann SF. (2000). Subunit composition of kainate receptors in hippocampal interneurons. *Neuron* **28,** 475-484.

Mulle C, Steriade M & Deschenes M. (1985). The effects of QX314 on thalamic neurons. *Brain Res* **333,** 350-354.

Mustafa AK, Gadalla MM & Snyder SH. (2009). Signaling by gasotransmitters. *Sci Signal* **2,** re2.

Nakamura T, Yamashita T, Saitoh N & Takahashi T. (2008). Developmental changes in calcium/calmodulin-dependent inactivation of calcium currents at the rat calyx of Held. *J Physiol* **586,** 2253-2261.

Nakamura Y & Takahashi T. (2007). Developmental changes in potassium currents at the rat calyx of Held presynaptic terminal. *J Physiol* **581,** 1101-1112.

Nathan C & Xie QW. (1994). Nitric oxide synthases: roles, tolls, and controls. *Cell* **78,** 915-918.

Neher E. (1992). Correction for liquid junction potentials in patch clamp experiments. *Methods Enzymol* **207,** 123-131.

Neher E & Sakaba T. (2008). Multiple roles of calcium ions in the regulation of neurotransmitter release. *Neuron* **59,** 861-872.

Newcomb R, Szoke B, Palma A, Wang G, Chen X, Hopkins W, Cong R, Miller J, Urge L, Tarczy-Hornoch K, Loo JA, Dooley DJ, Nadasdi L, Tsien RW, Lemos J & Miljanich G. (1998). Selective peptide antagonist of the class E calcium channel from the venom of the tarantula Hysterocrates gigas. *Biochemistry* **37,** 15353-15362.

Ngo-Anh TJ, Bloodgood BL, Lin M, Sabatini BL, Maylie J & Adelman JP. (2005). SK channels and NMDA receptors form a Ca2+-mediated feedback loop in dendritic spines. *Nat Neurosci* **8,** 642-649.

Noda M, Ikeda T, Kayano T, Suzuki H, Takeshima H, Kurasaki M, Takahashi H & Numa S. (1986a). Existence of distinct sodium channel messenger RNAs in rat brain. *Nature* **320,** 188-192.

Noda M, Ikeda T, Suzuki H, Takeshima H, Takahashi T, Kuno M & Numa S. (1986b). Expression of functional sodium channels from cloned cDNA. *Nature* **322,** 826-828.

Norris CM, Halpain S & Foster TC. (1998). Reversal of age-related alterations in synaptic plasticity by blockade of L-type Ca2+ channels. *J Neurosci* **18,** 3171-3179.

Nowycky MC, Fox AP & Tsien RW. (1985). Three types of neuronal calcium channel with different calcium agonist sensitivity. *Nature* **316,** 440-443.

O'Leary T, van Rossum MC & Wyllie DJ. (2010). Homeostasis of intrinsic excitability in hippocampal neurones: dynamics and mechanism of the response to chronic depolarization. *J Physiol* **588,** 157-170.

Ohtsuki G, Piochon C, Adelman JP & Hansel C. (2012). SK2 Channel Modulation Contributes to Compartment-Specific Dendritic Plasticity in Cerebellar Purkinje Cells. *Neuron* **75,** 108-120.

Olverman HJ, Jones AW & Watkins JC. (1984). L-glutamate has higher affinity than other amino acids for [3H]-D-AP5 binding sites in rat brain membranes. *Nature* **307,** 460-462.

Palmer RM, Ferrige AG & Moncada S. (1987). Nitric oxide release accounts for the biological activity of endothelium-derived relaxing factor. *Nature* **327,** 524-526.

Pape HC. (1996). Queer current and pacemaker: the hyperpolarization-activated cation current in neurons. *Annu Rev Physiol* **58,** 299-327.

Park JH, Straub VA & O'Shea M. (1998). Anterograde signaling by nitric oxide: characterization and in vitro reconstitution of an identified nitrergic synapse. *J Neurosci* **18,** 5463-5476.

Peterson BZ, DeMaria CD, Adelman JP & Yue DT. (1999). Calmodulin is the Ca2+ sensor for Ca2+ -dependent inactivation of L-type calcium channels. *Neuron* **22,** 549-558.

Petrovic MM, Nowacki J, Olivo V, Tsaneva-Atanasova K, Randall AD & Mellor JR. (2012). Inhibition of post-synaptic Kv7/KCNQ/M channels facilitates long-term potentiation in the hippocampus. *PLoS One* **7,** e30402.

Petzold GC, Scheibe F, Braun JS, Freyer D, Priller J, Dirnagl U & Dreier JP. (2005). Nitric oxide modulates calcium entry through P/Q-type calcium channels and N-methyl-d-aspartate receptors in rat cortical neurons. *Brain Res* **1063,** 9-14.

Postlethwaite M, Hennig MH, Steinert JR, Graham BP & Forsythe ID. (2007). Acceleration of AMPA receptor kinetics underlies temperature-dependent changes in synaptic strength at the rat calyx of Held. *J Physiol* **579,** 69-84.

Puzzo D, Staniszewski A, Deng SX, Privitera L, Leznik E, Liu S, Zhang H, Feng Y, Palmeri A, Landry DW & Arancio O. (2009). Phosphodiesterase 5 inhibition improves synaptic function, memory, and amyloid-beta load in an Alzheimer's disease mouse model. *J Neurosci* **29,** 8075-8086.

Raman IM & Bean BP. (1999). Ionic currents underlying spontaneous action potentials in isolated cerebellar Purkinje neurons. *J Neurosci* **19,** 1663-1674.

Rameau GA, Tukey DS, Garcin-Hosfield ED, Titcombe RF, Misra C, Khatri L, Getzoff ED & Ziff EB. (2007). Biphasic coupling of neuronal nitric oxide synthase phosphorylation to the NMDA receptor regulates AMPA receptor trafficking and neuronal cell death. *J Neurosci* **27,** 3445-3455.

Randall A & Tsien RW. (1995). Pharmacological dissection of multiple types of Ca2+ channel currents in rat cerebellar granule neurons. *J Neurosci* **15,** 2995-3012.

Randall AD. (1998). The molecular basis of voltage-gated Ca2+ channel diversity: is it time for T? *J Membr Biol* **161,** 207-213.

Rettig J, Heinemann SH, Wunder F, Lorra C, Parcej DN, Dolly JO & Pongs O. (1994). Inactivation properties of voltage-gated K+ channels altered by presence of beta-subunit. *Nature* **369,** 289-294.

Reyes-Haro D, Muller J, Boresch M, Pivneva T, Benedetti B, Scheller A, Nolte C & Kettenmann H. (2010). Neuron-astrocyte interactions in the medial nucleus of the trapezoid body. *J Gen Physiol* **135,** 583-594.

Russier M, Carlier E, Ankri N, Fronzaroli L & Debanne D. (2003). A-, T-, and H-type currents shape intrinsic firing of developing rat abducens motoneurons. *J Physiol* **549,** 21-36.

Sah P. (1996). Ca(2+)-activated K+ currents in neurones: types, physiological roles and modulation. *Trends Neurosci* **19,** 150-154.

Schneggenburger R & Forsythe ID. (2006). The calyx of Held. *Cell Tissue Res* **326,** 311-337.

Schneggenburger R, Meyer AC & Neher E. (1999). Released fraction and total size of a pool of immediately available transmitter quanta at a calyx synapse. *Neuron* **23,** 399-409.

Seutin V, Mkahli F, Massotte L & Dresse A. (2000). Calcium release from internal stores is required for the generation of spontaneous hyperpolarizations in dopaminergic neurons of neonatal rats. *J Neurophysiol* **83,** 192-197.

Shao LR, Halvorsrud R, Borg-Graham L & Storm JF. (1999). The role of BK-type Ca2+-dependent K+ channels in spike broadening during repetitive firing in rat hippocampal pyramidal cells. *J Physiol* **521 Pt 1,** 135-146.

Sheng J, He L, Zheng H, Xue L, Luo F, Shin W, Sun T, Kuner T, Yue DT & Wu LG. (2012). Calcium-channel number critically influences synaptic strength and plasticity at the active zone. *Nat Neurosci* **15,** 998-1006.

Sigel E, Baur R, Trube G, Mohler H & Malherbe P. (1990). The effect of subunit composition of rat brain GABAA receptors on channel function. *Neuron* **5,** 703-711.

Smith PH, Joris PX & Yin TC. (1998). Anatomy and physiology of principal cells of the medial nucleus of the trapezoid body (MNTB) of the cat. *J Neurophysiol* **79,** 3127-3142.

Sonntag M, Englitz B, Kopp-Scheinpflug C & Rubsamen R. (2009). Early postnatal development of spontaneous and acoustically evoked discharge activity of principal cells of the medial nucleus of the trapezoid body: an in vivo study in mice. *J Neurosci* **29,** 9510-9520.

Stanfield PR. (1970). The effect of the tetraethylammonium ion on the delayed currents of frog skeletal muscle. *J Physiol* **209,** 209-229.

Steinert JR, Chernova T & Forsythe ID. (2010). Nitric oxide signaling in brain function, dysfunction, and dementia. *Neuroscientist* **16,** 435-452.

Steinert JR, Kopp-Scheinpflug C, Baker C, Challiss RA, Mistry R, Haustein MD, Griffin SJ, Tong H, Graham BP & Forsythe ID. (2008). Nitric oxide is a volume transmitter regulating postsynaptic excitability at a glutamatergic synapse. *Neuron* **60,** 642-656.

Steinert JR, Postlethwaite M, Jordan MD, Chernova T, Robinson SW & Forsythe ID. (2011a). NMDAR-mediated EPSCs are maintained and accelerate in time course during maturation of mouse and rat auditory brainstem in vitro. *J Physiol* **588,** 447-463.

Steinert JR, Robinson SW, Tong H, Haustein MD, Kopp-Scheinpflug C & Forsythe ID. (2011b). Nitric oxide is an activity-dependent regulator of target neuron intrinsic excitability. *Neuron* **71,** 291-305.

Stocker M. (2004). Ca(2+)-activated K+ channels: molecular determinants and function of the SK family. *Nat Rev Neurosci* **5,** 758-770.

Stuehr DJ. (2004). Enzymes of the L-arginine to nitric oxide pathway. *J Nutr* **134,** 2748S-2751S; discussion 2765S-2767S.

Stuehr DJ, Santolini J, Wang ZQ, Wei CC & Adak S. (2004). Update on mechanism and catalytic regulation in the NO synthases. *J Biol Chem* **279,** 36167-36170.

Sun XP, Schlichter LC & Stanley EF. (1999). Single-channel properties of BK-type calcium-activated potassium channels at a cholinergic presynaptic nerve terminal. *J Physiol* **518 (Pt 3),** 639-651.

Tao X, West AE, Chen WG, Corfas G & Greenberg ME. (2002). A calcium-responsive transcription factor, CaRF, that regulates neuronal activity-dependent expression of BDNF. *Neuron* **33,** 383-395.

Thalhammer A, Rudhard Y, Tigaret CM, Volynski KE, Rusakov DA & Schoepfer R. (2006). CaMKII translocation requires local NMDA receptor-mediated Ca2+ signaling. *EMBO J* **25,** 5873-5883.

Thompson AM & Schofield BR. (2000). Afferent projections of the superior olivary complex. *Microsc Res Tech* **51,** 330-354.

Tong H, Steinert JR, Robinson SW, Chernova T, Read DJ, Oliver DL & Forsythe ID. (2010). Regulation of Kv channel expression and neuronal excitability in rat medial nucleus of the trapezoid body maintained in organotypic culture. *J Physiol* **588,** 1451-1468.

Tozer AJ, Forsythe ID & Steinert JR. (2012). Nitric oxide signalling augments neuronal voltage-gated L-type (ca(v)1) and p/q-type (ca(v)2.1) channels in the mouse medial nucleus of the trapezoid body. *PLoS One* **7,** e32256.

Tully K & Treistman SN. (2004). Distinct intracellular calcium profiles following influx through N- versus L-type calcium channels: role of Ca2+-induced Ca2+ release. *J Neurophysiol* **92,** 135-143.

Uwechue NM, Marx MC, Chevy Q & Billups B. (2012). Activation of glutamate transport evokes rapid glutamine release from perisynaptic astrocytes. *J Physiol* **590,** 2317-2331.

Vallance P & Leiper J. (2002). Blocking NO synthesis: how, where and why? *Nat Rev Drug Discov* **1,** 939-950.

Van Petegem F, Clark KA, Chatelain FC & Minor DL, Jr. (2004). Structure of a complex between a voltage-gated calcium channel beta-subunit and an alpha-subunit domain. *Nature* **429,** 671-675.

Wadel K, Neher E & Sakaba T. (2007). The coupling between synaptic vesicles and Ca2+ channels determines fast neurotransmitter release. *Neuron* **53,** 563-575.

Wahl-Schott C & Biel M. (2009). HCN channels: structure, cellular regulation and physiological function. *Cell Mol Life Sci* **66,** 470-494.

Waithe D, Ferron L, Page KM, Chaggar K & Dolphin AC. (2011). Beta-subunits promote the expression of Ca(V)2.2 channels by reducing their proteasomal degradation. *J Biol Chem* **286,** 9598-9611.

Walker D, Bichet D, Geib S, Mori E, Cornet V, Snutch TP, Mori Y & De Waard M. (1999). A new beta subtype-specific interaction in alpha1A subunit controls P/Q-type Ca2+ channel activation. *J Biol Chem* **274,** 12383-12390.

Wang LY, Gan L, Forsythe ID & Kaczmarek LK. (1998). Contribution of the Kv3.1 potassium channel to high-frequency firing in mouse auditory neurones. *J Physiol* **509 (Pt 1),** 183-194.

Wei AD, Gutman GA, Aldrich R, Chandy KG, Grissmer S & Wulff H. (2005). International Union of Pharmacology. LII. Nomenclature and molecular relationships of calcium-activated potassium channels. *Pharmacol Rev* **57,** 463-472.

Wendehenne D, Pugin A, Klessig DF & Durner J. (2001). Nitric oxide: comparative synthesis and signaling in animal and plant cells. *Trends Plant Sci* **6,** 177-183.

West AE, Chen WG, Dalva MB, Dolmetsch RE, Kornhauser JM, Shaywitz AJ, Takasu MA, Tao X & Greenberg ME. (2001). Calcium regulation of neuronal gene expression. *Proc Natl Acad Sci U S A* **98,** 11024-11031.

Wheeler DB, Randall A, Sather WA & Tsien RW. (1995). Neuronal calcium channels encoded by the alpha 1A subunit and their contribution to excitatory synaptic transmission in the CNS. *Prog Brain Res* **105,** 65-78.

Wheeler DB, Randall A & Tsien RW. (1994). Roles of N-type and Q-type Ca2+ channels in supporting hippocampal synaptic transmission. *Science* **264,** 107-111.

Willmott NJ, Wong K & Strong AJ. (2000). A fundamental role for the nitric oxide-G-kinase signaling pathway in mediating intercellular Ca(2+) waves in glia. *J Neurosci* **20,** 1767-1779.

Wilson GW & Garthwaite J. (2010). Hyperpolarization-activated ion channels as targets for nitric oxide signalling in deep cerebellar nuclei. *Eur J Neurosci* **31,** 1935-1945.

Wimmer VC, Horstmann H, Groh A & Kuner T. (2006). Donut-like topology of synaptic vesicles with a central cluster of mitochondria wrapped into membrane

protrusions: a novel structure-function module of the adult calyx of Held. *J Neurosci* **26,** 109-116.

Womack MD & Khodakhah K. (2004). Dendritic control of spontaneous bursting in cerebellar Purkinje cells. *J Neurosci* **24,** 3511-3521.

Wong AY, Graham BP, Billups B & Forsythe ID. (2003). Distinguishing between presynaptic and postsynaptic mechanisms of short-term depression during action potential trains. *J Neurosci* **23,** 4868-4877.

Wong EH, Kemp JA, Priestley T, Knight AR, Woodruff GN & Iversen LL. (1986). The anticonvulsant MK-801 is a potent N-methyl-D-aspartate antagonist. *Proc Natl Acad Sci U S A* **83,** 7104-7108.

Wu GY, Deisseroth K & Tsien RW. (2001). Activity-dependent CREB phosphorylation: convergence of a fast, sensitive calmodulin kinase pathway and a slow, less sensitive mitogen-activated protein kinase pathway. *Proc Natl Acad Sci U S A* **98,** 2808-2813.

Wu K, Xu JL, Suen PC, Huang YY & Mount HT. (1996). Nitric oxide increases calcium/calmodulin-dependent phosphorylation of proteins in the postsynaptic density of adult rat cerebral cortex. *Brain Res Mol Brain Res* **40,** 22-26.

Wu LG & Borst JG. (1999). The reduced release probability of releasable vesicles during recovery from short-term synaptic depression. *Neuron* **23,** 821-832.

Xia XM, Fakler B, Rivard A, Wayman G, Johnson-Pais T, Keen JE, Ishii T, Hirschberg B, Bond CT, Lutsenko S, Maylie J & Adelman JP. (1998). Mechanism of calcium gating in small-conductance calcium-activated potassium channels. *Nature* **395,** 503-507.

Youssoufian M, Oleskevich S & Walmsley B. (2005). Development of a robust central auditory synapse in congenital deafness. *J Neurophysiol* **94,** 3168-3180.

Yue DT, Backx PH & Imredy JP. (1990). Calcium-sensitive inactivation in the gating of single calcium channels. *Science* **250,** 1735-1738.

Zamponi GW, Bourinet E, Nelson D, Nargeot J & Snutch TP. (1997). Crosstalk between G proteins and protein kinase C mediated by the calcium channel alpha1 subunit. *Nature* **385,** 442-446.

Zhao R, Liu L & Rittenhouse AR. (2007). Ca2+ influx through both L- and N-type Ca2+ channels increases c-fos expression by electrical stimulation of sympathetic neurons. *Eur J Neurosci* **25,** 1127-1135.

Zong X, Krause S, Chen CC, Kruger J, Gruner C, Cao-Ehlker X, Fenske S, Wahl-Schott C & Biel M. (2012). Regulation of Hyperpolarization-activated Cyclic Nucleotide-gated (HCN) Channel Activity by cCMP. *J Biol Chem* **287,** 26506-26512.

Zucker RS & Regehr WG. (2002). Short-term synaptic plasticity. *Annu Rev Physiol* **64,** 355-405.